ABSTRACT

Title of Dissertation: GEOMETRIC COOPERATIVE CONTROL OF FORMATIONS

Fumin Zhang, Doctor of Philosophy, 2004

Dissertation directed by: Professor P.S. Krishnaprasad
Department of Electrical & Computer Engineering

Robots in a team are modeled as particles which obey simple, second order dynamics. The whole team can be viewed as a deformable body with changing shape and orientation. Jacobi shape theory is applied to model such a formation.

We derive the controlled system equations using the Lagrange-D'Alembert principle. Control forces on each robot are combined and reorganized as controls for the center, for rotation and for shape changes. From a shape-theoretic point of view, general feedback control laws are designed to achieve desired formations.

The system equations on shape space provide possibilities for achieving formations without communication links between team members equipped

with sufficient sensing ability. We allow each robot freedom to establish a coordinate system in which shape dynamics of the whole formation is computed. Without knowing such coordinate systems of other robots, each robot is able to perform cooperative control. This is made possible by a class of gauge covariant control laws. We argue that freedom of choosing gauge frame helps to improve controller performance.

When all robots are required to have common constant speed, the control forces have to be of gyroscopic nature. Previous works of Justh and Krishnaprasad has inspired us to study the obstacle avoidance and navigation problem from a point of view of formation shape control. We achieve gyroscopic control laws to achieve boundary following behavior when the particle encounters an obstacle. The "steady state" trajectory of the particle forms a Bertrand pair with the boundary curve of the obstacle. This steady state behavior correspond to a relative equilibrium for a non-autonomous system on special Euclidean groups. Our control law achieves asymptotic convergence of the non-autonomous system dynamics.

The boundary following behavior is a building block for robot navigation in a cluttered environment. Based on the configuration of the obstacles and the target, we may construct virtual boundary curves by analyzing sensory data. Such virtual boundary curves lead the robot to the target without collision.

We have also studied the problem of establishing a formation of satellites with periodic shape changes near an elliptic earth orbit. We propose a control

law that would set up a given formation near a given orbit. This law also allows a satellite formation to achieve orbit transfer.

GEOMETRIC COOPERATIVE CONTROL OF FORMATIONS

by
Fumin Zhang

Dissertation submitted to the Faculty of the Graduate School of the
University of Maryland, College Park in partial fulfillment
of the requirements for the degree of
Doctor of Philosophy
2004

Advisory Committee:

Professor P.S. Krishnaprasad, Chairman/Advisor
Professor Eyad Abed
Professor Stuart Antman
Professor John Baras
Professor Steven Marcus

DEDICATION

Dedicated to my parents, my sister and my wife.

ACKNOWLEDGEMENTS

In 1998, Dr. Krishnaprasad offered me financial aid to come to University of Maryland as a Ph.D. student. The thoughts and results presented in this thesis started then. During the six years, Dr. Krishnaprasad has spent uncountable days with me offering guidance, advice and corrections. He has contributed significantly to every result documented in this thesis. Other than the technical results, my skills of scientific communication are also in great debt to his educating effort.

The research work presented in Chapter 4 has benefited significantly from my collaboration with Dr. Eric Justh. The first version of the idea of using a detected point on obstacle boundary as a virtual vehicle was written as an internal report in the spring of 2003. Since then, Dr. Eric Justh has read every version of the report, helped to establish the current formulation and coauthored a conference paper in which convergence results for boundary-tracking laws (for circular and linear obstacle boundaries) were presented. He has also helped to extend the two dimensional boundary tracking law to a simple case in three dimension.

The simulations and experiments in Chapter 3 and Chapter 4 were performed with the help from Mr. Salman Haq, Mr. Micheal Goldgeier and Mr.

Alan O'Connor who spent many hours with me when they were undergraduates in or visiting University of Maryland. Although not presented in this thesis, the curvature estimation research work related to the boundary tracking algorithms in Chapter 4 benefits from the help of Mr. Alan O'Connor and Mr. Derek Luebke. The MDLe system, upon which many experiments are performed, bears marks from Dr. Dimitrios Hristu, Dr. Sean Andersson, Mr. Patrick Sodre , Mr. Aaron Greene, Mr. Adrian Cottin and all the people mentioned before. I really appreciate the Institute of Systems Research and the Department of Electrical and Computer Engineering for bringing all the young and talented undergraduate students together to take part in serious research works.

I would like to thank Dr. Naomi Loenard of Princeton University and Dr. Vladimir Lumelsky of the University of Wisconsin for advices on possible extensions of the results in Chapter 4.

I would also like to thank Dr. Dong Eui Chang and Dr. Jerald Marsden for lending a preprint upon which results in Chapter 5 are built. Mr. Steven Cooley from NASA has kindly verified those results on FreeFlyer. Dr. Ed Belbruno successfully organized ASTROCON2003 and helped to publish the results in Annals of the New York Academy of Sciences.

My research was supported in part by the National Aeronautics and Space Administration under NASA-GSFC Grant No. NAG5-10819, by the Air Force Office of Scientific Research under AFOSR Grant No. F49620-01-0415, by the Army Research Office under ODDR&E MURI97 Program Grant No.

DAAG55-97-1-0114 to the Center for Dynamics and Control of Smart Structures (through Harvard University), and under ODDR&E MURI01 Program Grant No. DAAD19-01-1-0465 to the Center for Communicating Networked Control Systems (through Boston University).

TABLE OF CONTENTS

LIST OF TABLES

LIST OF FIGURES

Chapter 1

Introduction and Preliminaries

In human societies, formations are formed deliberately in numerous situations to achieve goals beyond individual ability. The shapes of formations are determined according to target applications. For example, rectangles are formed to transport heavy burdens. Lines are used for hunting or attacking. Circles are used for defense...etc. In sports and entertainment, keeping and changing formations is appreciated as a form of art.

Human ability to achieve and maintain formations is acquired by learning and training. The algorithms are based on a set of rules. Commands or drums are used as synchronization mechanisms. However, this type of rule-based formation control requires very high level intelligence which will not be reached by any man-made device in the near future. On the other hand, many examples of formations have been observed in mammals, birds, fish and insects with much lower level intelligence. The most popular one is the

V-shape formation formed by geese and various kinds of birds. Researchers have come up with different explanations of why and how this shape is formed but the problem is still an open one([12]). What has been observed is that formations will help animals to cooperate effectively to face challenges from nature. A formation will provide more information sharing, more opportunities in reproducing, safer environment and less consumption of energy. Many attempts have been made in both explaining and simulating the behaviors of animal formations([27],[17]). Although the results are heuristic and approximate, they can serve as inspirations for designing and controlling multi-robot formations.

In physics, the world without intelligence, various structures of molecules and the structure of the solar system all suggest that formations can be achieved by basic interactions between objects. The problem of determining motion of a group of particles with mutual interactions is called the many-body problem. This problem has a history back to Kepler, Newton and Euler and is still a focus of research in modern physics. What are the interactions which allow particles to form a meaningful formation is the problem we want to address in this thesis.

This problem is not only interesting theoretically, but also very much relevant to applications. Some recent development in distributed sensor networks and adaptive sampling raised many interests in formation control that is able to react to environment changes, c.f. [11].

One must keep in mind that Nature does not know how to determine

the coordinates of the particles. The laws of physics, usually represented in formulas involving coordinates, are actually coordinate independent. A robot can be viewed as a physical object with low level intelligence. Without help from a fixed coordinate frame, only shape variables can be determined using its on-board sensors. As students of Nature, we can artificially introduce simulated physical interactions between robots to achieve formations. This serves as the main theme of this thesis. We justify this claim by suggesting mathematically justified interaction laws for mobile robots, unmanned aerial vehicles and man-made satellites.

1.1 Contributions of the thesis

Jacobi proposed a special class of coordinates ([23]) which served as the starting point to what we call the Jacobi shape space. On this shape space, global displacements (of translation and rotation) are not present. What remain are quantities which are coordinate free. In fact, the gravitational potential function and electric potential function, which induce the two basic natural forces, are functions on this Jacobi shape space. It suggests that Nature knows how to measure shapes.

The Jacobi shape space can be parametrized in different ways. Working independently, a statistician D. G. Kendall developed his notion of size-shape space ([15], [16]) which turns out to be a specially parametrized Jacobi shape space. Kendall defined a size variable which we prove to be the virial function

well known in physics. After the size information is removed from the Jacobi shape space, one gets a compact space of "pure shapes" which is the Kendall shape space.

The above discussions of shape spaces are elaborated in chapter 2. These insightful results provides mathematical tools describing formations. To show that we can take advantage of the knowledge of shape spaces. We give two examples at the end of chapter 2 . In the first example, we analyze a classical example of sequential pursuit. We discovered that the gauge covariant angular velocity is a conserved quantity which contributes to the beauty of system trajectories. The second example is controlling line formations with possible applications in automated highway systems. In these examples, our results benefit from Kendall's notion of size and shape.

In this spirit, we present some results using Lyapunov-based design methods. The central idea is to find a candidate function with compact sub-level sets. Then design a control law which produces semi-negative derivative for this function. We can then argue by using LaSalle's invariance principle that the controlled dynamics converges to the maximal invariant set. If the Lyapunov candidate function is a function on shape space, then the feedback control law only depends on shape variables.

In chapter 3, a formation of Newtonian particles is modeled as a controlled Lagrangian system. When there is symmetry in the Lagrangian function, the dynamics can be reduced to either the shape space or the pre-shape space. Then it is possible to design a control law based on a Lyapunov function on

the pre-shape space or shape space. Theorem 3.2.1 claims that a simple control law using measurements of Jacobi vectors can be utilized to setup a given formation. However, those measurements require the real time availability of GPS and high speed communication links. Theorem 3.3.1 and 3.3.2 claims that a desired formation can be set up by using measurements of shape variables. Since the measurements can be obtained through sensors of the robot, no GPS is required. To stop the rotation motion of the formation, in theorem 3.3.1, measurements of the angular velocity are employed as feedback. Theorem 3.3.2 states that if there exists certain friction in the environment then the formation will stop rotation without using a controller. The motivation to study such control laws is to lessen the demands on communication links posed by formation controllers.

The robots that form a formation usually have reasonably strong computing and sensing ability. An ideal cooperative control law should be able to allow maximum freedom for each robot in addition to achieving cooperation. The geometry of the tangent bundle on the shape space provides a class of gauge invariant and gauge covariant objects. When measured in different coordinate systems, these objects will either not change its value in different gauge coordinate frame or the change is compatible with the frame transform. Theorem 3.4.1 shows one way to utilize the gauge invariant and gauge covariant objects to allow each robot freedom to establish its own choice of gauge coordinate frame. Simulation shows that by having this freedom, noise in the sensor data might have less effect on the performance

of formation controllers.

The construction of Jacobi shape space inspired us to look into the possibilities of constructing other shape spaces suitable for specific context. In applications involving unmanned aerial vehicles (UAVs) and mobile robots, the configuration space of each robot is a Euclidean group $SE(2)$ or $SE(3)$. Meanwhile, regardless of its shape, the whole formation can be described by one group element that belongs to the same Euclidean group. Then shape variables are derived by computing the relative displacement between the group element of each member and the group element for the formation.

Due to fuel efficiency and dynamical stability, UAVs and high speed mobile robots are preferred to maintain constant speed. With the constant speed constraint, the interactions between the formation members are of gyroscopic nature. Several ways of designing gyroscopic interactions to achieve formations have been proposed by [14]. We discovered that the formation control technique can be applied to generate a control law for obstacle avoidance and navigation for constant speed vehicles.

Our navigation algorithms are based on a class of control laws that produce boundary following behaviors for moving vehicles. The steady state trajectory achieved by this control law is a Bertrand mate of the boundary curve of an obstacle. We describe the pair of planar Bertrand curves using the Frenet-Serret formulation. Theorem 4.2.2 shows that if a Bertrand pair of curves is traversed by a pair of points, then there is at least one configuration where the shape of the points remains constant. Theorem 4.3.1 claims

that a Bertrand pair can be viewed as a relative equilibrium for the motion of a pair of particles. We discovered that if one particle is a constant speed vehicle, then the other particle correspond to the closest point to the vehicle on the boundary curve. To make the vehicle follow the boundary curve, all we have to do now is to find control laws to achieve this equilibrium.

We have proposed two such control laws. The first control law assumes that the boundary curve is smooth. The resulting tracking behavior is independent of the choice for the direction of boundary curve. The second control law only assumes piecewise smoothness of the boundary curve. The vehicle is controlled to track the boundary in a given direction.

When there are multiple static obstacles and a fixed target in the environment, in order to navigate the robot to the target collision free, we construct virtual obstacle boundaries based on local measurements of the vehicle. These virtual boundaries are straight lines which go through the target. Algorithm 4.7.7 proposed one way to construct the virtual boundaries. Theorem 4.7.10 states that using such an algorithm and following the virtual boundaries, the vehicle is able to reach the target without collision.

In the context of the man-made satellites, a space of Keplerian orbits for single satellite is defined in [7] and [5]. We point out that if the earth is considered as a member of this two-body formation, the space of Keplerian orbits can be seen as part of a shape space. When the energy of each orbit is the same, although the geometric shape of the formation goes under periodic changes, the difference in the mean anomalies between members are constant.

Thus we name the space of Keplerian orbits of multiple satellites plus the differences between the mean anomalies as the shape space for a satellite formation. [47].

In chapter 5, we derived the Gaussian perturbation equations using shape variables. We then propose a Lyapunov function based control which is able to set up a periodic satellite formation on elliptic orbits and proved its convergence in theorem 5.5.2. In the next step, we address the issue of setting up satellite formations on circular orbits. The difficulty in this case lies in the fact that on a circular orbit, the mean anomaly cannot be measured from the perigee since there is no perigee or apogee. The problem is solved by measuring the mean anomaly from the ascending node instead of the perigee. Theorem 5.6.2 provides convergence results for the transfer algorithm to set up formation on circular orbits[48].

1.2 Lie groups and group actions

This section provides a concise review of knowledge related to Lie groups which is necessary in understanding the proofs and technical details in the following chapters. However, most of the results in this thesis are accessible without such knowledge. We also try to explain the concepts in the context where it is needed.

An algebraic set G is called a *group* if the following conditions are true:

1. It is equipped with a binary operation "$\cdot$" between members of the set.

Furthermore, the operation is closed and associative i.e. if $g, h, k \in G$, then $g \cdot h \in G$ and $(g \cdot h) \cdot k = g \cdot (h \cdot k)$. One often writes $g \cdot h$ as gh.

2. There exists a special member i_d, called the identity such that $i_d \cdot g = g \cdot i_d = g$.

3. For any member g, there exists a unique member, denoted by g^{-1} such that $g \cdot g^{-1} = g^{-1} \cdot g = i_d$.

Members of a group are often called group elements. We say a group is *Abelian* if $g \cdot h = h \cdot g$ for all elements.

If the notion of open set is defined on a group G s.t. (1) $\emptyset$ and G are open sets, (2) the intersection between two open sets is open, and (3) unions of countable open sets are open, we say G has a topology. Furthermore, if the topology is well defined s.t. the group operation "$\cdot$" and the inverse mapping that maps g to g^{-1} are continuous, then G becomes a *topological group*.

A *Lie group* is a topological group where the group operation and the inverse mapping are *differentiable*. Hence, a Lie group not only has the algebraic properties of a group, but also is viewed as a manifold with metric and geometric properties.

The most intensively studied Lie groups are *matrix groups*. The group elements are finite dimensional matrices. The group operation is the matrix multiplication and the inverse mapping is the matrix inverse. It is known that all finite dimensional Lie groups can be represented by matrix groups. Therefore the study of matrix groups is very important both practically and

theoretically.

Throughout the thesis we are going to use only two matrix groups, the orthogonal group $O(n)$ and the special Euclidean group $SE(n)$ where n is a positive integer. Furthermore, in most cases we let $n = 2$ or 3.

The *Orthogonal group* $O(n)$ is the collection of all $n \times n$ matrices g satisfying $g^T g = I_{n\times n}$ where ^{T} denotes the matrix transpose. $O(n)$ has two disconnected pieces. One piece contains all the g s.t. $det(g) = -1$. The other piece contains all the g s.t. $det(g) = 1$. We call the piece where $\det(g) = 1$ the *special orthogonal group* $SO(n)$.

The *special Euclidean group* $SE(n)$ is constructed by combining $SO(n)$ and the Euclidean vector space $\mathcal{R}^n$ in the following way. Let $g \in SO(n)$ and $\mathbf{r} \in \mathcal{R}^n$, then a group element $h \in SE(n)$ is a $(n+1) \times (n+1)$ matrix of the following form

$$h = \left[\begin{array}{ccc|c} & g & & \mathbf{r} \\ \hline 0 & \dots & 0 & 1 \end{array}\right] . \tag{1.1}$$

Given a Lie group G and a manifold M, in many situations we are able to define an operation Φ_g for each $g \in G$ on every $q \in M$. If the operation is smooth in both g and q, $\Phi_g[\Phi_h[q]] = \Phi_{gh}[q]$ and $\Phi_{i_d}[q] = q$, we call Φ a *left action* of G on M. For example, if G is $SO(n)$ and M is $\mathcal{R}^n$, we can define $\Phi_g[q] = gq$. When $n = 3$, this action produces a rotation of vector q. If instead of $\Phi_g[\Phi_h[q]] = \Phi_{gh}[q]$ one has $\Phi_g[\Phi_h[q]] = \Phi_{hg}[q]$, then Φ is called a *right action*. We often denote a left action by L_g and a right action by R_g. If G is $SE(3)$, then the left action of $h \in G$ on $\mathcal{R}^3$ is obtained by first enlarging

$\mathbf{x} \in \mathcal{R}^3$ to a vector of four elements $(\mathbf{x}^T, 1)^T$ and then multiply by the 4×4 dimensional matrix h to the left.

For each q in M, the action Φ produces an *orbit*, which is a subset of M defined as $O_q = \{x \in M | x = \Phi_g[q] \text{ for some } g \in G\}$. An action is *free* if all group orbits are diffeomorphic to the group G. Another way of saying this is that $\Phi_g[q] = \Phi_h[q]$ if and only if $g = h$. For example, the left action of $SO(2)$ on $\mathcal{R}^2 - \{0\}$ is free, but the left action of $SO(3)$ on $\mathcal{R}^3$ is not free because there is a subgroup of rotations that fixes a given vector.

Because G is also a manifold, at any point h_0, one can draw curves passing through this point. The linear approximation of a curve near h_0 is a *tangent vector*. The collection of all tangent vectors is called the *tangent space*, denoted as $T_{h_0}G$. A tangent space is well defined at each point (which is also a group element) on this manifold. The dimension of the tangent space is proved to be the same as the dimension of the Lie group.

The Lie group G acts on itself through the group operation. The action can be a left action or a right action. The left self action maps curves near a point, say h_0 to curves near a new point, say h_1. Therefore, it *induces* an operation on the tangent vectors by translating one vector in the tangent space of h_0 to a new vector in the tangent space of h_1. We would like to define this induced operation as an action. Because the operation involves tangent spaces at every point on the Lie group, it is necessary for us to consider the collection of all tangent spaces of the Lie group G. We define this large space

as the *tangent bundle* TG. Formally,

$$TG = \bigcup_{h \in G} T_h G \tag{1.2}$$

We define the induced action on the tangent spaces as the *lifted action* $T\Phi_g$ on the tangent bundle TG.

Under the lifted action $T\Phi_g$, starting from an element ξ of the tangent space near the identity, the orbit is a vector field on G viewed as a manifold. This vector field, denoted by X_ξ, is called a *left invariant vector field*, because (1) the vector at each point can be obtained by transporting the tangent vector ξ near the identity using the lifted left action and (2) if the lifted action $T\Phi_g$ is applied to this vector field, the resulting vector field is the same as the original one.

For a Lie group G, the tangent space at the identity is called its *Lie algebra*, denoted by $\mathfrak{g}$. The Lie algebra is equipped with a bracket operation which is defined as

$$[\xi, \eta]_l = [X_\xi, X_\eta]_L|_{i_d} \tag{1.3}$$

where the bracket between the two left invariant vector field is the Jacobi-Lie bracket defined as

$$[X, Y]_L(f) = X(Y(f)) - Y(X(f)) \tag{1.4}$$

where f is a smooth function on the Lie group. For $G = SO(n)$, its Lie algebra is denoted as $so(n)$ which contains $n \times n$ skew-symmetric matrices. And the Lie bracket is just the bracket operation between matrices. When $n = 3$,

the Lie algebra $so(3)$ is diffeomorphic to $\mathcal{R}^3$ and the Lie bracket is the cross product between vectors. Therefore, it is often more convenient to represent elements of $so(3)$ as three dimensional vectors. In such a context, one often use ξ for the vector representation and use $\widehat{\xi}$ for the matrix representation. We have, for $\xi, \eta \in so(3)$,

$$[\widehat{\xi}, \widehat{\eta}]_l = \widehat{\xi \times \eta} \ . \tag{1.5}$$

For an element $\xi \in \mathfrak{g}$, we define the *exponential map* $\exp : \mathfrak{g} \to G$ s.t.

$$\frac{d}{dt}\exp(t\xi)|_{t=0} = \xi \ , \tag{1.6}$$

and $\exp((t+s)\xi) = \exp(t\xi)\exp(s\xi)$. For each ξ one obtains a group element $\exp(\xi)$. The exponential map is a diffeomorphism between the Lie algebra and an open neighborhood of the Lie group G near the identity element.

An important action is the *adjoint action* where group G acts on its Lie algebra. Let L_g and R_g denote the left and right self action of a Lie group G. For $\xi \in \mathfrak{g}$, the adjoint action of G on $\mathfrak{g}$ is defined as:

$$Ad_g[\xi] = \frac{d}{dt} L_g[R_g^{-1}[\exp(t\xi)]]|_{t=0} \tag{1.7}$$

For $G = SO(3)$, the adjoint action is

$$Ad_g[\widehat{\xi}] = g\widehat{\xi}g^{-1} \ \text{ or } \ Ad_g[\xi] = g\xi \ . \tag{1.8}$$

For an element $\xi \in G$, there exists a one parameter subgroup $\exp(t\xi) \in G$. If we already defined an action Φ of G on some manifold M, then $\Phi_{\exp(t\xi)}$ is the action of the one parameter subgroup on M. We can define the *infinitesimal*

generator of the action as

$$\xi_G(q) = \frac{d}{dt}\Phi_{\exp(t\xi)}[q]|_{t=0} \ . \tag{1.9}$$

For $G = SO(3)$, the infinitesimal generator is

$$\xi_G(q) = \widehat{\xi} q = \xi \times q \ . \tag{1.10}$$

Given a vector field $X(q)$ on a manifold M, suppose G acts on M by the action Φ_g. A point $q_e \in M$ is a *relative equilibrium* of $X(q)$ if there exists $\xi \in \mathfrak{g}$ s.t.

$$X(q_e) = \xi_G(q_e) \ . \tag{1.11}$$

Unlike at an equilibrium, the vector field at a relative equilibrium does not vanish. Instead, it coincides with the tangent vector of a group orbit. We note that if the vector field X is non-autonomous, then ξ is allowed to be time-dependent. If this is the case, we say q_e is a relative equilibrium for the non-autonomous vector field $X(q,t)$ if there exists $\xi(t) \in \mathfrak{g}$ s.t.

$$X(q_e, t) = \xi_G(q_e, t) \ . \tag{1.12}$$

Chapter 2

Shape Space and Geometry

The many body problem has been a focus of classical mechanics and quantum mechanics for more than two centuries. During the last 30 years, modern geometry started to play an important role toward getting insights on classical results and explaining new observations. From a geometric point of view, the shape of a formation is invariant under left action of a Euclidean group, i.e. rotation and translation. Under appropriate technical assumptions, one can split the entire configuration space into two parts. One space corresponds to a group orbit, which has the same structure as the group. The other space is the collection of points, each point represents one group orbit. We call the first space a fiber and the second space the base space. Points that belong to the base space describe the shape of the formation, hence the base space is also called the shape space. Bearing the similarity with the framework for studying non-holonomic mechanical system (c.f. [43]), such decomposition is

called a principal fiber bundle.

Motions in the configuration space can also split, resulting in motions in the shape space and motions in the fiber. One interesting phenomenon happens here: one motion in the shape space may cause another motion in the fiber. To describe the relationship between the two motions, we need two mathematical tools. First we shall establish a gauge convention, which assign each point on the fiber a unique group element. We can then slice the configuration space into sections, each section contains points that correspond to an identical group element. Secondly, we shall define a connection form, which describes the drift along fibers when one tries to move within a section. In another words, the connection form tells us how much rotation of a formation is produced by changing the shape of the formation. This connection form is represented as gauge potentials in physics [23].

On another track, mathematicians working in the field of statistical pattern recognition started to develop their own notion of size-shape space from the late 70s and early 80s. Kendall is one of them[15] [16]. If we assume all the particles in a many body problem have the same mass, then a shape space in physics sense will be further decomposed into a size variable and a shape space in Kendall's notion. Hence the Kendall shape space is a compact manifold equipped with a Riemannian metric. This will allow us to control the size and the shape of a formation separately.

Other than the two shape spaces defined above, in the context of satellite formations, the space of Keplerian orbits is introduced in [7] [5]. Shape space

is also defined when ensembles of rigid bodies such as **G**-snakes [39] [40] are studied. Those shape spaces are utilized later in other chapters to solve specific problems. In this section we will study the Jacobi and Kendall shape spaces and the geometric structures associated to them.

2.1 Jacobi shape space of the many-body problem

To describe the motion of a cluster of particles, we set up a fixed coordinate frame first. We call it the space frame or the fixed lab frame. Let $q_i \in \mathcal{R}^3$, $i = 1, 2, ..., N$, denote the coordinates of N particles with mass m_i. The kinetic energy of this cluster is

$$K^{\text{tot}} = \frac{1}{2} \sum_{i=1}^{N} m_i \parallel \dot{q}_i \parallel^2 \ . \tag{2.1}$$

This kinetic energy is invariant under translation, because if the positions of all particles are subjected to the transform $q_i \rightarrow q_i + \mathbf{z}_c$ for all i where $\mathbf{z}_c$ is a given vector in $\mathcal{R}^3$, then the value of K^{tot} is unchanged. Let

$$M = \sum_{i=1}^{N} m_i \ . \tag{2.2}$$

Let

$$q_c = \frac{\sum_{i=1}^{N} m_i q_i}{M} \ . \tag{2.3}$$

We can see q_c is the coordinate for the center of mass. Now one can define a new set of coordinates $\mathbf{c}_{\mathrm{f}i}$ as

$$\mathbf{c}_{\mathrm{f}i} = q_i - q_c \ . \tag{2.4}$$

Then the kinetic energy can be expressed as

$$K^{\mathrm{tot}} = \frac{1}{2} M \parallel \dot{q}_c \parallel^2 + \frac{1}{2} \sum_{i=1}^{N} m_i \parallel \dot{\mathbf{c}}_{\mathrm{f}i} \parallel^2 \ . \tag{2.5}$$

Hence K is separated into two parts. The first part is the translational kinetic energy which only depends on $\parallel \dot{q}_c \parallel$. The second part is the internal kinetic energy which only depends on the internal variables $\mathbf{c}_{\mathrm{f}i}$. But since

$$\sum_{i=1}^{N} m_i \mathbf{c}_{\mathrm{f}i} = 0, \tag{2.6}$$

we can find $(N-1)$ independent vectors $(\rho_{\mathrm{f}i}, i = 1, 2, ..., N-1)$ from $span(\mathbf{c}_{\mathrm{f}i}, i = 1, 2, ..., N)$. We want $\rho_{\mathrm{f}i}$ be chosen such that the kinetic energy has the form

$$K^{\mathrm{tot}} = \frac{1}{2} M \parallel \dot{q}_c \parallel^2 + \frac{1}{2} \sum_{i=1}^{N-1} \parallel \dot{\rho}_{\mathrm{f}i} \parallel^2 \ . \tag{2.7}$$

Such a set of $\rho_{\mathrm{f}i}$ are called *the Jacobi coordinates*.

One way of constructing the Jacobi coordinates is to let

$$\begin{aligned}
\rho_{\mathrm{f}1} &= \sqrt{\mu_1}(\mathbf{c}_{\mathrm{f}2} - \mathbf{c}_{\mathrm{f}1}) \\
\rho_{\mathrm{f}2} &= \sqrt{\mu_2}(\mathbf{c}_{\mathrm{f}3} - \frac{m_1 \mathbf{c}_{\mathrm{f}1} + m_2 \mathbf{c}_{\mathrm{f}2}}{m_1 + m_2}) \\
&\vdots \\
\rho_{\mathrm{f}i} &= \sqrt{\mu_i}(\mathbf{c}_{\mathrm{f}(i+1)} - \frac{\sum_{k=1}^{i} m_k \mathbf{c}_{\mathrm{f}k}}{\sum_{k=1}^{i} m_k}) \\
&\vdots
\end{aligned}$$

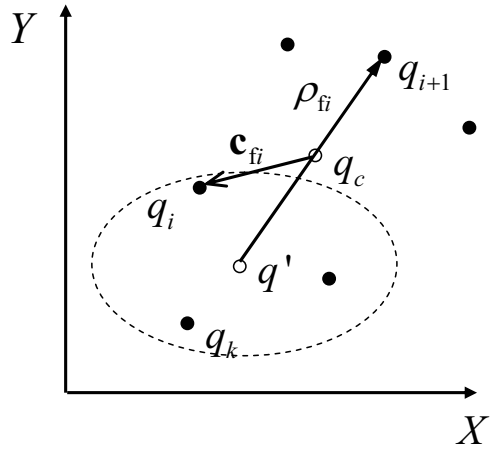

Figure 2.1: *q_c is the center of mass. q' is the center of mass of the cluster containing the first i particles. The Jacobi vector ρ_{fi} will be the vector between q' and q_{i+1} scaled by $\sqrt{\mu_i}$.*

$$\rho_{f(N-1)} = \sqrt{\mu_{N-1}}(\mathbf{c}_{fN} - \frac{\sum_{k=1}^{N-1} m_k \mathbf{c}_{fk}}{\sum_{k=1}^{N-1} m_k}) \tag{2.8}$$

where

$$\frac{1}{\mu_i} = \frac{1}{\sum_{k=1}^{i} m_k} + \frac{1}{m_{i+1}} \text{ for } i = 1, 2, ..., N-1 \ . \tag{2.9}$$

The proof for this construction satisfying (2.7) will be provided later (see proposition 2.3.1 and its proof).

By constructing the Jacobi coordinates, we have implemented a linear transformation Φ from q_i to (q_c, ρ_{fi}). If we express Φ in a $(N \times N)$ matrix, we have:

$$[q_c, \rho_{f1}, ..., \rho_{f(N-1)}] = [q_1, q_2, ..., q_N]\Phi \tag{2.10}$$

$$\Phi_{i1} = \frac{m_i}{M} \quad (i = 1, 2, ...N)$$

$$\begin{aligned}
\Phi_{ii} &= \sqrt{\mu_{i-1}} \quad (i>1) \\
\Phi_{ij} &= -\sqrt{\mu_{j-1}}\frac{m_i}{\sum_{k=1}^{j-1} m_k} \quad (j>1;\ i<j) \\
\Phi_{ij} &= 0 \quad (j>1;\ i>j)
\end{aligned} \tag{2.11}$$

As one can see from the definitions and figure 2.1, the vectors $\rho_{\mathrm{f}i}$ are constructed by finding the scaled relative displacement between the $(i+1)$th particle and the center of mass of the sub-cluster of first i particles. This process depends on how the particles are labeled. We can also change the way we sub-cluster particles as in [2], [22] and [23]. Hence Jacobi coordinates are not unique. However, between any two sets of Jacobi coordinates there exists an element $\mathbf{h} \in \mathrm{O(N-1)}$ s.t.

$$[\rho^1_{\mathrm{f}1}, \rho^1_{\mathrm{f}2}, ..., \rho^1_{\mathrm{f}(N-1)}] = [\rho^2_{\mathrm{f}1}, \rho^2_{\mathrm{f}2}, ..., \rho^2_{\mathrm{f}(N-1)}]\mathbf{h}\ . \tag{2.12}$$

This representation of the orthogonal group $O(N-1)$ is called *the democracy group* [23].

The existence of the democracy group gives us an immediate advantage in computing the transform from $(q_c, \rho_{\mathrm{f}1}, \rho_{\mathrm{f}2}, \ldots, \rho_{\mathrm{f}(N-1)})$ to $(q_1, q_2, \ldots, q_N)$ i.e. the inverse of the transform that defines q_c and $\rho_{\mathrm{f}i}$. If we can compute the inverse map for one set of Jacobi variables, say Φ_1^{-1}, then for another set of Jacobi variables, the inverse map Φ_2^{-1} can be obtained by

$$\Phi_2^{-1} = \begin{bmatrix} 1 & 0 \\ 0 & \mathbf{h} \end{bmatrix} \Phi_1^{-1}\ . \tag{2.13}$$

Therefore it is only necessary to compute one such inverse map, namely Φ^{-1}. We have the following lemma:

Lemma 2.1.1 *Let*

$$\nu_i = \frac{1}{\sum_{j=1}^{i} m_j} - \frac{1}{\sum_{j=1}^{i+1} m_j} \tag{2.14}$$

for $i = (1, 2, \ldots, N-1)$. *Suppose* $\rho_{\mathrm{f}i}$, $(i = 1, 2, \ldots, N-1)$ *are defined by equation (2.8). Then*

$$q_k = q_c + \left(\sqrt{\frac{1}{m_k} - \frac{1}{\sum_{j=1}^{k} m_j}} \right) \rho_{\mathrm{f}(k-1)} - \sum_{j=k}^{N-1} (\sqrt{\nu_j}) \rho_{\mathrm{f}j} \ , \tag{2.15}$$

where we let $\rho_{\mathrm{f}0} = 0$ *and* $k = 1, 2, ..., N$

Proof By using equation (2.8), we can verify that

$$\begin{aligned} q_{k+1} - q_k &= \frac{1}{\sqrt{\mu_k}} \rho_{\mathrm{f}k} - \left(\sqrt{\frac{1}{m_k} - \frac{1}{\sum_{j=1}^{k} m_j}} \right) \rho_{\mathrm{f}(k-1)} \\ q_1 &= q_c - \sum_{j=1}^{N-1} (\sqrt{\nu_j}) \rho_{\mathrm{f}j} \ , \end{aligned} \tag{2.16}$$

for $k = 1, 2, \ldots, N-1$, by evaluating the right hand side. We can also verify that q_k given by equation (2.15) satisfies equation (2.16). But in the non-degenerate case the solution to equation (2.16) is unique. Therefore (2.15) gives the transform from $(q_c, \rho_{\mathrm{f}1}, \rho_{\mathrm{f}2}, \ldots, \rho_{\mathrm{f}(N-1)})$ to $(q_1, q_2, \ldots, q_N)$. ■

Let $Q = \mathcal{R}^{3N}$ be the total configuration space of the formation. The space of Jacobi coordinates is $\mathcal{R}^{3N-3}$. We define

$$K = \frac{1}{2} \sum_{i=1}^{N-1} \| \dot{\rho}_{\mathrm{f}i} \|^2 \ . \tag{2.17}$$

This K is invariant under the diagonal left action on $\mathcal{R}^{3N-3}$ by the special orthogonal group $\mathbf{G} = SO(3)$. The action is:

$$\Phi_g(\rho_{\mathrm{f}i}) = g\rho_{\mathrm{f}i} \ \text{ for } g \in \mathbf{G} \ . \tag{2.18}$$

This symmetry group $\mathbf{G}$ acts on $\mathcal{R}^{3N-3}$ properly and freely except for the shapes where all $\rho_{\mathrm{f}i}$ are collinear. We let the set F_0 be the set of all the Jacobi coordinates corresponding to collinear shapes. Let $F = \mathcal{R}^{3N-3} - F_0$ and call it the *Jacobi pre-shape space*. It is an open sub-manifold of the configuration space. Since $\mathbf{G}$ acts properly and freely on F, the base space $B = F/\mathbf{G}$ is a smooth manifold and the canonical projection $\pi : F \to B$ is differentiable. B is called the *Jacobi shape space*.

In dropping from F to B, we get rid of the $SO(3)$ symmetry from the Jacobi coordinates. After the reduction, the dimension of the shape space B is $(3N-6)$. On this shape space we can define *shape coordinates* s_j as

$$s_j = s_j(\rho_{\mathrm{f}1}, \rho_{\mathrm{f}2}, ..., \rho_{\mathrm{f}(N-1)}) \text{ for } j = 1, 2, ...(3N-6) \tag{2.19}$$

s.t.

$$s_j(g\rho_{\mathrm{f}1}, g\rho_{\mathrm{f}2}, ..., g\rho_{\mathrm{f}(N-1)}) = s_j(\rho_{\mathrm{f}1}, \rho_{\mathrm{f}2}, ..., \rho_{\mathrm{f}(N-1)}) \tag{2.20}$$

for all $g \in SO(3)$. Candidates for s^j are functions of dot products $(\rho_{\mathrm{f}i} \cdot \rho_{\mathrm{f}j})$ and triple products $(\rho_{\mathrm{f}i} \cdot (\rho_{\mathrm{f}j} \times \rho_{\mathrm{f}k}))$. Thus, mutual distances, bearing angles, areas and volumes formed by the line segments connecting the particles all serve as candidates for shape variables.

One can establish a body coordinate system on a formation with certain shape. The reference orientation of this formation can be defined as the orientation when the body coordinate frame and the lab coordinate frame coincide. Then the orientation of this formation with the *same* shape can be described by an element $g \in SO(3)$. The Jacobi coordinates in these two

coordinate systems have the following relationship:

$$\rho_{\mathrm{f}i} = g\rho_i(s) \tag{2.21}$$

where

$$s = (s_1, s_2, ..., s_{3N-6})^T. \tag{2.22}$$

ρ_i are Jacobi coordinates in the body coordinate frame which only depend on shape coordinates.

Taking derivative on both sides of (2.21), we get

$$\dot{\rho}_{\mathrm{f}i} = \dot{g}\rho_i + g\dot{\rho}_i \ . \tag{2.23}$$

On a matrix Lie group $\mathbf{G}$, $\dot{g} \in T_g\mathbf{G}$. There exists $\widehat{\Omega} \in \mathfrak{g}$ the Lie algebra s.t. $\dot{g} = g\widehat{\Omega}$. In our case, $\mathbf{G} = SO(3)$, so $\mathfrak{g} = (\mathcal{R}^3, \times)$. Thus the derivative of $\dot{\rho}_{\mathrm{f}i}$ is

$$\dot{\rho}_{\mathrm{f}i} = g(\Omega \times \rho_i + \sum_{j=1}^{3N-6} \frac{\partial \rho_i}{\partial s_j}\dot{s}_j) \ . \tag{2.24}$$

In the body coordinate frame, the *angular momentum* of the whole system J can be calculated as

$$\begin{aligned} J &= g^{-1}\sum_{i=1}^{N-1}(\rho_{\mathrm{f}i} \times \dot{\rho}_{\mathrm{f}i}) \\ &= I(\Omega + \sum_{i=1}^{3N-6} A_j\dot{s}_j) \ , \end{aligned} \tag{2.25}$$

where

$$I(s) = \sum_{i=1}^{N-1}(\| \rho_i \|^2 \mathbf{e} - \rho_i\rho_i^T) \tag{2.26}$$

is defined as the *locked inertia tensor* of the formation in the body coordinate frame and

$$A_j(s) = I^{-1} \sum_{i=1}^{N-1} \rho_i \times \frac{\partial \rho_i}{\partial s_j} \tag{2.27}$$

are *vector potential functions*. These quantities are defined on the shape space because ρ_i only depend on shape coordinates.

2.2 Gauge transform

As discussed in the previous section, for a given shape s_0, one can establish a body coordinate system and obtain a group element in $SO(3)$ which measures the orientation of the formation and serves as the transform between the lab coordinate system and the body coordinate system. If the shape of the formation has changed to s_1, in order to compare the orientation, one has to make sure that the body coordinate system is established in a consistent way. Therefore, the procedure to establish a body coordinate system should be shape independent. Such a shape independent procedure for establishing body coordinate system on a deformable body is called a *gauge convention*. Formally, a *gauge convention* is a diffeomorphism between F and $G \times B$ mapping any point $\rho_{\mathrm{f}} \in F$ to $(g, s) \in G \times B$ s.t. $\Phi_{g_1}[\rho_{\mathrm{f}}]$ is mapped to $(g_1 g, s)$. Notice that g serves as part of the coordinates for ρ_{f} independent of s. For example, let (q_1, q_2, q_3) describe three points in $\mathcal{R}^3$. Except for the singular cases of collinear shapes, one can establish the body coordinate system of this triangular formation as follows:

1. Place the origin at center of mass, let the x-axis be aligned with vector $q_1\vec{q}_2$.

2. Let the y-axis be in the plane formed by triangle $q_1q_2q_3$, perpendicular to the x-axis and points towards point q_3.

3. Let the z-axis form a right handed coordinate system with x-axis and y-axis.

It is easy to see that this method is truly shape independent.

Gauge conventions are generally not unique. Let $g \in SO(3)$ describes the orientation of the formation for any $s \in B$ under one gauge convention. Let $g_1 \in SO(3)$ describes the orientation of the formation for the same $s \in B$ under another gauge convention. Then by the property of $SO(3)$, there exists $h(s)$ such that

$$g = g_1 h^T(s) \tag{2.28}$$

where $h : B \to SO(3)$ is a $SO(3)$ valued function on B. This right action of $h(s)$ on $SO(3)$ is called a *gauge transform*. Because a gauge transform is a shape dependent group action, an object which obeys certain transformation rules under rigid group action by $SO(3)$ may violate such rules under a gauge transform. We say an object is *gauge invariant* if it is invariant under any gauge transform. We say an object is *gauge covariant* if it obeys the transformation rules for rigid group action by $SO(3)$ when it is subjected to gauge transforms. An obvious example of a gauge invariant object is the shape variable s. The tangent vectors to the shape space B are also gauge invariant. An obvious example of a gauge covariant object is the Jacobi

vectors ρ_i. Because

$$g\rho_i = \rho_{\mathrm{f}i} = g_1\rho_{i1} \ , \tag{2.29}$$

this implies that

$$\rho_i = h(s)\rho_{i1} \ . \tag{2.30}$$

Hence ρ_{i1} is transformed to ρ_i via the left action by $SO(3)$.

In the applications of cooperative control, gauge invariance and gauge covariance are desired because of the distributed nature of the computing power. Each agent within a team has its own freedom or limitation on how to describe the combined system. A gauge invariant or covariant object can be shared across multiple agents with little or no conversion.

Let F denote the Jacobi Pre-shape space coordinated by (g, s) where $g \in SO(3)$ and $s = (s_1, s_2, \ldots, s_{3N-6}) \in B$ where B is the Jacobi shape manifold. A point in the tangent space $TF(g, s)$ can be represented by $(g, s, g\widehat{\Omega}, v)$ where $\widehat{\Omega} \in so(3)$. However, such representation of TF is not gauge covariant. Under a gauge transform

$$g = g_1 h^T(s) \ , \tag{2.31}$$

then we can calculate the transform of $\widehat{\Omega}$ as

$$\begin{aligned} \widehat{\Omega} &= g^{-1}\dot{g} \\ &= h(s)g_1^T(\dot{g}_1 h^T(s) + g_1\dot{h}^T(s)) \\ &= h(s)\widehat{\Omega}_1 h^T(s) + h(s)\dot{h}^T(s) \\ &= h(s)(\widehat{\Omega}_1 + \dot{h}^T(s)h(s))h^T(s) \ . \end{aligned} \tag{2.32}$$

Since $h^T(s)h(s) = i_d$ where i_d is the identity, we know that $\dot{h}^T(s)h(s) = -h^T(s)\dot{h}(s)$. We then define

$$\Gamma_i = h^T \frac{\partial h}{\partial s_i} \quad for \quad i = 1, 2, \ldots, 3N-6 \; . \tag{2.33}$$

It is easy to see that $\Gamma_i \in so(3)$. Therefore, we can let γ_i denote the vector representation of Γ_i. Hence equation (2.32) becomes

$$\widehat{\Omega} = h(s)(\widehat{\Omega}_1 - \sum_{i=1}^{3N-6} \Gamma_i \dot{s}_i) h^T(s) \; . \tag{2.34}$$

Its vector form is

$$\Omega = h(s)(\Omega_1 - \sum_{i=1}^{3N-6} \gamma_i \dot{s}_i) \; . \tag{2.35}$$

It is clearly not gauge-covariant because Ω_1 can not be transformed to Ω by any lifted action of $SO(3)$ on $so(3)$. We now define

$$\Upsilon = \Omega + \sum_{j=1}^{3N-6} A_j s_j \; . \tag{2.36}$$

Lemma 2.2.1 *Υ is gauge covariant and*

$$\Upsilon = h(s)\Upsilon_1 \tag{2.37}$$

under the gauge transform

$$g = g_1 h^T(s) \; . \tag{2.38}$$

Proof

Under the gauge transform, a Jacobi vector is transformed as

$$\rho_i = h(s)\rho_{i1} \; . \tag{2.39}$$

Therefore, according to the definition of the locked inertia tensor in equation (2.26), one can verify that

$$I(s) = h(s)I_1(s)h^T(s) \tag{2.40}$$

i.e. the locked inertia tensor is gauge covariant.

According to equation (2.27),

$$\begin{aligned} A_j &= I^{-1}\sum_{i=1}^{N-1}(h(s)\rho_{i1}) \times \frac{\partial h(s)\rho_{i1}}{\partial s_j} \\ &= h(s)I_1^{-1}h^T(s)h(s)\sum_{i=1}^{N-1}\rho_{i1} \times (\frac{\partial \rho_{i1}}{\partial s_j} + h^T(s)\frac{\partial h(s)}{\partial s_j}\rho_{i1}) \\ &= h(s)(A_{j1} + I_1^{-1}\sum_{i=1}^{N-1}\rho_{i1} \times (\gamma_j \times \rho_{i1})) \\ &= h(s)(A_{j1} + I_1^{-1}\sum_{i=1}^{N-1}(\| \rho_{i1} \|^2 - \rho_{i_1}\rho_{i_1}^T)\gamma_j) \\ &= h(s)(A_{j1} + \gamma_j)\ . \end{aligned} \tag{2.41}$$

Therefore,

$$\begin{aligned} \Upsilon &= \Omega + \sum_{j=1}^{3N-6} A_j\dot{s}_j \\ &= h(s)(\Omega_1 - \sum_{j=1}^{3N-6}\gamma_j\dot{s}_j) + \sum_{j=1}^{3N-6} h(s)(A_{j1} + \gamma_j)\dot{s}_j \\ &= h(s)(\Omega_1 + \sum_{j=1}^{3N-6} A_{j1}\dot{s}_j) \\ &= h(s)\Upsilon_1\ . \end{aligned} \tag{2.42}$$

■

Thus, a gauge co-variant coordinates for a point in the tangent space $TF(g,s)$ is $(g, s, g\Upsilon, v)$.

2.2.1 Connections and gauge kinematics

In the previous sections, objects such as I, J and A arise when we tried to write the kinetic energy in a split form. We have given formulas for computing those objects in either the fixed lab coordinate system or the body coordinate system. Although the results are necessary and preferred by engineering applications, the mathematical properties of these objects are not fully shown. Therefore, we would like to redefine the objects including I, J and A, and concepts such as gauge convention and gauge transform, by taking a geometrically intrinsic approach. This approach provides a clearer image for the underlying structure of the problem and may also lead to generalization of our results to a larger class of systems.

A function with multiple arguments can often be viewed as an operator acting on the domain of one of its arguments. The other arguments can then be viewed as parameters for this operator. To distinguish the argument being operated from the parameters, we use [ ] to enclose the argument and use ( ) to enclose the parameters.

We first point out that $(F, B, \pi, \mathbf{G})$ forms a principal fiber bundle with shape space at the base and $SO(3)$ orbits as fibers. Let $T_{\rho_\mathrm{f}}F$ be the tangent space of F at point $\rho_\mathrm{f} \in F$. Let $s = \pi(\rho_\mathrm{f})$ be the base point of ρ_f in B. The tangent space to B at point s is T_sB. Let $TF = \bigcup_{\rho_\mathrm{f}\in F} T_{\rho_\mathrm{f}}F$, $TB = \bigcup_{s\in B} T_sB$. TF, TB are called the *tangent bundles* of F and B respectively. Here, a point of the tangent bundle TF represents a point ρ_f of F paired with a tangent

vector v_{ρ_f} to F, while a point of the tangent bundle TB represents a point s of B paired with a tangent vector v_s to B. Since the canonical mapping π maps ρ_f to s, if the tangent vectors to F and B are viewed as infinitesimal approximations for curves in F and B passing through ρ_f and s, then π induces a tangent map $T\pi$ which maps a tangent vector v_{ρ_f} in $T_{\rho_\mathrm{f}}F$ to a tangent vector v_s in T_sB. Therefore, the map $(\pi, T\pi)$ defines a projection map from tangent bundle TF to tangent bundle TB. This projection map $(\pi, T\pi)$ annihilates tangent vectors to the fibers (group orbits). Such tangent vectors to the fibers are closely related to the tangent vectors to the Lie group $\mathbf{G}$.

For a Lie group $\mathbf{G}$, the tangent space at the identity is called the *Lie algebra associated with* $\mathbf{G}$, denoted by $\mathfrak{g}$. Then any curve $g(t) \in \mathbf{G}$ passing $g(0)$ when $t = 0$, can be expressed as $\Psi_{g(0)}[\exp(t\xi)]$ where Ψ denotes the group operator, ξ denotes a vector in $\mathfrak{g}$ and $\exp(\cdot)$ is the exponential map between tangent space and base space. If we take derivative with respect to t along those curves, we obtain a linear map $T_{g(0)}\Psi : \mathfrak{g} \to T_{g(0)}\mathbf{G}$ between the Lie algebra and the tangent space at $g(0)$. Furthermore, any tangent vector to the Lie group $\mathbf{G}$ at point $g(0)$ can be represented by $T_{g(0)}\Psi[\xi]$.

Other than $T_{g(0)}\Psi$, we can define another linear operator $Ad_{g(0)} : \mathfrak{g} \to \mathfrak{g}$, which we call the *adjoint operator*, as follows:

$$Ad_{g(0)}[\xi] = \frac{d}{dt}\Psi_{g(0)}[\Psi_{\exp(t\xi)}[g^{-1}(0)]] \,, \tag{2.43}$$

where $\xi \in \mathfrak{g}$.

We now compute the tangent vector to the fibers of F. Let $\xi_F(\rho_{\rm f}) \in T_{\rho_{\rm f}}F$ be the *infinitesimal generator* of the group action Φ_g on F induced by $\xi \in \mathfrak{g}$, which is defined as

$$\xi_F(\rho_{\rm f}) = \frac{d}{dt}\Phi_{\exp(t\xi)}[\rho_{\rm f}]|_{t=0} \ . \tag{2.44}$$

Then the tangent vector to a fiber of F at point $\rho_{\rm f} = (g, s)$ is

$$\begin{aligned} \frac{d}{dt}\Phi_{\Psi_g[\exp(t\xi)]}[\rho_{\rm f}]|_{t=0} &= \frac{d}{dt}(\Phi_g\Phi_{\exp(t\xi)}[\rho_{\rm f}])|_{t=0} \\ &= T\Phi_g[\xi_F(\rho_{\rm f})] \ . \end{aligned} \tag{2.45}$$

This equation implies that at any given point in F, there is a one to one correspondence between a tangent vector to the fiber and a vector in the Lie algebra $\mathfrak{g}$ of the Lie group $\mathbf{G}$.

The map $T\pi$ and the infinitesimal generator indicate that the tangent bundle TF can be viewed as a combination of the tangent bundle TB and a Lie algebra $\mathfrak{g}$. Therefore, a tangent vector to F can be represented by a tangent vector to B and a vector in the Lie algebra. However, this separation does not mean that TB and $\mathfrak{g}$ are decoupled or unrelated. In fact, because of the existence of a Riemannian metric on F, there exists interesting coupling between TB and $\mathfrak{g}$. Mathematically, we say there exists a connection between a tangent vector to F and a vector in $\mathfrak{g}$.

To describe such a connection, we need a mathematical object called a *lie algebra valued one form*. It is a linear operator $\omega_{\rm f} : TF \to \mathfrak{g}$ represented as $\omega(\rho_{\rm f})[v_{\rm f}]$ for $\rho_{\rm f} \in F$ and $v_{\rm f} \in T_{\rho_{\rm f}}F$. Concerning the group action Φ_g and the induced tangent operator $T\Phi_g$, we use the notation $\Phi_g^*\omega_{\rm f}(\rho_{\rm f})[v_{\rm f}]$ to represent

$\omega(\Phi_g[\rho_{\rm f}])[T\Phi_g[v_{\rm f}]]$. $\Phi_g^*\omega_{\rm f}$ is called the *pull-back* of the one form $\omega_{\rm f}$. We call $\omega_{\rm f}$ a *connection form* on F if the following two properties are satisfied:

(1) $\omega_{\rm f}(\rho_{\rm f})[\xi_F] = \xi$

(2) $\Phi_g^*\omega_{\rm f}(\rho_{\rm f})[X] = Ad_g[\omega_{\rm f}[X]]$

for all vector fields $X \in TF$. This connection form tells us what is the vector in $\mathfrak{g}$ that is associated with a tangent vector to F. It also puts a restriction on this association by requiring that the vector in $\mathfrak{g}$ must satisfy the second property under group action Φ_g. Specially, if $v = T\Phi_g[\xi_F]$ is a tangent vector to a fiber at certain point $\rho_{\rm f} = (g, s)$. Then

$$\omega_{\rm f}[v] = \omega_{\rm f}[T\Phi_g[\xi_F]] = \Phi_g^*\omega_{\rm f}[\xi_F] = Ad_g[\xi] \; . \tag{2.46}$$

Once a connection form $\omega_{\rm f}$ is defined, a given vector field X with $X(\rho_{\rm f}) \in T_{\rho_{\rm f}}F$ can be decomposed as

$$X(\rho_{\rm f}) = X^v(\rho_{\rm f}) + X^h(\rho_{\rm f}) \tag{2.47}$$

with

$$\begin{aligned} \omega_{\rm f}[X^v(\rho_{\rm f})] &= \omega_{\rm f}[X(\rho_{\rm f})] \\ \omega_{\rm f}[X^h(\rho_{\rm f})] &= 0 \; . \end{aligned} \tag{2.48}$$

Here, X^v and X^h are called vertical and horizontal components of X. This suggests that the tangent space $T_{\rho_{\rm f}}F$ can be decomposed into vertical subspace $V_{\rho_{\rm f}}$ and horizontal subspace $H_{\rho_{\rm f}}$.

$$T_{\rho_{\rm f}}F = V_{\rho_{\rm f}} \oplus H_{\rho_{\rm f}} \tag{2.49}$$

where

$$\begin{aligned} V_{\rho_{\mathrm{f}}} &= \{v_1 \in T_{\rho_{\mathrm{f}}}F | v_1 = T\Phi_g[\xi_F], \text{ for some } \xi \in \mathfrak{g}\} \\ H_{\rho_{\mathrm{f}}} &= \{v_2 \in T_{\rho_{\mathrm{f}}}F | \omega_{\mathrm{f}}[v_2] = 0\} \ . \end{aligned} \tag{2.50}$$

Since the vertical vectors are tangent vectors to fibers, we know that $T_{\rho_{\mathrm{f}}}\pi[v] = 0$ for $v \in V_{\rho_{\mathrm{f}}}$. This is to say that the projection of $T_{\rho_{\mathrm{f}}}F$ on to $T_{\rho_{\mathrm{f}}}B$ eliminates the vertical space $V_{\rho_{\mathrm{f}}}$.

On a principal fiber bundle, usually the connection form ω_{f} is not uniquely defined. For a certain class of system called the simple mechanical system with symmetry, a canonical connection form called the mechanical connection exists.

A *simple mechanical system with symmetry* is a quintuple $(Q, K_m, \mathbf{G}, V, \Phi)$. Q is the configuration space. K_m is a Riemannian metric on Q. V is a smooth function on Q. $\mathbf{G}$ is a Lie group and Φ defines the action of $\mathbf{G}$ on Q. For $q \in Q$, $\frac{1}{2}K_m(\dot{q}, \dot{q})$ is called the kinetic energy and $V(q)$ is called the potential energy. The kinetic energy $\frac{1}{2}K_m(\dot{q}, \dot{q})$ and potential energy V should be invariant under the group action Φ, that is,

$$\begin{aligned} K_m(\Phi_g[q])(T\Phi_g[\dot{q}], T\Phi_g[\dot{q}]) &= K_m(q)(\dot{q}, \dot{q}) \\ V(\Phi_g[q]) &= V(q) \ . \end{aligned} \tag{2.51}$$

By this definition, our formation system with $V = 0$ is a simple mechanical system with configuration space $Q = \mathcal{R}^3 \times F$, kinetic energy K^{tot} and the group $\mathbf{G}$ acting trivially on $\mathcal{R}^3$(coordinate of center of mass) but diagonally on F (the Jacobi coordinates). For such a system, we can define a

locked inertia tensor and a momentum map. These two objects can both be viewed as linear operators on $\mathfrak{g}$. Thus they belong to the *dual space* of the Lie algebra $\mathfrak{g}$, denoted by $\mathfrak{g}^*$.

The *locked inertia tensor* of the system is $I_{\mathrm{f}} : F \times \mathfrak{g} \to \mathfrak{g}^*$ satisfying

$$I_{\mathrm{f}}(\rho_{\mathrm{f}}, \xi)[\eta] = K_m(\rho_{\mathrm{f}})(\xi_F, \eta_F) \ , \tag{2.52}$$

where $\xi, \eta \in \mathfrak{g}$ and $\rho_{\mathrm{f}} \in F$.

The *momentum map* is $J_{\mathrm{f}} : TF \to \mathfrak{g}^*$ satisfying

$$J_{\mathrm{f}}(\rho_{\mathrm{f}}, v_{\rho_{\mathrm{f}}})[\xi] = K_m(\rho_{\mathrm{f}})(v_{\rho_{\mathrm{f}}}, \xi_F) \ , \tag{2.53}$$

where $\xi \in \mathfrak{g}$, $\rho_{\mathrm{f}} \in F$ and $v_{\rho_{\mathrm{f}}} \in T_{\rho_{\mathrm{f}}}F$.

For the formation system, the *mechanical connection* is defined as $\omega_{\mathrm{f}}(\rho_{\mathrm{f}})$ s.t.

$$\omega_{\mathrm{f}}(\rho_{\mathrm{f}})[v_{\rho_{\mathrm{f}}}] = I_{\mathrm{f}}(\rho_{\mathrm{f}})^{-1}[J_{\mathrm{f}}(\rho_{\mathrm{f}}, v_{\rho_{\mathrm{f}}})] \ . \tag{2.54}$$

It satisfies the first condition for a connection form because

$$\begin{aligned} \omega_{\mathrm{f}}(\rho_{\mathrm{f}})[\xi_F] &= I_{\mathrm{f}}(\rho_{\mathrm{f}})^{-1}[J_{\mathrm{f}}(\rho_{\mathrm{f}}, \xi_F)] \\ &= I_{\mathrm{f}}(\rho_{\mathrm{f}})^{-1}[I_{\mathrm{f}}(\rho_{\mathrm{f}}, \xi)] \\ &= \xi \ . \end{aligned} \tag{2.55}$$

Let us now check for the second condition for a connection form. We want to know how I_{f}, J_{f} and ω_{f} are transformed under the group action Φ_g. We first compute the transformation rule for an infinitesimal generator $\xi_F(\rho_{\mathrm{f}})$.

$$\xi_F(\Phi_g[\rho_{\mathrm{f}}]) = \frac{d}{dt}\Phi_{\exp(t\xi)}\Phi_g[\rho_{\mathrm{f}}]$$

$$
\begin{aligned}
&= T\Phi_{g^{-1}} \frac{d}{dt} \Phi_{g^{-1}} \Phi_{\exp(t\xi)} \Phi_g[\rho_{\mathrm{f}}] \\
&= T\Phi_{g^{-1}} \frac{d}{dt} \Phi_{\exp(tAd_{g^{-1}}[\xi])}[\rho_{\mathrm{f}}] \\
&= T\Phi_{g^{-1}}[(Ad_{g^{-1}}[\xi])_F] \ . \qquad (2.56)
\end{aligned}
$$

Then,

$$
\begin{aligned}
\Phi_g^* I_{\mathrm{f}}(\rho_{\mathrm{f}}, \xi)[\eta] &= I_{\mathrm{f}}(\Phi_g[\rho_{\mathrm{f}}], \xi)[\eta] \\
&= K_m(\Phi_g[\rho_{\mathrm{f}}])(\xi_F(\Phi_g[\rho_{\mathrm{f}}]), \eta_F(\Phi_g[\rho_{\mathrm{f}}])) \\
&= K_m(\Phi_g[\rho_{\mathrm{f}}])(T\Phi_g[(Ad_{g^{-1}}[\xi])_F], T\Phi_g[(Ad_{g^{-1}}[\eta])_F]) \\
&= K_m(\rho_{\mathrm{f}})((Ad_{g^{-1}}[\xi])_F, (Ad_{g^{-1}}[\eta])_F) \\
&= I_{\mathrm{f}}(\rho_{\mathrm{f}}, Ad_{g^{-1}}[\xi])[Ad_{g^{-1}}[\eta]] \\
&= (Ad^T_{g^{-1}}[I_{\mathrm{f}}(\rho_{\mathrm{f}}, Ad_{g^{-1}}[\xi])])[\eta]; , \qquad (2.57)
\end{aligned}
$$

and

$$
\begin{aligned}
\Phi_g^* J_{\mathrm{f}}(\rho_{\mathrm{f}}, v)[\xi] &= J_{\mathrm{f}}(\Phi_g[\rho_{\mathrm{f}}], T\Phi_g[v])[\xi] \\
&= K_m(\Phi_g[\rho_{\mathrm{f}}])(T\Phi_g[v], \xi_F(\Phi_g[\rho_{\mathrm{f}}])) \\
&= K_m(\Phi_g[\rho_{\mathrm{f}}])(T\Phi_g[v], T\Phi_g[(Ad_{g^{-1}}[\xi])_F]) \\
&= K_m(\rho_{\mathrm{f}})(v, (Ad_{g^{-1}}[\xi])_F) \\
&= J_{\mathrm{f}}(\rho_{\mathrm{f}}, v)[Ad_{g^{-1}}[\xi]] \\
&= (Ad^T_{g^{-1}}[J_{\mathrm{f}}(\rho_{\mathrm{f}}, v)])[\xi] \ . \qquad (2.58)
\end{aligned}
$$

Here, Ad_g^T is the conjugate operator of Ad_g. If Ad_g is represented by a matrix, then Ad_g^T is represented by the transpose of the matrix. We can rewrite the above results as

$$
\Phi_g^* I_{\mathrm{f}} = (Ad^T_{g^{-1}}[I_{\mathrm{f}}])[Ad_{g^{-1}}]
$$

$$\Phi_g^* J_{\mathrm{f}} \;=\; Ad^T_{g^{-1}}[J_{\mathrm{f}}]\;. \tag{2.59}$$

Therefore

$$\begin{aligned}
\Phi_g^* \omega_{\mathrm{f}} &= \Phi_g^*(I_{\mathrm{f}}^{-1} J_{\mathrm{f}}) \\
&= (\Phi_g^* I_{\mathrm{f}})^{-1}[\Phi_g^* J_{\mathrm{f}}] \\
&= Ad_g[I_{\mathrm{f}}^{-1}[Ad_g^T[Ad^T_{g^{-1}}[J_{\mathrm{f}}]]]] \\
&= Ad_g[I_{\mathrm{f}}^{-1}[J_{\mathrm{f}}]] \\
&= Ad_g[\omega_{\mathrm{f}}]\;,
\end{aligned} \tag{2.60}$$

that is, ω_{f} satisfies the second property of a connection.

With the connection form well defined, we are now ready to define the relationship between TB and $\mathfrak{g}$. We first notice that the base space B is embedded in F by a mapping τ such that $\pi \circ \tau = i_{dm}$ where i_{dm} denotes the identity map. Unlike the mapping π, τ is not uniquely determined. Let τ_1 be one possible choice and τ_2 be another. $\tau_1(s)$ and $\tau_2(s)$ lie on the same fiber (group orbit) because they are mapped to the same point on the base space by π. Then for each $s \in B$, there exists a group element $h(s) \in \mathbf{G}$ s.t.

$$\tau_1(s) = \Phi_{h(s)}[\tau_2(s)] \tag{2.61}$$

We define a *gauge convention* to be a choice of map τ. The set $\tau(B)$ is called the *zero section* of the principal fiber bundle. A point in $\tau(B)$ is represented by (i_d, s) where i_d is the identity element of the Lie group $\mathbf{G}$. We define the action of the group valued function $h(s)$ described in equation (2.61) as a *gauge transform*. One can verify that if the group $\mathbf{G}$ is $SO(3)$ and the action

Φ_g is the left action, then these definitions are equivalent to the definitions for gauge convention and gauge transform in section 2.2.

Furthermore, the map $\tau(\cdot)$ induces a tangent map $T\tau$ which maps a tangent vector to B to a tangent vector to F. Then, we can define the *pull-back* of the connection form ω under the map τ, denoted by $\tau^*\omega$ as

$$\tau^*\omega[v_s] = \omega[T\tau[v_s]] \tag{2.62}$$

for $v_s \in T_sB$. This $\tau^*\omega$ is a one form on B. It is also called the *pull-down connection form*. Such a form defines a relationship between a tangent vector to B and a vector in the Lie algebra $\mathfrak{g}$.

We point out that the notion of gauge invariant and gauge covariant can be well understood in this framework. The locked inertia tensor I_{f}, the angular momentum J_{f} and the connection form ω_{f} are gauge invariant since they are defined regardless of the choice for τ. Next, we create representations for I_{f}, J_{f} and ω_{f} when they are restricted to the zero section $\tau(B)$. We define

$$\begin{aligned} I(\rho,\xi) &= I_{\mathrm{f}}(\rho_{\mathrm{f}},\xi)|_{\rho_{\mathrm{f}}\in\tau(B)} \\ J(\rho,v_\rho) &= J_{\mathrm{f}}(\rho_{\mathrm{f}},v_{\rho_{\mathrm{f}}})|_{(\rho_{\mathrm{f}}\in\tau(B),v_{\rho_{\mathrm{f}}}\in T_{\rho_{\mathrm{f}}}F)} \\ \omega &= I^{-1}[J]\ . \end{aligned} \tag{2.63}$$

When the group $\mathbf{G}$ is $SO(3)$, I and J represent the locked inertia tensor and angular momentum in the body coordinate system. These representations are gauge dependent because they depend on the construction of τ. To see what the dependency is, we introduce a gauge transform $\Phi_{h(s)}$, which by

definition, produces $\rho_{\rm f}^1 = \Phi_{h(s)}[\rho_{\rm f}^2]$ where $\rho_{\rm f}^1 \in \tau_1(B)$ and $\rho_{\rm f}^2 \in \tau_2(B)$. The following calculations show how I,J and ω are transformed.

$$\begin{aligned}
I(\rho^1, \xi) &= I_{\rm f}(\rho_{\rm f}^1, \xi)|_{\rho_{\rm f}^1 \in \tau_1(B)} \\
&= I_{\rm f}(\Phi_{h(s)}[\rho_{\rm f}^2], \xi)|_{\rho_{\rm f}^2 \in \tau_2(B)} \\
&= \Phi_{h(s)}^* I_{\rm f}(\rho_{\rm f}^2, \xi) \\
&= Ad_{h^{-1}(s)}^T [I_{\rm f}(\rho_{\rm f}^2, Ad_{h^{-1}(s)}[\xi])] \\
&= Ad_{h^{-1}(s)}^T [I(\rho^2, Ad_{h^{-1}(s)}[\xi])] \\
J(\rho^1, v_\rho^1) &= J_{\rm f}(\rho_{\rm f}^1, v_{\rho_{\rm f}}^1)|_{\rho_{\rm f}^1 \in \tau_1(B)} \\
&= J_{\rm f}(\Phi_{h(s)}[\rho_{\rm f}^2], T\Phi_{h(s)}[v_{\rho_{\rm f}}^2])|_{\rho_{\rm f}^2 \in \tau_2(B)} \\
&= \Phi_{h(s)}^* J_{\rm f}(\rho_{\rm f}^2, v_{\rho_{\rm f}}^2) \\
&= Ad_{h^{-1}(s)}^T [J_{\rm f}(\rho_{\rm f}^2, v_{\rho_{\rm f}}^2)] \\
&= Ad_{h^{-1}(s)}^T [J(\rho^2, v_\rho^2)] \\
\omega(\rho^1) &= I(\rho^1)^{-1} J(\rho^1) \\
&= Ad_{h(s)}[I(\rho^2)^{-1}[Ad_{h(s)}^T [Ad_{h^{-1}(s)}^T [J(\rho^2)]]]] \\
&= Ad_{h(s)}[I(\rho^2)^{-1}[J(\rho^2)]] \\
&= Ad_{h(s)}[\omega(\rho^2)] \ . \qquad (2.64)
\end{aligned}$$

In these transformation rules, $h(s)$ appears as if s is a constant i.e. there is no term involving $\frac{\partial h(s)}{\partial s}$. We say I,J and ω are gauge covariant because the transformation rules are the same as the rigid body transformation rules.

The angular velocity and the pull-down connection form also depend on specific gauge convention. Because their transformation rules involve $\frac{\partial h(s)}{\partial s}$, they are neither gauge invariant nor gauge covariant.

We mention that although the intrinsic approach is abstract, it is able to produce the same set of formulas as seen previously in both the lab coordinate system and the body coordinate system. We would like to show this process as a validation to the intrinsic approach.

In our context, since the group $\mathbf{G}$ is SO(3), the Lie algebra $\mathfrak{g}$ is $so(3)$. We can represent the elements of $so(3)$ by 3-dimensional vectors ξ, η and also by (3×3) skew symmetric matrices $\widehat{\xi}, \widehat{\eta}$.

In the lab coordinate system,

$$\xi_F(\rho_{\mathrm{f}}) = (\xi \times \rho_{\mathrm{f}1}, \xi \times \rho_{\mathrm{f}2}, ...\xi \times \rho_{\mathrm{f}(N-1)}) \ . \tag{2.65}$$

By the definition of the locked inertia tensor, we have

$$\begin{aligned} I_{\mathrm{f}}(\rho_{\mathrm{f}}, \xi)[\eta] &= K(\xi_F, \eta_F) \\ &= \sum_{i=1}^{N-1} (\xi \times \rho_{\mathrm{f}i})^T (\eta \times \rho_{\mathrm{f}i}) \\ &= \sum_{i=1}^{N-1} \xi^T (\| \rho_{\mathrm{f}i} \|^2 \mathbf{e} - \rho_{\mathrm{f}i} \rho_{\mathrm{f}i}^T) \eta \end{aligned} \tag{2.66}$$

where $\mathbf{e}$ is the 3×3 identity matrix. Hence

$$I_{\mathrm{f}}(\rho_{\mathrm{f}}) = \sum_{i=1}^{N-1} (\| \rho_{\mathrm{f}i} \|^2 \mathbf{e} - \rho_{\mathrm{f}i} \rho_{\mathrm{f}i}^T) \ . \tag{2.67}$$

By similar calculations we find the expression for the momentum map J to be:

$$J_{\mathrm{f}}(\rho_{\mathrm{f}}, \dot{\rho}_{\mathrm{f}}) = \sum_{i=1}^{N-1} \rho_{\mathrm{f}i} \times \dot{\rho}_{\mathrm{f}i} \ . \tag{2.68}$$

The expressions in body coordinates can be derived by applying equation

(2.63). The locked inertia tensor in body frame is

$$I(\rho) = \sum_{i=1}^{N-1} (\| \rho_i \|^2 \mathbf{e} - \rho_i \rho_i^T) \ . \tag{2.69}$$

We can see that $I_{\mathrm{f}} = gIg^T$. Next, we notice that if $\rho_{\mathrm{f}} \in \tau(B)$, then according to equation (2.23), its coordinates satisfy

$$\dot{\rho}_{\mathrm{f}i} = \Omega \times \rho_i + \dot{\rho}_i \ . \tag{2.70}$$

For the momentum map, we have

$$J(\rho, \dot{\rho}) = J_{\mathrm{f}}(\rho_{\mathrm{f}}, \dot{\rho}_{\mathrm{f}})|_{(\rho_{\mathrm{f}} \in \tau(B), \dot{\rho}_{\mathrm{f}} \in T_{\rho_{\mathrm{f}}} F)} = \sum_{i=1}^{N-1} (\rho_i \times (\Omega \times \rho_i) + \rho_i \times \dot{\rho}_i) \ . \tag{2.71}$$

Obviously, $J_{\mathrm{f}} = gJ$. After simplification we have:

$$J(\rho, \dot{\rho}) = I\Omega + \sum_{i=1}^{N-1} \rho_i \times \dot{\rho}_i \ . \tag{2.72}$$

Hence, the mechanical connection in body frame is

$$\begin{aligned} \omega(\rho)[\dot{\rho}] &= I^{-1} J \\ &= \Omega + I^{-1} \sum_{i=1}^{N-1} \rho_i \times \dot{\rho}_i \ . \end{aligned} \tag{2.73}$$

Therefore, one can see the relation between ω_{f} and ω as,

$$\omega_{\mathrm{f}}(\rho_{\mathrm{f}})[\dot{\rho}_{\mathrm{f}}] = I_{\mathrm{f}}^{-1} J_{\mathrm{f}} = g I^{-1} J = g\omega(\rho)[\dot{\rho}] \ . \tag{2.74}$$

After we choose shape coordinates s_j on the shape space B, we already know that

$$\rho_i = \rho_i(s_1, s_2, ...s_{3N-6}) \ . \tag{2.75}$$

Therefore, let $v_s \in T_sB$, the lift of v_s to $T_{\tau(s)}F$ is

$$\begin{aligned} T_s\tau[v_s] &= \frac{d}{dt}(\rho_1(s+tv_s), \rho_2(s+tv_s), ..., \rho_{N-1}(s+tv_s), i_d)|_{t=0} \\ &= (\sum_{j=1}^{3N-6} \frac{\partial \rho_1}{\partial s_j} v_{sj}, \sum_{j=1}^{3N-6} \frac{\partial \rho_2}{\partial s_j} v_{sj}, ..., \sum_{j=1}^{3N-6} \frac{\partial \rho_{N-1}}{\partial s_j} v_{sj}, \Omega = 0). \end{aligned} \quad (2.76)$$

Then by equation (2.73),

$$\begin{aligned} \tau^*\omega(s)[v_s] &= \omega(\rho_{\rm f})[T\tau[v_s]]|_{\rho_{\rm f}\in\tau(B)} \\ &= I^{-1}(\Omega + \sum_{i=1}^{N-1}(\rho_i \times \sum_{j=1}^{3N-6} \frac{\partial \rho_i}{\partial s_j} v_{sj})) \\ &= I^{-1} \sum_{i=1}^{N-1}(\rho_i \times \sum_{j=1}^{3N-6} \frac{\partial \rho_i}{\partial s_j} v_{sj}) \\ &= \sum_{j=1}^{3N-6} (I^{-1} \sum_{i=1}^{N-1} \rho_i \times \frac{\partial \rho_i}{\partial s_j}) v_{sj} \ . \end{aligned} \quad (2.77)$$

Define A_j as

$$A_j = I^{-1} \sum_{i=1}^{N-1} \rho_i \times \frac{\partial \rho_i}{\partial s_j} \ . \quad (2.78)$$

Then the representation of $\tau^*\omega$ in shape coordinates is $\sum_{j=1}^{3N-6} A_j ds_j$ where A_j are lie algebra valued functions. A_j are called the *gauge potentials* on the shape space B. Because

$$I^{-1} \sum_{i=1}^{N-1} \rho_i \times \dot{\rho}_i = \sum_{j=1}^{3N-6} A_j \dot{s}_j \ , \quad (2.79)$$

we also obtained a simpler form for ω as

$$\omega(g, s, \Omega, \dot{s}) = \Omega + \sum_{i=1}^{3N-6} A_j \dot{s}_j \quad (2.80)$$

This is identical with the definition of Υ in equation (2.36). The gauge covariant property of Υ comes from the fact that ω is gauge covariant.

We found the information in [43] and the references therein very helpful in understanding gauge theory. The block diagonalization technique can be found in [25, 35, 36, 20, 42].

2.3 Kendall's notion of size and shape

For a while, statisticians have been asking the following questions: Given data points on a line, plane, ... $\mathcal{R}^m$, how can one describe the shape of the data? distinguish between two shapes? determine the distance between two shapes? Starting from the knowledge that shape information is invariant under translation and rotation, D.G. Kendall rediscovered Jacobi vectors but with the assumption that all the particles have unit mass [15]. Given N points in R^m, $N \geq 2$, as x_1^*,x_2^*,...,x_N^*, written as columns of matrix X^*. Then Kendall's coordinates are

$$\begin{aligned} x_0 &= \sqrt{N} x_c^* \\ &= \frac{1}{\sqrt{N}}(x_1^* + x_2^* + \cdots + x_N^*) \\ \widetilde{x}_j &= \frac{1}{\sqrt{j+j^2}}(j x_{j+1}^* - (x_1^* + x_2^* + \cdots + x_j^*)) \end{aligned} \tag{2.81}$$

where $1 \leq j \leq (N-1)$. In matrix form,

$$\widetilde{X} = [x_0, \widetilde{x}_1, ..., \widetilde{x}_{N-1}] = X^* Q_N \ , \tag{2.82}$$

for example:

$$Q_3 = \begin{bmatrix} \frac{1}{\sqrt{3}} & \frac{-1}{\sqrt{2}} & \frac{-1}{\sqrt{6}} \\ \frac{1}{\sqrt{3}} & \frac{1}{\sqrt{2}} & \frac{-1}{\sqrt{6}} \\ \frac{1}{\sqrt{3}} & 0 & \frac{2}{\sqrt{6}} \end{bmatrix} . \tag{2.83}$$

In fact, if we let $m_1 = m_2 =, ..., m_N = 1$ in the definition of Jacobi coordinates, then

$$\mu_j = \frac{m_{j+1} \sum_{k=1}^{j} m_k}{\sum_{k=1}^{j+1} m_k} = \frac{j}{j+1} . \tag{2.84}$$

Hence by letting $q_i = x_i^*$ for $i = 1, 2, ..., N$, we have

$$\begin{aligned} q_c &= \frac{\sum_{i=1}^{N} m_i q_i}{M} = \frac{1}{\sqrt{N}} x_0 \\ \rho_{\mathrm{f}j} &= \sqrt{\mu_j}(\mathbf{c}_{\mathrm{f}(j+1)} - \frac{\sum_{k=1}^{j} m_k \mathbf{c}_{\mathrm{f}k}}{\sum_{k=1}^{j} m_k}) \\ &= \sqrt{\frac{j}{j+1}}(q_{j+1} - \frac{q_1 + q_2 + ... + q_j}{j}) \\ &= \sqrt{\frac{1}{j(j+1)}}(jq_{j+1} - (q_1 + q_2 + ... + q_j)) \\ &= \widetilde{x}_j . \end{aligned} \tag{2.85}$$

Thus we have proved that Kendall coordinates are Jacobi coordinates with the unit mass assumption.

The Kendall size variable is defined as

$$S = \sqrt{\sum_{i=1}^{N} \| x_i^* - x_c^* \|^2} = \sqrt{\sum_{i=1}^{N-1} \| \widetilde{x}_i \|^2} . \tag{2.86}$$

Assuming $S \neq 0$, we have removed degeneracy of total collision, corresponding to the case when the formation will shrink to one point so that no shape

need to be studied. After dropping the first column in matrix $\widetilde{X}$, then divide the result by S, we get an $(m \times (N-1))$ matrix

$$X = [x_1, x_2..., x_{N-1}] \tag{2.87}$$

where $x_i = \widetilde{x}_i/S$. X is a point in a $(m(N-1)-1)$ dimensional sphere which is defined as the *Kendall pre-shape sphere* S_m^N. A *Kendall shape* is an equivalence class $[X]$ on the pre-shape sphere where the equivalence relation $\sim$ is :

$$X \sim Y \ ,$$

if there exists $T \in SO(m)$ s.t. $X = TY$. The *Kendall shape space* is the space of such equivalence classes, denoted by Σ_m^N. It is the shape space of N data points in $\mathcal{R}^m$. Notice that only the case where *all* particles collide has been excluded from this shape space.

The similarity between Kendall's procedure and Jacobi's procedure is very clear. After the unit mass assumption is dropped, we can make a small extension to the definitions of Kendall's size variable so that

$$S = \sqrt{\sum_{i=1}^{N-1} \| \rho_{\mathrm{f}i} \|^2} \ . \tag{2.88}$$

In fact, this size variable S can be viewed as a special choice of Jacobi shape variable. We extend the Kendall coordinates to be the Jacobi coordinates. Then this extended Kendall shape space is a compact sub-manifold of Jacobi shape space. All the future arguments about Kendall shape space is applicable to the extended one if we replace the Kendall coordinates by the Jacobi

coordinates.

From now on, the terms *shape variable(s)* or *shape coordinate(s)* will refer to variables or coordinates on the Jacobi shape space. The terms *pure shape variable(s)* or *pure shape coordinate(s)* will refer to variables or coordinates on the extended Kendall shape space where size information has been removed.

We discovered an interesting fact. The size variable S is equivalent to the virial function which has been used for measuring the size of star clusters much earlier than Kendall's work. The virial function is defined as

$$V_I = \sum_{i=1}^{N} \frac{1}{2} m_i \parallel \mathbf{c}_{\mathrm{f}i} \parallel^2 \tag{2.89}$$

where $\mathbf{c}_{\mathrm{f}i}$ is defined in Equation (2.4).

Proposition 2.3.1 $\frac{1}{2}S^2 = V_I$.

Proof

We are going to use the induction method. Starting from $N = 2$, we have

$$\rho_{\mathrm{f}1} = \sqrt{\mu_1}(\mathbf{c}_{\mathrm{f}2} - \mathbf{c}_{\mathrm{f}1}) \ . \tag{2.90}$$

But since we already know that

$$m_1\mathbf{c}_{\mathrm{f}1} + m_2\mathbf{c}_{\mathrm{f}2} = 0 \ . \tag{2.91}$$

Then

$$\mathbf{c}_{\mathrm{f}2} = -\frac{m_1}{m_2}\mathbf{c}_{\mathrm{f}1} \ . \tag{2.92}$$

Thus replace $\mathbf{c}_{\mathrm{f}2}$ in equation (2.90) by equation (2.92), we get

$$\rho_{\mathrm{f}1} \quad = \quad -\sqrt{\mu_1}\frac{m_1 + m_2}{m_2}\mathbf{c}_{\mathrm{f}1}$$

$$= -\sqrt{\frac{m_1(m_2+m_1)}{m_2}}\mathbf{c}_{\mathrm{f}1} \ . \tag{2.93}$$

Hence

$$\begin{aligned}
\frac{1}{2}S_2^2 &= \frac{1}{2}\parallel \rho_{\mathrm{f}1} \parallel^2 \\
&= \frac{m_1(m_2+m_1)}{2m_2}\parallel \mathbf{c}_{\mathrm{f}1} \parallel^2 \\
&= \frac{1}{2}m_1 \parallel \mathbf{c}_{\mathrm{f}1} \parallel^2 + \frac{1}{2}\frac{m_1^2}{m_2}\parallel \mathbf{c}_{\mathrm{f}1} \parallel^2 \\
&= \frac{1}{2}m_1 \parallel \mathbf{c}_{\mathrm{f}1} \parallel^2 + \frac{1}{2}m_2 \parallel \mathbf{c}_{\mathrm{f}2} \parallel^2 \\
&= V_I \ .
\end{aligned} \tag{2.94}$$

Now, suppose the proposition holds for N particles i.e.

$$\text{induction hypothesis} \quad \sum_{i=1}^{N}\frac{1}{2}m_i \left\| \mathbf{c}_{\mathrm{f}i}^N \right\|^2 = \sum_{i=1}^{N-1}\frac{1}{2}\parallel \rho_{\mathrm{f}i} \parallel^2 \ , \tag{2.95}$$

we want to show it holds for $(N+1)$ particles. Notice the addition of the $(N+1)$th particle has changed the center of mass from q_c^N to q_c^{N+1}. By definition of the Jacobi vectors we get

$$\rho_{\mathrm{f}N} = \sqrt{\mu_{N+1}}(\mathbf{c}_{\mathrm{f}(N+1)}^{N+1} - (q_c^N - q_c^{N+1})) \tag{2.96}$$

where

$$\mu_{N+1} = \frac{M_N\, m_{N+1}}{M_N + m_{N+1}} \tag{2.97}$$

where $M_N = \sum_{i=1}^{N} m_i$. We also have

$$M_N(q_c^N - q_c^{N+1}) + m_{N+1}\mathbf{c}_{\mathrm{f}(N+1)}^{N+1} = 0 \ . \tag{2.98}$$

Thus equation (2.96) can be rewritten as

$$\rho_{\mathrm{f}N} = \sqrt{\frac{(M_N + m_{N+1})m_{N+1}}{M_N}}\mathbf{c}_{\mathrm{f}(N+1)}^{N+1} \ . \tag{2.99}$$

$\mathbf{c}_{\mathrm{f}i}^N$ and $\mathbf{c}_{\mathrm{f}i}^{N+1}$ are also related by:

$$\begin{aligned}\mathbf{c}_{\mathrm{f}i}^N &= \mathbf{c}_{\mathrm{f}i}^{N+1} + q_c^{N+1} - q_c^N \\ &= \mathbf{c}_{\mathrm{f}i}^{N+1} + \frac{m_{N+1}}{M_N}\mathbf{c}_{\mathrm{f}(N+1)}^{N+1} \,. \end{aligned} \tag{2.100}$$

Therefore

$$\begin{aligned}\frac{1}{2}S_{N+1}^2 &= \sum_{i=1}^{N-1}\frac{1}{2}\parallel\rho_{\mathrm{f}i}\parallel^2 + \frac{1}{2}\parallel\rho_{\mathrm{f}N}\parallel^2 \\ &= \sum_{i=1}^{N}\frac{1}{2}m_i\left\|\,\mathbf{c}_{\mathrm{f}i}^N\,\right\|^2 + \frac{1}{2}\parallel\rho_{\mathrm{f}N}\parallel^2 \\ &= \sum_{i=1}^{N}\frac{1}{2}m_i\left\|\,\mathbf{c}_{\mathrm{f}i}^{N+1} + \frac{m_{N+1}}{M_N}\mathbf{c}_{\mathrm{f}(N+1)}^{N+1}\,\right\|^2 \\ &\quad + \frac{1}{2}\frac{(M_N+m_{N+1})m_{N+1}}{M_N}\left\|\,\mathbf{c}_{\mathrm{f}(N+1)}^{N+1}\,\right\|^2 \\ &= \sum_{i=1}^{N}\frac{1}{2}m_i\left\|\,\mathbf{c}_{\mathrm{f}i}^{N+1}\,\right\|^2 + (\sum_{i=1}^{N}m_i\mathbf{c}_{\mathrm{f}i}^{N+1})\frac{m_{N+1}}{M_N}\mathbf{c}_{\mathrm{f}(N+1)}^{N+1} \\ &\quad + \frac{1}{2}(\sum_{i=1}^{N}m_i)\frac{m_{N+1}^2}{M_N^2}\left\|\,\mathbf{c}_{\mathrm{f}(N+1)}^{N+1}\,\right\|^2 + \frac{1}{2}m_{N+1}\left\|\,\mathbf{c}_{\mathrm{f}(N+1)}^{N+1}\,\right\|^2 \\ &\quad + \frac{1}{2}\frac{m_{N+1}^2}{M_N}\left\|\,\mathbf{c}_{\mathrm{f}(N+1)}^{N+1}\,\right\|^2 \\ &= \sum_{i=1}^{N}\frac{1}{2}m_i\left\|\,\mathbf{c}_{\mathrm{f}i}^{N+1}\,\right\|^2 - \frac{1}{2}\frac{m_{N+1}^2}{M_N}\left\|\,\mathbf{c}_{\mathrm{f}(N+1)}^{N+1}\,\right\|^2 \\ &\quad + \frac{1}{2}m_{N+1}\left\|\,\mathbf{c}_{\mathrm{f}(N+1)}^{N+1}\,\right\|^2 + \frac{1}{2}\frac{m_{N+1}^2}{M_N}\left\|\,\mathbf{c}_{\mathrm{f}(N+1)}^{N+1}\,\right\|^2 \\ &= \sum_{i=1}^{N+1}\frac{1}{2}m_i\left\|\,\mathbf{c}_{\mathrm{f}i}^{N+1}\,\right\|^2 \\ &= V_I \,. \end{aligned} \tag{2.101}$$

Notice that we used the fact $\sum_{i=1}^{N} m_i\mathbf{c}_{\mathrm{f}i}^{N+1} = -m_{N+1}\mathbf{c}_{\mathrm{f}(N+1)}^{N+1}$. By induction the proposition is proved. ■

This proof can be easily modified as a proof to equation (2.7). Hence it must have been known by Jacobi.

The topology of Kendall shape space has been partially classified in [16]. Some interesting special cases are listed as follows:

- Points on a line: $\Sigma_1^N = S^{N-2}(1)$ a unit sphere.
- Points on a plane: $\Sigma_2^N = CP^{N-2}(4)$ a complex projective space where 4 is curvature parameter. Specifically, $\Sigma_2^3 = S^2(\frac{1}{2})$.
- Higher dimension: $\Sigma_m^{m+1} \approx S^{m(m+1)/2-1}$ where $\approx$ means homeomorphism. This is a theorem proved by Casson.

On Kendall pre-shape space, for $m \geq 2$, we define a metric

$$d(X,Y) = 2\text{arcsin}(\frac{1}{2} \parallel X - Y \parallel) = \arccos(tr(XY^T)) \tag{2.102}$$

where $X, Y \in S_m^N$. It is not difficult to see that d is the great-circle metric on the unit sphere S_m^N, topologically equivalent to the *chordal metric* inherited from $R^{m(N-1)}$. Then on Kendall shape space Σ_m^N, we can define a metric δ which is the quotient metric of d.

$$\delta(\pi(X), \pi(Y)) = \min_{T \in SO(m)} d(X, TY) = \arccos(\max_{T \in SO(m)} tr(TXY^T)) \tag{2.103}$$

where π is the canonical projection.

2.4 Examples

2.4.1 A conserved quantity of sequential pursuit

In this section we apply shape theory to analyze the problem of sequential pursuit. The simplest such problem is of the following form.

Let (q_1, q_2, q_3) denote the positions of three particles in $\mathcal{R}^3$. Suppose they satisfy the equations

$$\begin{aligned} \dot{q}_1 &= q_2 - q_1 \\ \dot{q}_2 &= q_3 - q_2 \\ \dot{q}_3 &= q_1 - q_3 \ . \end{aligned} \tag{2.104}$$

We want to show that from any initial configuration, (q_1, q_2, q_3) will converge to the centroid of the initial shape. This result is known to Brocard in 1877 [4]. It was studied later in [3] and more recently in [21].

The proof for convergence is straight forward after we express the system equations using the Jacobi shape coordinates. It is obvious that

$$\dot{q}_c = \frac{1}{3}(\dot{q}_1 + \dot{q}_2 + \dot{q}_3) = 0 \ . \tag{2.105}$$

Then according to the definition of the Jacobi vectors in equation (2.8)

$$\begin{aligned} \dot{\rho}_{\mathrm{f}1} &= \frac{1}{\sqrt{2}}(\dot{q}_2 - \dot{q}_1) = \frac{1}{\sqrt{2}}(q_3 - 2q_2 + q_1) \\ \dot{\rho}_{\mathrm{f}2} &= \sqrt{\frac{2}{3}}\left(\dot{q}_3 - \frac{\dot{q}_2 + \dot{q}_1}{2}\right) = \left(\sqrt{\frac{3}{2}}\right)(q_1 - q_3) \ . \end{aligned} \tag{2.106}$$

According to the inverse transform presented in (2.15), we have

$$q_1 = q_c - \frac{\sqrt{2}}{2}\rho_{\mathrm{f}1} - \frac{1}{\sqrt{6}}\rho_{\mathrm{f}2}$$

$$
\begin{aligned}
q_2 &= q_c + \frac{\sqrt{2}}{2}\rho_{\mathrm{f}1} - \frac{1}{\sqrt{6}}\rho_{\mathrm{f}2} \\
q_3 &= q_c + \frac{\sqrt{2}}{\sqrt{3}}\rho_{\mathrm{f}2} \, .
\end{aligned} \tag{2.107}
$$

Then, the equations in Jacobi coordinates are

$$
\begin{aligned}
\dot{\rho}_{\mathrm{f}1} &= -\frac{3}{2}\rho_{\mathrm{f}1} + \frac{\sqrt{3}}{2}\rho_{\mathrm{f}2} \\
\dot{\rho}_{\mathrm{f}2} &= -\frac{\sqrt{3}}{2}\rho_{\mathrm{f}1} - \frac{3}{2}\rho_{\mathrm{f}2} \, .
\end{aligned} \tag{2.108}
$$

One can see that the system is a linear system with eigenvalues equal to $-\frac{3}{2} \pm \mathbf{i}\frac{\sqrt{3}}{2}$. Therefore, as $t \to 0$, $\rho_{\mathrm{f}1}, \rho_{\mathrm{f}2} \to 0$. Since q_c is fixed, the three particles will converge to q_c. The eigenvalues are invariant under the action of the democracy group. Therefore the convergence does not depend on the choice for Jacobi coordinates.

Next, by using shape theory we are to analysis the geometric property of the convergence for triangular shapes. We want to understand how the shape of the "virtual" body formed by the three particles evolves in time and how fast the whole body is rotating around the centroid. It seems that these questions have not yet been answered in literature.

As shown in figure 2.2, we establish a gauge convention as discussed in section 2.2. The origin are chosen to be at the center of mass. The x-axis is aligned with the line joining particles 1 and 2 pointing towards particle 2. We choose the y-axis to be perpendicular to the x-axis in the plane formed by the three particles such that the $x-y$ coordinate system is a right handed system. We choose the z-axis to form a right handed 3-D coordinate system

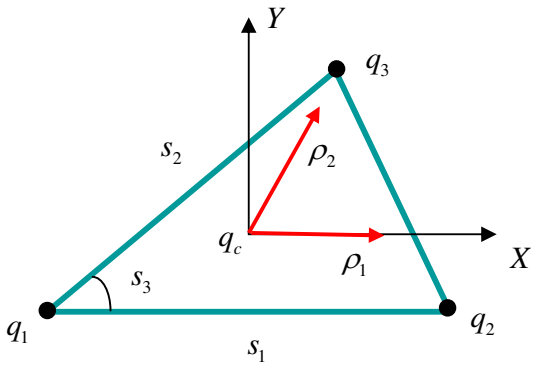

Figure 2.2: *Gauge convention for a triangular formation. The shape variable s_1 is the distance between particle 1 and 2. Shape variable s_2 measures distance between particle 1 and 3. Shape variable s_3 is the angle between $q_1\vec{q}_3$ and $q_1\vec{q}_2$.*

with x and y axis.

Three shape variables are chosen. The shape variable s_1 is the distance between particles 1 and 2. Shape variable s_2 measures distance between particles 1 and 3. Shape variable s_3 is the angle shown in figure 2.2. These three variables are enough to describe a triangle because according to previous discussions, the dimension of the Jacobi shape space formed by three particles is 3.

Under the chosen gauge convention, the coordinates of particle 2 are $(s_1, 0, 0)^T$. Particle 3 has the coordinates $(s_2\cos(s_3), s_2\sin(s_3), 0)^T$. Thus, the Jacobi vectors in this body frame are

$$\rho_1 \quad = \quad \sqrt{\mu_1}(s_1, 0, 0)^T$$

$$\rho_2 \;=\; \sqrt{\mu_2}(s_2\cos(s_3) - \frac{m_2}{m_1+m_2}s_1, s_2\sin(s_3), 0)^T \;. \qquad (2.109)$$

The following calculations can be carried out:

$$\begin{aligned}
\| \rho_1 \|^2 &= \mu_1 s_1^2 \\
\| \rho_2 \|^2 &= \mu_2((s_2\cos(s_3) - \frac{m_2}{m_1+m_2}s_1)^2 + s_2^2\sin^2(s_3)) \\
\rho_1\rho_1^T &= \mu_1 \begin{bmatrix} s_1^2 & 0 & 0 \\ 0 & 0 & 0 \\ 0 & 0 & 0 \end{bmatrix} \\
\rho_2\rho_2^T &= \\
\mu_2 \begin{bmatrix} (s_2\cos(s_3) - \frac{m_2}{m_1+m_2}s_1)^2 & s_2\sin(s_3)(s_2\cos(s_3) - \frac{m_2}{m_1+m_2}s_1) & 0 \\ s_2\sin(s_3)(s_2\cos(s_3) - \frac{m_2}{m_1+m_2}s_1) & s_2^2\sin^2(s_3) & 0 \\ 0 & 0 & 0 \end{bmatrix} &.
\end{aligned}$$

Thus, we can calculate the locked inertia tensor I. Since

$$I = \| \rho_1 \|^2 \mathbf{e} - \rho_1\rho_1^T + \| \rho_2 \|^2 \mathbf{e} - \rho_2\rho_2^T \;, \qquad (2.110)$$

we have

$$\begin{aligned}
I_{11} &= \mu_2 s_2^2\sin^2(s_3) \\
I_{12} &= I_{21} = -\mu_2 s_2\sin(s_3)(s_2\cos(s_3) - \frac{m_2}{m_1+m_2}s_1) \\
I_{22} &= \mu_1 s_1^2 + \mu_2(s_2\cos(s_3) - \frac{m_2}{m_1+m_2}s_1)^2 \\
I_{33} &= \mu_1 s_1^2 + \mu_2((s_2\cos(s_3) - \frac{m_2}{m_1+m_2}s_1)^2 + s_2^2\sin^2(s_3)) \\
I_{23} &= I_{32} = I_{13} = I_{31} = 0 \;. \qquad (2.111)
\end{aligned}$$

In order to calculate the gauge potential A, the following derivatives are calculated:

$$\begin{aligned}
\frac{\partial \rho_1}{\partial s_1} &= \sqrt{\mu_1}[1,0,0]^T \\
\frac{\partial \rho_1}{\partial s_2} &= [0,0,0]^T \\
\frac{\partial \rho_1}{\partial s_3} &= [0,0,0]^T \\
\frac{\partial \rho_2}{\partial s_1} &= \sqrt{\mu_2}[-\frac{m_2}{m_1+m_2},0,0]^T \\
\frac{\partial \rho_2}{\partial s_2} &= \sqrt{\mu_2}[\cos(s_3),\sin(s_3),0]^T \\
\frac{\partial \rho_2}{\partial s_3} &= \sqrt{\mu_2}[-s_2\sin(s_3),s_2\cos(s_3),0]^T \ . \qquad (2.112)
\end{aligned}$$

Since

$$A_j = I^{-1}(\rho_1 \times \frac{\partial \rho_1}{\partial s_j} + \rho_2 \times \frac{\partial \rho_2}{\partial s_j}) \qquad (2.113)$$

for $j = 1, 2, 3$, the results are:

$$\begin{aligned}
A_1 &= \mu_2 \frac{1}{I_{33}}[0,0,\frac{m_2}{m_1+m_2}s_2\sin(s_3)]^T \\
A_2 &= \mu_2 \frac{1}{I_{33}}[0,0,-\frac{m_2}{m_1+m_2}s_1\sin(s_3)]^T \\
A_3 &= \mu_2 \frac{1}{I_{33}}[0,0,s_2^2-\frac{m_2}{m_1+m_2}s_1 s_2\cos(s_3)]^T \ . \qquad (2.114)
\end{aligned}$$

We want to find Ω, the rotation speed of the body and $\dot{s}_i$ for $i = 1, 2, 3$. There are altogether six unknowns. These unknowns can be solved from the six equations given by

$$\dot{\rho}_j = \Omega \times \rho_j + \sum_{i=1}^{3} \frac{\partial \rho_j}{\partial s_i}\dot{s}_i \qquad (2.115)$$

for $j = 1, 2$. In our context, we assume that $m_1 = m_2 = m_3 = 1$. Therefore, when $j = 1$, according to equation (2.108) and equation (2.115), the first three equations are

$$\begin{aligned}\Omega \times \begin{bmatrix} \frac{1}{\sqrt{2}} s_1 \\ 0 \\ 0 \end{bmatrix} + \dot{s}_1 \begin{bmatrix} \frac{1}{\sqrt{2}} \\ 0 \\ 0 \end{bmatrix} &= -\frac{3}{2}\rho_1 + \frac{\sqrt{3}}{2}\rho_2 \\ = -\frac{3}{2} \begin{bmatrix} \frac{1}{\sqrt{2}} s_1 \\ 0 \\ 0 \end{bmatrix} &+ \frac{\sqrt{3}}{2} \cdot \sqrt{\frac{2}{3}} \begin{bmatrix} s_2 \cos(s_3) - \frac{1}{2} s_1 \\ s_2 \sin(s_3) \\ 0 \end{bmatrix} . \end{aligned} \tag{2.116}$$

We let $\Omega = [\Omega_x, \Omega_y, \Omega_z]^T$. The above equations are simplified to

$$\begin{bmatrix} 0 \\ \frac{1}{\sqrt{2}} \Omega_z s_1 \\ -\frac{1}{\sqrt{2}} \Omega_y s_1 \end{bmatrix} + \begin{bmatrix} \frac{1}{\sqrt{2}} \dot{s}_1 \\ 0 \\ 0 \end{bmatrix} = \begin{bmatrix} -\frac{3}{4}\sqrt{2} s_1 + \frac{1}{\sqrt{2}}(s_2 \cos(s_3) - \frac{1}{2} s_1) \\ \frac{1}{\sqrt{2}} s_2 \sin(s_3) \\ 0 \end{bmatrix} . \tag{2.117}$$

We can then get the following solutions

$$\begin{aligned} \dot{s}_1 &= -2s_1 + s_2 \cos(s_3) \\ \Omega_y &= 0 \\ \Omega_z &= \frac{s_2}{s_1} \sin(s_3) . \end{aligned} \tag{2.118}$$

On the next step, we can write the remaining three equations as

$$\Omega \times \rho_2 + \dot{s}_1 \begin{bmatrix} -\frac{1}{\sqrt{6}} \\ 0 \\ 0 \end{bmatrix} + \dot{s}_2 \cdot \sqrt{\frac{2}{3}} \begin{bmatrix} \cos(s_3) \\ \sin(s_3) \\ 0 \end{bmatrix} + \dot{s}_3 \cdot \sqrt{\frac{2}{3}} \begin{bmatrix} -s_2 \sin(s_3) \\ s_2 \cos(s_3) \\ 0 \end{bmatrix}$$

$$= -\frac{\sqrt{3}}{2}\rho_1 - \frac{3}{2}\rho_2 = \begin{bmatrix} -\frac{3}{2}\sqrt{\frac{2}{3}}s_2\cos(s_3) \\ -\frac{3}{2}\sqrt{\frac{2}{3}}s_2\sin(s_3) \\ 0 \end{bmatrix} . \tag{2.119}$$

One can verify that

$$\Omega \times \rho_2 = \begin{bmatrix} -\sqrt{\frac{2}{3}} \cdot \frac{s_2^2\sin^2(s_3)}{s_1} \\ \sqrt{\frac{2}{3}} \cdot \frac{s_2}{s_1}\sin(s_3)(s_2\cos(s_3) - \frac{1}{2}s_1) \\ \sqrt{\frac{2}{3}}s_2\sin(s_3)\Omega_x \end{bmatrix} . \tag{2.120}$$

Then we can observe that

$$\Omega_x = 0 . \tag{2.121}$$

The remaining two equations are simplified to

$$\begin{aligned} \dot{s}_2\cos(s_3) - \dot{s}_3 s_2\sin(s_3) &= -s_2\cos(s_3) - s_1 + \frac{s_2^2\sin^2(s_3)}{s_1} \\ \dot{s}_2\sin(s_3) + \dot{s}_3 s_2\cos(s_3) &= -s_2\sin(s_3) - \frac{s_2^2\sin(s_3)\cos(s_3)}{s_1} . \end{aligned} \tag{2.122}$$

We find the solutions to be

$$\begin{aligned} \dot{s}_2 &= -s_2 - s_1\cos(s_3) \\ \dot{s}_3 &= (\frac{s_1}{s_2} - \frac{s_2}{s_1})\sin(s_3) \end{aligned} \tag{2.123}$$

We now let

$$\begin{aligned} S_1 &= s_1^2 + s_2^2 + (s_1^2 + s_2^2 - 2s_1 s_2\cos(s_3)) \\ S_2 &= \frac{1}{2}s_1 s_2\sin(s_3) . \end{aligned} \tag{2.124}$$

We see S_1 is the square sum of the length of the three edges. If we denote the size of the formation as Z in Kendall sense and let V_I be the virial of

the three particles, then $\sqrt{S_1} = \sqrt{3}\ Z = \sqrt{6V_I}$. S_2 measures the area of the triangle. Then

$$\begin{aligned}
\dot{S}_1 &= 2(2s_1\dot{s}_1 + 2s_2\dot{s}_2 - \dot{s}_1 s_2\cos(s_3) - s_1\dot{s}_2\cos(s_3) + s_1 s_2 sin(s_3)\dot{s}_3) \\
&= -6(s_1^2 + s_2^2 - s_1 s_2\cos(s_3)) \\
&= -3S_1 \qquad (2.125)
\end{aligned}$$

and

$$\begin{aligned}
\dot{S}_2 &= \frac{1}{2}(\dot{s}_1 s_2\sin(s_3) + s_1\dot{s}_2\sin(s_3) + s_1 s_2\cos(s_3)\dot{s}_3) \\
&= -\frac{3}{2}s_1 s_2\sin(s_3) \\
&= -3S_2\ . \qquad (2.126)
\end{aligned}$$

It is obvious that $S_1 \to 0$ and $S_2 \to 0$ as $t \to \infty$.

We now prove that the gauge covariant angular speed $\Upsilon = \Omega + \sum_{i=1}^{3} A_i\dot{s}_i$ is a constant. From equations (2.114) and the fact that $\Omega_x = \Omega_y = 0$, we conclude that $\Upsilon_x = \Upsilon_y = 0$. Then

$$\begin{aligned}
\Upsilon_z &= \Omega_z + A_{1z}\dot{s}_1 + A_{2z}\dot{s}_2 + A_{3z}\dot{s}_3 \\
&= \frac{s_2}{s_1}\sin(s_3) + \frac{2}{3I_{33}}\left[\frac{1}{2}s_2\sin(s_3)(-2s_1 + s_2\cos(s_3))\right. \\
&\quad \left. + \frac{1}{2}s_1\sin(s_3)(s_2 + s_1\cos(s_3)) + \left(s_2^2 - \frac{1}{2}s_1 s_2\cos(s_3)\right)\left(\frac{s_1}{s_2} - \frac{s_2}{s_1}\right)\sin(s_3)\right] \\
&= \frac{s_2}{s_1}\sin(s_3) + \frac{2}{3I_{33}}\left(\frac{s_2}{s_1}\sin(s_3)\right)\left(s_1 s_2\cos(s_3) + \frac{1}{2}s_1^2 - s_2^2\right) \\
&= \frac{s_1 s_2\sin(s_3)}{I_{33}} \\
&= 6\,\frac{S_2}{S_1} \\
&= 2\frac{S_2}{Z^2} = \frac{S_2}{V_I}\ . \qquad (2.127)
\end{aligned}$$

This means that the rotational speed is the proportion between the area and the virial of the formation. We can calculate the derivative of Υ_z as

$$\begin{aligned} \dot{\Upsilon}_z &= \frac{S_1\dot{S}_2 - S_2\dot{S}_1}{S_1^2} \\ &= 3\frac{-S_1S_2 + S_2S_1}{S_1^2} \\ &= 0\ . \end{aligned} \tag{2.128}$$

This proves that Υ is a constant.

2.4.2 Line formations: controlling shape and size separately

In this subsection we try to control formations of N mobile robots moving along a predefined straight line. This line can be either the configuration space of the robots like a trail for trains or a holonomic constraint maintained by steering control in the situation of keeping vehicles in the same lane on a highway. In either of the two cases, the position of each robot can be described as a scalar. A formation of such robots is represented by the relative distance between adjacent robots. The relative distance is often of great importance and need to be adjusted according to safety standards and communication requirements. For example, consider the case where one vehicle is following another on a highway, in the presence of constant communication delays, the distance between these two vehicles is increased when the traveling speed is increased because if the front one has to perform an

emergent stop, the back one need a longer braking distance to avoid hitting the front one. On the other hand, the distance between the two vehicles should not be too big to maintain the wireless communication link between them. The safe distance will also depend on whether the back vehicle is a truck or a compact size car. Thus, there is an optimal distance. All the optimal distances hence determine an optimal formation which will satisfy all the safety and communication requirements. Here, we are not going to compute the optimal formation. In stead, we assume that the optimal formation is known and we want to achieve it from an arbitrary initial formation and maintain it after wards.

Suppose the formation contains N vehicles. The position q_c of the center of mass can be calculated according to equation (2.3). We can then calculate the Jacobi vectors $\rho_{\mathrm{f}i}$ by using equation (2.8). Since the configuration space for each vehicle is $\mathcal{R}$. The Jacobi vectors are now scalars. There are $N-1$ Jacobi vectors. Thus the pre-shape space F is $\mathcal{R}^{N-1}$. Because the symmetry group is trivial, the base space B coincide with the pre-shape space F, i.e. $\rho_i = \rho_{\mathrm{f}i}$. This is to say that we do not have to worry about connections and gauge potentials.

Let S_N denote the size of the formation calculated according to equation (2.88). We define $s_i = \rho_i/S_N$, $(i = 1, 2, ...N-2)$ as the pure shape variables. It is obvious that the Kendall shape space B_K is a $(N-2)$ sphere embedded in $B = \mathcal{R}^{N-1}$.

Suppose the vehicles obey the simple equations

$$\dot{q}_i = \frac{u_i}{m_i} \tag{2.129}$$

where u_i are speed controls. The system equations for (q_c, ρ_i) can be derived as follows

$$\begin{aligned} \dot{q}_c &= \frac{1}{M}\sum_{i=1}^{N} u_i \\ \dot{\rho}_i &= \sqrt{\mu_i}(u_{(i+1)} - \frac{\sum_{k=1}^{i} u_k}{\sum_{k=1}^{i} m_k}) \end{aligned} \tag{2.130}$$

where $(i = 1, 2, ..., N-1)$. Then the system equations for the size and pure shape variables are

$$\dot{S}_N = \frac{\sum_{i=1}^{N-1} \rho_i \dot{\rho}_i}{S_N} \tag{2.131}$$

$$\dot{s}_i = \frac{\sum_{k\neq i}^{N-1} \rho_k(\rho_k\dot{\rho}_i - \rho_i\dot{\rho}_k)}{S_N^3} \tag{2.132}$$

where $(i = 1, 2, ..., N-2)$.

Now we want to find a control law s.t. s_i will be kept constant when we change the size of the formation to a non zero value S^0. For this purpose we let $\dot{s}_i = 0$. Hence one solution is

$$\frac{\dot{\rho}_k}{\rho_k} = \frac{\dot{\rho}_i}{\rho_i} \tag{2.133}$$

for any pair of k and i. If this is true, the derivative of the size variable is

$$\dot{S}_N = \frac{\sum_{k=1}^{N} \rho_k^2}{S_N}\frac{\dot{\rho}_1}{\rho_1} = S_N\frac{\dot{\rho}_1}{\rho_1}\ . \tag{2.134}$$

A very simple choice of control is to let

$$\frac{\dot{\rho}_i}{\rho_i} = -k\frac{(S_N - S^0)}{S_N} \tag{2.135}$$

for $i = 1, 2, ...N-1$. Then we can drive S_N to S^0. The controls u_i can be calculated from (2.130) and (2.133). Notice that we have N controls but only $N-1$ equations. We can add another equation to either let u_1 or $\dot{q}_c$ be some predefined speed.

On the other hand, we can find a control law to keep the size constant while making shape changes. Then from equation (2.131) we have,

$$\sum_{i=1}^{N-1} \rho_i \dot{\rho}_i = 0 \ . \tag{2.136}$$

Then we can represent $\dot{\rho}_{(N-1)}$ in terms of other $\dot{\rho}_i$ as

$$\dot{\rho}_{(N-1)} = -\sum_{i=1}^{N-2} \frac{\rho_i}{\rho_{(N-1)}} \dot{\rho}_i \ . \tag{2.137}$$

The system equations (2.132) are then simplified as

$$\dot{s}_i = \frac{\dot{\rho}_i}{S_N} \ . \tag{2.138}$$

Suppose we want the controlled pure shape variables to trace geodesics on the $(N-2)$ sphere. The reason is that following the geodesics is the fastest way to change shape with a given control magnitude. Let ρ^0 and ρ denote two points on the $(N-2)$ sphere. Suppose $\rho^0 \neq \rho$, the shortest path between ρ^0 and ρ is the intersection of the plane spanned by vectors ρ^0 and ρ and the sphere S^{N-1}. The tangent vector $\dot{\rho}$ of this curve at point ρ should lie in the tangent space of S^{N-1}, Hence

$$\rho \cdot \dot{\rho} = 0 \ . \tag{2.139}$$

On the other hand, this tangent vector $\dot{\rho}$ must also lie in the plane spanned by ρ^0 and ρ i.e.

$$\dot{\rho} = l\rho^0 + k\rho \ . \tag{2.140}$$

Combining the above two equations we can solve for k and l as

$$k = -l\frac{(\rho \cdot \rho^0)}{(\rho \cdot \rho)} \ . \tag{2.141}$$

Hence, the controls can be solved from

$$\dot{\rho} = l(\rho^0 - \rho\frac{(\rho \cdot \rho^0)}{(\rho \cdot \rho)}) \tag{2.142}$$

and equation (2.130) where $l > 0$ is free to choose. In fact, l determines how fast we want to go along the geodesic.

Proposition 2.4.1 *If we apply the control law such that (2.142) is satisfied, then $\rho \to \rho^0$ asymptotically if the starting position $\rho \neq -\rho^0$.*

Proof Let

$$V_L = \frac{1}{2} \left\| \rho - \rho^0 \right\|^2 \ . \tag{2.143}$$

Then

$$\begin{aligned} \dot{V}_L &= (\rho - \rho^0) \cdot \dot{\rho} \\ &= l(\rho - \rho^0) \cdot (\rho^0 - \rho\frac{(\rho \cdot \rho^0)}{(\rho \cdot \rho)}) \\ &= l(-\left\| \rho^0 \right\|^2 + \frac{(\rho \cdot \rho^0)^2}{\left\| \rho \right\|^2}) \\ &= l(\frac{-\left\| \rho^0 \right\|^2 \left\| \rho \right\|^2 + (\rho \cdot \rho^0)^2}{\left\| \rho \right\|^2}) \ . \end{aligned} \tag{2.144}$$

According to Cauchy-Schwartz inequality we have

$$\left\| \rho^0 \right\|^2 \| \rho \|^2 \geq (\rho \cdot \rho^0)^2 \, . \tag{2.145}$$

Thus $\dot{V}_L \leq 0$ where the equality is true if and only if ρ and ρ^0 is aligned. In our case, since $\| \rho \| = \| \rho^0 \|$, the only chances are $\rho = \rho_0$ or $\rho = -\rho_0$. But the configuration for $\rho = -\rho^0$ is unstable because V_L achieve its maximum value there. Hence $\rho \to \rho^0$ is proved. ■

Chapter 3

Feedback Control of Small Formations

Robots in a formation can be viewed as particles subjected to control forces. Hence a robot formation can be modeled as a controlled Lagrangian system of particles. What are the interactions, which allow particles (robots) to form a stable formation, is the problem we want to investigate.

A formation can be studied as a deformable body. Its shape is invariant under translation and rotation, and is also independent of the coordinate system in which we choose to describe it. On the Jacobi shape space, the global displacements, i.e. translation and rotation for the entire body, are not present. As mentioned in the previous chapter, shape variables are rigid motion invariants such as inter-particle distances, areas or angles made by lines connecting the particles.

In a fixed inertial frame, if the position of each robot can be determined by using localization technology such as GPS, then Jacobi vectors are convenient to describe the shape and orientation of the whole formation. A simple controller is proposed in section 3.2. Under such controller, we use estimates of Jacobi vectors as feedback to stabilize shape and orientation of a formation.

When no positioning system is available, without knowing robot coordinates in a fixed coordinate system, only shape variables, which are measured using on-board sensors of robots, can be used to control the formation. In this case, a gauge convention will be established which provides a gauge frame for any given shape of the formation.

In a chosen gauge frame, we compute the controlled dynamics of the whole formation using the Lagrange-D'Alembert principle. In the resulting equations, control forces of all robots are combined and are represented as controls for the shape, the position and the orientation respectively. We are now able to design formation control by starting from designing the combined forces. The goal is to compute control force on each robot to implement those combined forces.

Under the assumption that each robot is able to measure the shape and rotation for the whole formation, we allow no communication between the robots. If all the robots agree on a unified way to establish a gauge frame for the whole formation, a simple control law proposed in section 3.3 can be employed. In section 3.5, we allow each robot the freedom to attach its own choice of gauge frame to observe the whole formation. This requirement

often arises when a certain coordinate system is more convenient than others for getting more accurate estimates from sensory data. Geometric properties associated with the Jacobi shape space allow us to utilize gauge invariant and gauge covariant objects to design a cooperative control law to satisfy this requirement.

3.1 Lagrangian dynamics of formations

Suppose a manifold M is the configuration space of a mechanical system. Let TM be the tangent bundle of the configuration space. If the system is Lagrangian, then there exists a function L on the tangent bundle TM, such that the motion of the mechanical system is described by a set of equations obtained by applying the Lagrange-D'Alembert principle. We call the function a Lagrangian function. Let (q, v) denote a point on TM where $q \in M$ and $v \in T_qM$. Then the Lagrange-D'Alembert principle asserts that

$$\frac{d}{dt} D_v L - D_q L = \mathbf{f} \tag{3.1}$$

where $\mathbf{f}$ represents external force.

By defining Jacobi vectors and then Jacobi shape variables we have gone through a sequence of changes of coordinates on the configuration space Q for the entire formation. In the first step, the transform is a diffeomorphism between Q and R^{3N} mapping configuration variables q_i to the position of the center of mass q_c and the Jacobi vectors $\rho_{\mathrm{f}i}$. In the second step, the transform

is a local diffeomorphism between $R^3 \times F$ and $R^3 \times \mathbf{G} \times B$ mapping $(q_c, \rho_{\mathrm{f}i})$ where $i = 1, 2, ..., (N-1)$ to (q_c, g, s_j) where $j = 1, 2, ...(3N-6)$ s.t.

$$\rho_{\mathrm{f}i} = g\rho_i(s_1, s_2, ...s_{3N-6}) \ . \tag{3.2}$$

The Lagrangian on TQ is given by $L(q, \dot{q}) = K^{\mathrm{tot}}(\dot{q}) - V(q)$. Before the coordinate transformation, K^{tot} has the form

$$K^{\mathrm{tot}}(\dot{q}) = \frac{1}{2} \sum_{i=1}^{N} m_i \parallel \dot{q}_i \parallel^2 \ . \tag{3.3}$$

The Lagrange equations for the system are just the Newton's equations:

$$m_i \ddot{q}_i = \mathbf{f}_i - \frac{\partial V}{\partial q_i} \tag{3.4}$$

for $i = 1, 2, ..., N$ where $\mathbf{f}_i$ are control forces.

Apply the Lagrange-D'Alembert principle to Jacobi pre-shape space. The Lagrange equations for the Lagrangian $L(q_c, \rho_{\mathrm{f}}, \dot{q}_c, \dot{\rho}_{\mathrm{f}})$ are

$$\begin{aligned} \frac{d}{dt}\frac{\partial L}{\partial \dot{q}_c} - \frac{\partial L}{\partial q_c} &= u_c \\ \frac{d}{dt}\frac{\partial L}{\partial \dot{\rho}_{\mathrm{f}}} - \frac{\partial L}{\partial \rho_{\mathrm{f}}} &= u_{\mathrm{f}} \ , \end{aligned} \tag{3.5}$$

where u_c is the equivalent force on the center of mass and u_{f} represent the equivalent control on Jacobi vectors. Now the Lagrangian function becomes

$$L = \frac{1}{2} M \parallel \dot{q}_c \parallel^2 + \frac{1}{2} \sum_{i=1}^{N-1} \parallel \dot{\rho}_{\mathrm{f}i} \parallel^2 - V(q_c, \rho_{\mathrm{f}1}, ..., \rho_{\mathrm{f}(N-1)}) \ . \tag{3.6}$$

Hence, we can calculate the partial derivatives in equation (3.5) to obtain the system equations in Jacobi coordinates

$$M\ddot{q}_c = -\frac{\partial V}{\partial q_c} + u_c$$

$$\ddot{\rho}_{\mathrm{f}i} \;=\; -\frac{\partial V}{\partial \rho_{\mathrm{f}i}} + u_{\mathrm{f}i} \tag{3.7}$$

for $i = 1, 2, ...N-1$. We notice that the control forces $\mathbf{f}_i$ are combined into controls u_c and $u_{\mathrm{f}i}$.

We now go one step further. Let F denote the Jacobi Pre-shape space coordinated by (g, s) where $g \in SO(3)$ and $s = (s_1, s_2, \ldots, s_{3N-6}) \in B$ where B is the Jacobi shape manifold. A point in the tangent bundle TF can be represented by $(g, s, g\widehat{\Omega}, v)$ where $\widehat{\Omega} \in so(3)$ and v represents $\dot{s}$.

Let

$$A = [A_1, A_2, ..., A_{3N-6}] \tag{3.8}$$

Then we can rewrite the kinetic energy in block diagonalized form as

$$K^{\mathrm{tot}} = \frac{1}{2} M \parallel \dot{q}_c \parallel^2 + \frac{1}{2}(\Omega + A\dot{s})^T I(\Omega + A\dot{s}) + \frac{1}{2}\dot{s}^T G \dot{s} \tag{3.9}$$

where

$$G_{jk} = -A_j^T I A_k + \sum_{i=1}^{N-1} \frac{\partial \rho_i}{\partial s_j} \frac{\partial \rho_i}{\partial s_k} \tag{3.10}$$

According to the arguments in chapter 2 regarding the decomposition of a tangent vector into horizontal and vertical components, given a tangent vector $(\Omega, \dot{s})$, $(\Omega + A\dot{s})$ is its vertical component. Equation (3.9) tells us that the Riemannian metric which gives rise to K^{tot} induces a Riemannian metric G on the horizontal subspace and a Riemannian metric I on the Lie algebra.

Suppose V is translation invariant. Omitting the center of mass, we are given a Lagrangian function

$$L = \frac{1}{2}(\Omega + A\dot{s})^T I(\Omega + A\dot{s}) + \frac{1}{2}\dot{s}^T G \dot{s} - V(g, s) \tag{3.11}$$

In order to apply the Lagrange-D'Alembert principle we shall calculate the derivatives

$$dL = (D_g L, D_s L, D_{g\widehat{\Omega}} L, D_v L). \tag{3.12}$$

Here dL represents a one form on the tangent bundle TF. This one form will be evaluated at a tangent vector to TF. Let Y be such a tangent vector, then $Y \in TTF$. We shall first compute Y.

The tangent vector Y contains four components. The first two components come from taking Frechet derivatives of the configuration variables (g, s). We use $(g\widehat{\Omega}_1, v_1)$ to represent these two components. The last two components come from taking Frechet derivatives of the velocity variables $(g\widehat{\Omega}, v)$ as follows

$$\frac{d}{d\epsilon} g \, \exp(\epsilon\widehat{\Omega}_1)(\widehat{\Omega} + \epsilon\widehat{w})|_{\epsilon=0} = g(\widehat{\Omega}_1\widehat{\Omega} + \widehat{w}) \, , \tag{3.13}$$

and

$$\frac{d}{d\epsilon}(v + \epsilon z)|_{\epsilon=0} = z \, . \tag{3.14}$$

Therefore

$$Y = (g\widehat{\Omega}_1, v_1, g(\widehat{\Omega}_1\widehat{\Omega} + \widehat{w}), z) \, . \tag{3.15}$$

Next, we want to solve for dL from the equation

$$dL[Y] = \frac{d}{d\epsilon} L|_{\epsilon=0} \, . \tag{3.16}$$

We compute the left hand side of this equation as

$$dL[Y] \;\; = \;\; \langle D_g L, g\widehat{\Omega}_1 \rangle_M + \langle D_s L, v_1 \rangle$$

$$+\langle D_{g\widehat{\Omega}}L, g(\widehat{\Omega}_1\widehat{\Omega}+\widehat{w})\rangle_M + \langle D_v L, z\rangle \ . \tag{3.17}$$

Here the operation $\langle\ ,\ \rangle_M$ is the inner product between matrices defined as

$$\langle A, B\rangle_M = \frac{1}{2}tr(A^T B) \ . \tag{3.18}$$

We then compute the right hand side of equation (3.16) as

$$\begin{aligned}
\frac{d}{d\epsilon}L|_{\epsilon=0} &= \frac{d}{d\epsilon}|_{\epsilon=0}(\frac{1}{2}(\Omega+\epsilon w + A(s+\epsilon v_1)(\dot{s}+\epsilon z))^T I(s+\epsilon v_1)(\Omega+\epsilon w \\
&\quad +A(s+\epsilon v_1)(\dot{s}+\epsilon z)) + \frac{1}{2}(\dot{s}+\epsilon z)^T G(s+\epsilon v_1)(\dot{s}+\epsilon z) \\
&\quad -V(g\ \exp(\epsilon\Omega_1), s+\epsilon v_1)) \\
&= w^T I(\Omega+A\dot{s}) + \left(\frac{\partial A}{\partial s}[v_1,\dot{s}]\right)^T I(\Omega+A\dot{s}) \\
&\quad +\frac{1}{2}\frac{\partial I}{\partial s}[v_1, \Omega+A\dot{s}, \Omega+A\dot{s}] \\
&\quad +(Az)^T I(\Omega+A\dot{s}) + \frac{1}{2}\frac{\partial G}{\partial s}[v_1,\dot{s},\dot{s}] + z^T G\dot{s} \\
&\quad +\frac{\partial V}{\partial s}v_1 + \langle D_g V, g\widehat{\Omega}_1\rangle_M \ .
\end{aligned} \tag{3.19}$$

Comparing equation (3.17) and (3.19), we first noticed that there is only one term involving w. Therefore,

$$\langle D_{g\widehat{\Omega}}L, g\widehat{w}\rangle_M = w^T I(\Omega+A\dot{s}) \tag{3.20}$$

which implies

$$D_{g\widehat{\Omega}}L = g\widehat{(}I(\Omega+A\dot{s})\widehat{)} \ . \tag{3.21}$$

Here we use the notation $\widehat{(\ )}$ to denote the skew symmetric matrix representation of a three dimensional vector inside the bracket.

Next, there is only one term involving Ω_1 in (3.19), hence

$$\langle D_g L, g\widehat{\Omega}_1\rangle_M + \langle D_{g\widehat{\Omega}} L, g(\widehat{\Omega}_1\widehat{\Omega})\rangle_M = \langle D_g V, g\widehat{\Omega}_1\rangle_M \tag{3.22}$$

which implies that

$$D_g L = \widehat{g(I(\Omega + A\dot{s})}\,\widehat{\Omega} + D_g V \ . \tag{3.23}$$

Observing the terms involving z in (3.19), we obtain

$$\langle D_v L, z\rangle = (A\,z)^T I(\Omega + A\dot{s}) + z^T G\dot{s} \ . \tag{3.24}$$

Here, the inner product is the inner product between vectors. Therefore,

$$D_v L = A^T I(\Omega + A\dot{s}) + G\dot{s} \ . \tag{3.25}$$

Finally, we gather the terms in (3.19) that contain v_1 and obtain

$$\begin{aligned}\langle D_s L, v_1\rangle &= \left(\frac{\partial A}{\partial s}[v_1, \dot{s}]\right)^T I(\Omega + A\dot{s}) + \frac{1}{2}\frac{\partial I}{\partial s}[v_1, \Omega + A\dot{s}, \Omega + A\dot{s}] \\ &\quad + \frac{1}{2}\frac{\partial G}{\partial s}[v_1, \dot{s}, \dot{s}] + \frac{\partial V}{\partial s}v_1 \ .\end{aligned} \tag{3.26}$$

In this equation $\frac{\partial A}{\partial s}$, $\frac{\partial I}{\partial s}$ and $\frac{\partial G}{\partial s}$ are rank three tensors. We have

$$\begin{aligned}\left(\frac{\partial A}{\partial s}[v_1, \dot{s}]\right)^T I(\Omega + A\dot{s}) &= \frac{\partial A}{\partial s}[v_1, \dot{s}, I(\Omega + A\dot{s})] \\ &= (\frac{\partial A}{\partial s})^*[\dot{s}, I(\Omega + A\dot{s}), v_1]\end{aligned} \tag{3.27}$$

where $(\frac{\partial A}{\partial s})^*$ is the cyclic transpose of $\frac{\partial A}{\partial s}$. Similarly,

$$\frac{\partial I}{\partial s}[v_1, \Omega + A\dot{s}, \Omega + A\dot{s}] = (\frac{\partial I}{\partial s})^*[\Omega + A\dot{s}, \Omega + A\dot{s}, v_1] \tag{3.28}$$

and

$$\frac{\partial G}{\partial s}[v_1, \dot{s}, \dot{s}] = (\frac{\partial G}{\partial s})^*[\dot{s}, \dot{s}, v_1] \ , \tag{3.29}$$

c.f. [41] and [1]. Therefore, we can solve for $D_s L$ as

$$\begin{aligned} D_s L &= (\frac{\partial A}{\partial s})^*[\dot{s}, I(\Omega + A\dot{s})] + \frac{1}{2}(\frac{\partial I}{\partial s})^*[\Omega + A\dot{s}, \Omega + A\dot{s}] \\ &\quad + \frac{1}{2}(\frac{\partial G}{\partial s})^*[\dot{s}, \dot{s}] + \frac{\partial V}{\partial s} \ . \end{aligned} \tag{3.30}$$

The Lagrange-D'Alembert principle tells us

$$\frac{d}{dt}\begin{bmatrix} D_{g\widehat{\Omega}} L \\ D_v L \end{bmatrix} - \begin{bmatrix} D_g L \\ D_s L \end{bmatrix} = \begin{bmatrix} g u_g \\ u_s \end{bmatrix} \ . \tag{3.31}$$

Because

$$\begin{aligned} \frac{d}{dt} D_{g\widehat{\Omega}} L &= \frac{d}{dt}(g\widehat{(I(\Omega + A\dot{s}))}\,) \\ &= g\widehat{\Omega}\,\widehat{(I(\Omega + A\dot{s}))} + g\frac{d}{dt}\widehat{(I(\Omega + A\dot{s}))} \ , \end{aligned} \tag{3.32}$$

we obtain the equation for rotation as

$$g\frac{d}{dt}\widehat{(I(\Omega + A\dot{s}))} + g\widehat{\Omega}\,\widehat{(I(\Omega + A\dot{s}))} - g\widehat{(I(\Omega + A\dot{s}))}\,\widehat{\Omega} - D_g V = g u_g \tag{3.33}$$

which implies

$$\frac{d}{dt}\widehat{(I(\Omega + A\dot{s}))} + [\widehat{\Omega}, \widehat{(I(\Omega + A\dot{s}))}\,]_l = g^{-1} D_g V + u_g \tag{3.34}$$

where we use $[\ ,\ ]_l$ to denote the Lie bracket operation between two matrices. In vector form, this equation is

$$\frac{d}{dt} I(\Omega + A\dot{s}) = -\Omega \times I(\Omega + A\dot{s}) + g^{-1}\frac{\partial V}{\partial g} + u_g \ . \tag{3.35}$$

Next, we have

$$\begin{aligned}\frac{d}{dt}D_vL &= \frac{d}{dt}(A^TI(\Omega+A\dot{s})+G\dot{s}) \\ &= \frac{\partial A}{\partial s}[\dot{s},I(\Omega+A\dot{s})]+A^T\frac{d}{dt}(I(\Omega+A\dot{s}))+\frac{d}{dt}(G\dot{s})\ . \quad (3.36)\end{aligned}$$

Therefore, the equation for shape changes are

$$\begin{aligned}A^T\frac{d}{dt}(I(\Omega+A\dot{s}))+\frac{d}{dt}(G\dot{s}) &= ((\frac{\partial A}{\partial s})^*-\frac{\partial A}{\partial s})[\dot{s},I(\Omega+A\dot{s})] \\ &\quad +\frac{1}{2}(\frac{\partial I}{\partial s})^*[\Omega+A\dot{s},\Omega+A\dot{s}] \\ &\quad +\frac{1}{2}(\frac{\partial G}{\partial s})^*[\dot{s},\dot{s}]+\frac{\partial V}{\partial s}+u_s\ . \quad (3.37)\end{aligned}$$

After adding in the equation for the center of mass, the set of Lagrange equations takes the form

$$M\ddot{q}_c = u_c \quad (3.38)$$

$$\frac{d}{dt}(I(\Omega+A\dot{s})) = -\Omega\times I(\Omega+A\dot{s})-g^{-1}\frac{\partial V}{\partial g}+u_g \quad (3.39)$$

$$\begin{aligned}\frac{d}{dt}(G\dot{s}) \ + \ A^T\frac{d}{dt}(I(\Omega+A\dot{s})) &= ((\frac{\partial A}{\partial s})^*-\frac{\partial A}{\partial s})[\dot{s},I(\Omega+A\dot{s})] \\ &\quad +\frac{1}{2}[\frac{\partial I}{\partial s}]^*:(\Omega+A\dot{s},\Omega+A\dot{s}) \\ &\quad +\frac{1}{2}[\frac{\partial G}{\partial s}]^*(\dot{s},\dot{s})-\frac{\partial V}{\partial s}+u_s\ . \quad (3.40)\end{aligned}$$

The relationship between the control forces $\mathbf{f}_{\mathrm{i}}$, the control on Jacobi pre-shape space $(u_c,u_{\mathrm{f}i})$ and the control on Jacobi shape space (u_c,u_g,u_s) comes from a well known fact for controlled Lagrangian system: if the coordinate transformation $r=r(q)$ is a local diffeomorphism, which implies that

$$\dot{r}=\frac{\partial r}{\partial q}\dot{q}\ , \quad (3.41)$$

then

$$u_r = (\frac{\partial r^T}{\partial q})^{-1} u_q \tag{3.42}$$

so that $\langle u_r, \dot{r} \rangle = \langle u_q, \dot{q} \rangle$. Therefore, from equation (2.8), we can calculate the relations between $(\mathbf{f}_1, \mathbf{f}_2, ..., \mathbf{f}_\mathrm{i}, ..., \mathbf{f}_\mathrm{N})$ and $(u_c, u_{\mathrm{f}1}, ..., u_{\mathrm{f}i} ..., u_{\mathrm{f}(N-1)})$ as:

$$\mathbf{f}_i = \frac{m_i}{M} u_c + \sqrt{\mu_{i-1}} u_{f(i-1)} - m_i \sum_{j=i}^{N-1} \frac{\sqrt{\mu_j} u_{fj}}{m_1 + m_2 + \cdots + m_j} \ . \tag{3.43}$$

for $i = 1, 2, ..., N$ with the assumption that $\mu_0 = 0$ and $u_0 = 0$. In the next step, equation (2.24) plays the role of equation (3.41). Then u_g and u_s can be solved from

$$\begin{aligned} u_g &= \sum_{j=1}^{N-1} \rho_j \times u_j \\ u_{sk} &= \sum_{j=1}^{N-1} (\frac{\partial \rho_j}{\partial s_k})^T u_j \ . \end{aligned} \tag{3.44}$$

where $k = 1, 2, ..., (3N-6)$ and $u_j = g^{-1} u_{fj}$.

3.2 Feedback law in lab coordinate system

If the coordinates of the robots in fixed lab frame are available using GPS or other navigation technique, due to the structures in the definition of Jacobi vectors, we find that the Jacobi vectors can be easily calculated.

Suppose each robot has GPS receiver on board with its coordinate q_i measured. Then we can rewrite the definitions for Jacobi vectors in (2.8) as

$$\rho_{\mathrm{f}1} = \sqrt{\mu_1}(q_2 - q_1)$$

$$
\begin{aligned}
\rho_{\mathrm{f}2} &= \sqrt{\mu_2}((q_3 - q_2) + \frac{m_1}{m_1 + m_2}(q_2 - q_1)) \\
\rho_{\mathrm{f}3} &= \sqrt{\mu_3}((q_4 - q_3) + \frac{m_1 + m_2}{m_1 + m_2 + m_3}(q_3 - q_2) + \frac{m_1}{m_1 + m_2 + m_3}(q_2 - q_1)) \\
&\ldots
\end{aligned} \tag{3.45}
$$

The formula for $\dot{\rho}_{\mathrm{f}i}$ has similar form with q_i replaced by $\dot{q}_i$.

Hence, the Jacobi vector $\rho_{\mathrm{f}i}$ and its derivative $\dot{\rho}_{\mathrm{f}i}$ will be calculated on the $(i+1)$th robot. A one directional communication link should be established between robot $(i-1)$ and i so that robot $(i-1)$ will report $(q_{i-1}, \dot{q}_{i-1})$ and $(q_k - q_{k-1}, \dot{q}_k - \dot{q}_{k-1})$ where $(1 \leq k < i-1)$ to robot i. The coordinate of the center of mass q_c and its derivative $\dot{q}_c$ are computable on the last robot.

The system can be described using system equation (3.7). Suppose the potential function V is translation invariant. Then we must have

$$
\frac{\partial V}{\partial q_c} = 0 \; . \tag{3.46}
$$

Thus $\frac{\partial V}{\partial \rho_{\mathrm{f}i}}$ do not depend on q_c. The two equations in (3.7) are decoupled. This means the dynamics described by the second equation is the reduced dynamics on the tangent bundle of Jacobi pre-shape space. On this tangent bundle, consider a function defined as

$$
V_L = \sum_{i=1}^{N-1} (h_{\mathrm{f}i}(\rho_{\mathrm{f}i}) + \frac{1}{2} \parallel \dot{\rho}_{\mathrm{f}i} \parallel^2) \; . \tag{3.47}
$$

Let ρ_i^0 be constant vectors specifying the desired shape and orientation. The functions $h_{\mathrm{f}i}(z)$ satisfies the following conditions

1. $\frac{dh_{\mathrm{f}i}}{dz}$ exists for all $z \in \mathcal{R}^3$.

2. $\frac{dh_{\mathrm{f}i}}{dz} = 0$ if and only if $z = \rho_i^0$.

3. Every $h_{\mathrm{f}i}$ is bounded below.

The derivative of this function V_L along the trajectory of the reduced dynamics is

$$\begin{aligned} \dot{V}_L &= \sum_{i=1}^{N-1} (\frac{dh_{\mathrm{f}i}}{d\rho_{\mathrm{f}i}} \cdot \dot{\rho}_{\mathrm{f}i} + \dot{\rho}_{\mathrm{f}i} \cdot \ddot{\rho}_{\mathrm{f}i}) \\ &= \sum_{i=1}^{N-1} \dot{\rho}_{\mathrm{f}i} (\frac{dh_{\mathrm{f}i}}{d\rho_{\mathrm{f}i}} + \ddot{\rho}_{\mathrm{f}i}) \\ &= \sum_{i=1}^{N-1} \dot{\rho}_{\mathrm{f}i} (\frac{dh_{\mathrm{f}i}}{d\rho_{\mathrm{f}i}} - \frac{\partial V}{\partial \rho_{\mathrm{f}i}} + u_{\mathrm{f}i}) \ . \end{aligned} \tag{3.48}$$

We can see by letting

$$u_{\mathrm{f}i} = -\dot{\rho}_{\mathrm{f}i} + \frac{\partial V}{\partial \rho_{\mathrm{f}i}} - \frac{dh_{\mathrm{f}i}}{d\rho_{\mathrm{f}i}} \ , \tag{3.49}$$

the derivative of V_L is

$$\dot{V}_L = -\sum_{i=1}^{N-1} \| \dot{\rho}_{\mathrm{f}i} \|^2 \leq 0 \ . \tag{3.50}$$

We can apply LaSalle's invariance principle to argue that the controlled dynamics converges to the maximal invariant set C_1 within the set M_1 where $\dot{V}_L = 0$. Hence

$$M_1 = \{(\rho_{\mathrm{f}}, \dot{\rho}_{\mathrm{f}}) \in TF | \dot{\rho}_{\mathrm{f}} = 0\} \tag{3.51}$$

and

$$C_1 = \{(\rho_{\mathrm{f}}, \dot{\rho}_{\mathrm{f}}) \in M_1 | \dot{\rho}_{\mathrm{f}} = 0, \ddot{\rho}_{\mathrm{f}} = 0\} \ . \tag{3.52}$$

Hence, on the set C_1, we must have

$$u_{\mathrm{f}i} - \frac{\partial V}{\partial \rho_{\mathrm{f}i}} = 0 \tag{3.53}$$

i.e.

$$\frac{dh_{\mathrm{f}i}}{d\rho_{\mathrm{f}i}} = 0 \ . \tag{3.54}$$

Thus, we have proved the following theorem

Theorem 3.2.1 *Suppose the Lagrangian L is translation invariant. By using the feedback control law (3.49), the system can be controlled to the formation specified by the set of Jacobi coordinates* $\{\rho_i^0\}$ *asymptotically.*

Notice that the control law u_i is calculated on the $(i+1)$th robot where $\rho_{\mathrm{f}i}$ and $\dot{\rho}_{\mathrm{f}i}$ are available due to the communication scheme mentioned before. Now according to equation (3.43), the actual force $\mathbf{f}_{i+1}$ on robot $(i+1)$ can only be computed if $(u_i, u_{i+1}, ..., u_{N-1})$ are known. Therefore, in addition to the communication link from robot i to $(i+1)$ reporting $(q_1, q_2, ..., q_i)$ to robot $(i+1)$, we need a communication link from robot $(i+1)$ to i reporting $(u_i, u_{i+2}..., u_{N-1})$. Hence, if the messages are delivered in this manner, the smallest time interval between two consecutive control actions on robot 1 would be greater than twice the delay between node 1 and node N of the communication network. In addition, the form of $\frac{\partial V}{\partial \rho_{\mathrm{f}i}}$ will determine whether more communication links are necessary.

3.3 Feedback law using shape measurements

The previous result assumes q_i are available in real time. This assumption is strong and not very realistic in many applications. In some situations, a GPS signal is not available. Even when GPS is available, the measurements have significant error in them or the time required to obtain an estimation is significant. It will be dangerous for robots staying near each other. On the other hand, the robots are usually equipped with on-board sensors such as laser range finders which are capable of measuring the mutual distances between robots and angles between lines of sight. These measurements are often reasonably accurate. They tell us the values of the Jacobi shape variables. We show that formation can be achieved by using only these shape measurements.

3.3.1 Lyapunov-based control for the general case

Suppose the potential function V is translation and rotation invariant i.e. V is only a function of the shape variables s. Then in the system equations (3.38), (3.39) and (3.40), the equation for q_c is decoupled from the other two. Also we may have $\frac{\partial V}{\partial g} = 0$. Then we can define a function on the tangent bundle of the pre-shape space as

$$V_L = h_s(s) + \frac{1}{2}(\Omega + A\dot{s})^T I(\Omega + A\dot{s}) + \frac{1}{2}\dot{s}^T G\dot{s} \; . \tag{3.55}$$

Let $s^0 \in \mathcal{R}^{3N-6}$ specify the desired formation. The function $h_s(z)$ satisfies the following:

1. $\frac{dh_s}{dz}$ exists for all $z \in \mathcal{R}^{3N-6}$ except for singular shapes.

2. $\frac{dh_s}{dz} = 0$ if and only if $z = s^0$.

3. h_s is bounded below.

The derivative of this function along the reduced dynamics (3.39) and (3.40) is

$$\begin{aligned} \dot{V}_L &= \langle \frac{dh_s}{ds}, \dot{s} \rangle + \langle \Omega, u_g \rangle + \langle \dot{s}, u_s - \frac{\partial V}{\partial s} \rangle \\ &= \langle \dot{s}, u_s - \frac{\partial V}{\partial s} + \frac{dh_s}{ds} \rangle + \langle \Omega, u_g \rangle \end{aligned} \tag{3.56}$$

where we use $\langle\ ,\ \rangle$ to denote the inner product. Hence by letting the control law to be

$$\begin{aligned} u_g &= -k_1 \Omega \\ u_s &= \frac{\partial V}{\partial s} - \frac{dh_s}{ds} - \dot{s} \end{aligned} \tag{3.57}$$

where $k_1 > 0$, we have

$$\dot{V}_L = - \parallel \dot{s} \parallel^2 - k_1 \parallel \Omega \parallel^2 \leq 0 \ . \tag{3.58}$$

We can apply LaSalle's invariance principle to argue that the controlled dynamics converge to the maximal invariant set C_2 within the set M_2 where $\dot{V}_L = 0$. Hence

$$M_2 = \{(g, s, \Omega, \dot{s}) \in TF | \Omega = 0, \dot{s} = 0\} \tag{3.59}$$

and

$$C_2 = \{(g, s, \Omega, \dot{s}) \in M_2 | \dot{\Omega} = 0, \ddot{s} = 0\} \ . \tag{3.60}$$

In the system equations (3.39) and (3.40), let $\Omega = 0$ and $\dot{s} = 0$, we have

$$\begin{aligned} I\dot{\Omega} &= u_g = 0 \\ G\ddot{s} + I\dot{\Omega} &= u_s - \frac{\partial V}{\partial s} = 0 \ . \end{aligned} \tag{3.61}$$

Thus on the set C_2, in order for $\dot{\Omega} = 0$ and $\ddot{s} = 0$, we must have

$$\frac{dh_s}{ds} = 0 \ . \tag{3.62}$$

Thus we have proved the following theorem

Theorem 3.3.1 *Suppose the Lagrangian L is both translation and rotation invariant. By using the feedback control law (3.57), the system can be controlled to the formation specified by the Jacobi shape variable s^0 asymptotically.*

However, by letting $u_g = -k_1\Omega$ we already made the assumption that Ω can be measured. In fact, Ω need not to be measured accurately. All we need is an estimation of the direction of Ω which will ensure $\| \Omega \|$ be decreasing. This estimation can not be obtained by only measuring s and $\dot{s}$. Some extra sensors has to be employed which will observe the relative movements of fixed landmarks to the formation.

Given the difficulty of measuring Ω, we proceed to explore the situations when no estimation of Ω is necessary. Notice that in most applications there exists dissipative forces such as the frictions of ground, air or water. Suppose those dissipative forces can be modeled by a Rayleigh dissipative function

$R(q, \dot{q})$. This dissipation must satisfy

$$\frac{\partial R}{\partial \dot{q}_i}\dot{q}_i \geq 0 \tag{3.63}$$

for $i = 1, 2, ...N$. The following assumptions are made:

1. This dissipation is translation invariant.

2. After the coordinate change from q to (q_c, g, s), this dissipation function can be separated into two parts as

$$R(g, s, \dot{q}_c, \Omega, \dot{s}) = R_c(\dot{q}_c) + R_s(g, s, \Omega, \dot{s}) \ . \tag{3.64}$$

3. R_s satisfies

$$\frac{\partial R_s}{\partial \dot{s}}\dot{s} + \frac{\partial R_s}{\partial \Omega}\Omega \geq 0 \tag{3.65}$$

where zero is obtained only if $\dot{s} = 0$ and $\Omega = 0$.

4. If $\dot{s} = 0$ and $\Omega = 0$, then we have

$$\begin{aligned} \frac{\partial R_s}{\partial \dot{s}} &= 0 \\ \frac{\partial R_s}{\partial \Omega} &= 0 \ . \end{aligned} \tag{3.66}$$

Among these assumptions, the strongest one is assumption 2. So far we only know

$$R(\dot{q}) = \frac{k}{2}\sum_{i=1}^{N} m_i \parallel \dot{q}_i \parallel^2 \tag{3.67}$$

with $k > 0$ satisfies all these assumptions.

When such a dissipative function is presented, the system equations should be modified to

$$M\ddot{q}_c = u_c - \frac{\partial R_c}{\partial q_c} \tag{3.68}$$

$$\frac{d}{dt}(I(\Omega + A\dot{s})) = -\Omega \times I(\Omega + A\dot{s}) - g^{-1}\frac{\partial V}{\partial g} + u_g - \frac{\partial R_s}{\partial \Omega} \tag{3.69}$$

$$\begin{aligned} \frac{d}{dt}(G\dot{s}) \quad + \quad & A^T \frac{d}{dt}(I(\Omega + A\dot{s})) = ((\frac{\partial A}{\partial s})^* - \frac{\partial A}{\partial s})[\dot{s}, I(\Omega + A\dot{s})] \\ + \quad & \frac{1}{2}[\frac{\partial I}{\partial s}]^* : (\Omega + A\dot{s}, \Omega + A\dot{s}) + \frac{1}{2}[\frac{\partial G}{\partial s}]^*(\dot{s}, \dot{s}) \\ & -\frac{\partial V}{\partial s} + u_s - \frac{\partial R_s}{\partial \dot{s}} \; . \end{aligned} \tag{3.70}$$

Then by using the same Lyapunov function as (3.55) on the tangent bundle of the pre-shape space, the derivative of this function along the reduced dynamics (3.69) and (3.70) is now

$$\begin{aligned} \dot{V}_L &= \langle \frac{dh_s}{ds}, \dot{s} \rangle + \langle \Omega, u_g - \frac{\partial R_s}{\partial \Omega} \rangle + \langle \dot{s}, u_s - \frac{\partial V}{\partial s} - \frac{\partial R_s}{\partial \dot{s}} \rangle \\ &= \langle \dot{s}, u_s - \frac{\partial V}{\partial s} + \frac{dh_s}{ds} \rangle + \langle \Omega, u_g \rangle - \frac{\partial R_s}{\partial \dot{s}}\dot{s} - \frac{\partial R_s}{\partial \Omega}\Omega \; . \end{aligned} \tag{3.71}$$

Hence the control law can be designed as

$$\begin{aligned} u_g &= 0 \\ u_s &= \frac{\partial V}{\partial s} - \frac{dh_s}{ds} \end{aligned} \tag{3.72}$$

such that

$$\dot{V}_L = -\frac{\partial R_s}{\partial \dot{s}}\dot{s} - \frac{\partial R_s}{\partial \Omega}\Omega \leq 0 \; . \tag{3.73}$$

We can apply LaSalle's invariance principle. By similar arguments as before we can prove the following theorem

Theorem 3.3.2 *Suppose the Lagrangian L is both translation and rotation invariant. Suppose there exists a Rayleigh dissipation satisfying assumptions*

1-4. Then by using the feedback control law (3.72), the system can be controlled to the formation specified by the Jacobi shape variable s^0 asymptotically.

3.3.2 Various Lyapunov functions and control laws

The Lyapunov function based control laws in the last section can be specialized to fit in different contexts. Furthermore, we can use different forms of h_s to avoid shapes that corresponding to collision between particles or collinear shapes.

Suboptimal distance function on shape space

In [45], we let

$$h_s(s) = \frac{1}{2} \left\| s - s^0 \right\|^2 . \tag{3.74}$$

The resulting control law is applicable to formations that contain an arbitrary number of robots. However, one drawback of this method is that by using $\| s - s_0 \|$, we are using the "chordal distance". Hence the controlled dynamics is not following the true geodesics on the shape space. The algorithm is not the most efficient. In fact, the geodesic distance between two points s and s^0 on the shape space B is

$$\delta_B^*(s, s^0) = \min_{g \in SO(3)} \sum_{i=1}^{N-1} \left\| \rho_i(s) - g\rho_i(s^0) \right\|^2 . \tag{3.75}$$

Generally, the minimizer g_{min} is hard to calculate and $\delta_B^*(s, s^0)$ is hard to compute.

Thus, we use a sub-optimal but easier to calculate distance

$$\delta_B(s, s^0) = \sum_{i=1}^{N-1} \| \rho_i(s) - \rho_i(s^0) \|^2 \ . \tag{3.76}$$

Let $h_s(s) = \frac{1}{2}\delta_B(s, s^0)$. The Lyapunov function is now

$$V_L = \frac{1}{2}\sum_{i=1}^{N-1} \| \rho_i(s) - \rho_i(s^0) \|^2 + \frac{1}{2}(\Omega + A\dot{s})^T I(\Omega + A\dot{s}) + \frac{1}{2}\dot{s}^T G\dot{s} \ . \tag{3.77}$$

The derivative of this function along the reduced dynamics (3.39) and (3.40) is

$$\begin{aligned} \dot{V}_L &= \sum_{i=1}^{N-1}\langle \rho_i(s) - \rho_i(s^0), \frac{\partial \rho_i}{\partial s}\dot{s}\rangle + \langle \Omega, u_g\rangle + \langle \dot{s}, u_s - \frac{\partial V}{\partial s}\rangle \\ &= \langle \dot{s}, u_s - \frac{\partial V}{\partial s} + \sum_{i=1}^{N-1}(\frac{\partial \rho_i}{\partial s})^T(\rho_i(s) - \rho_i(s^0))\rangle + \langle \Omega, u_g\rangle \ . \end{aligned} \tag{3.78}$$

Hence by letting the control law to be

$$\begin{aligned} u_g &= -k_1\Omega \\ u_s &= \frac{\partial V}{\partial s} - \sum_{i=1}^{N-1}(\frac{\partial \rho_i}{\partial s})^T(\rho_i(s) - \rho_i(s^0)) - \dot{s} \end{aligned} \tag{3.79}$$

where $k_1 > 0$, we have

$$\dot{V}_L = -\| \dot{s} \|^2 - k_1 \| \Omega \|^2 \leq 0 \ . \tag{3.80}$$

We know that on the tangent bundle TF of Jacobi pre-shape space F, V_L is radially unbounded. So we can apply LaSalle's invariance principle to argue that the controlled dynamics converge to the maximal invariant set C_3 within the set M_3 where $\dot{V}_L = 0$. Hence

$$M_3 = \{(g, s, \Omega, \dot{s}) \in TF | \Omega = 0, \dot{s} = 0\} \tag{3.81}$$

and

$$C_3 = \{(g, s, \Omega, \dot{s}) \in M_3 | \dot{\Omega} = 0, \ddot{s} = 0\} \ . \tag{3.82}$$

In the system equations (3.39) and (3.40), let $\Omega = 0$ and $\dot{s} = 0$. We have

$$\begin{aligned} I\dot{\Omega} &= u_g = 0 \\ G\ddot{s} + I\dot{\Omega} &= u_s - \frac{\partial V}{\partial s} = \sum_{i=1}^{N-1} (\frac{\partial \rho_i}{\partial s})^T (\rho_i(s) - \rho_i(s^0)) \ . \end{aligned} \tag{3.83}$$

Thus on the set C_3, in order for $\dot{\Omega} = 0$ and $\ddot{s} = 0$, we must have

$$\sum_{i=1}^{N-1} (\frac{\partial \rho_i}{\partial s})^T (\rho_i(s) - \rho_i(s^0)) = 0 \ . \tag{3.84}$$

The question is now whether this implies that $\rho_i(s) = \rho_i(s^0)$ for $i = 1, 2, ..., N-1$.

We now going to show that if $N = 3$, the answer is positive. In fact, from the calculations before, we have

$$(\frac{\partial \rho_1}{\partial s})^T = \begin{bmatrix} \sqrt{\mu_1} & 0 & 0 \\ 0 & 0 & 0 \\ 0 & 0 & 0 \end{bmatrix} \tag{3.85}$$

$$(\frac{\partial \rho_2}{\partial s})^T = \sqrt{\mu_2} \begin{bmatrix} -\frac{m_2}{m_1+m_2} & 0 & 0 \\ \cos(s_3) & \sin(s_3) & 0 \\ -s_2 \sin(s_3) & s_2 \cos(s_3) & 0 \end{bmatrix} \ . \tag{3.86}$$

Hence, let

$$\rho_2(s) - \rho_2(s^0) = \{\delta_x, \delta_y, 0\}^T \ . \tag{3.87}$$

We can calculate $(\frac{\partial \rho_1}{\partial s})^T(\rho_1(s) - \rho_1(s^0)) + (\frac{\partial \rho_2}{\partial s})^T(\rho_2(s) - \rho_2(s^0))$ to be:

$$\{\sqrt{\mu_1}(s_1 - s_1^0) + \sqrt{\mu_2}\frac{m_2}{m_1+m_2}\delta_x, \qquad \sqrt{\mu_2}(\delta_x \cos(s_3) + \delta_y \sin(s_3)),$$
$$\sqrt{\mu_2}(-\delta_x s_2 \sin(s_3) + \delta_y s_2 \cos(s_3))\}^T \qquad . \tag{3.88}$$

Thus on the invariant set the following equations has to be satisfied:

$$\begin{aligned} \sqrt{\mu_1}(s_1 - s_1^0) + \sqrt{\mu_2}\frac{m_2}{m_1+m_2}\delta_x &= 0 \\ \delta_x \cos(s_3) + \delta_y \sin(s_3) &= 0 \\ \delta_x s_2 \sin(s_3) + \delta_y s_2 \cos(s_3) &= 0\,. \end{aligned} \tag{3.89}$$

Notice that if $s_2 \neq 0$, the last two equations will give $\delta_x = 0$ and $\delta_y = 0$. Then the first equation will give $s_1 = s_1^0$. Thus we proved that $\rho_1(s) = \rho_1(s^0)$ and $\rho_2(s) = \rho_2(s^0)$. However, if $s_2 = 0$, then the second and third particle collide. Thus proper initial conditions should be chosen so that this case is avoided. In other words, we should choose the initial configuration sufficiently close to the desired configuration.

Collision Avoidance

For a three particle formation, shapes that corresponding to $s_1 = 0$ or $s_2 = 0$ have to be avoided because inter particle collision happens in these two cases. Shapes that corresponding to $s_3 = 0$ shall also be avoided since this is the collinear shape. To achieve these goals, in addition to the three conditions listed in section 3.3.1, $h_s(z)$ should satisfy one more condition

4. $h_s(s) = \infty$ when $s_i = 0$ for $i = 1$ or 2 or 3.

Then under control law (3.79), the desired shape s^0 can be established asymptotically without inter-particle collision.

3.4 Cooperative control form

Next, we point out that although controllers can be designed by computing (u_g, u_s) first and then find out $\mathbf{f}_i$, which is the actual force on each particle, this procedure is gauge dependent. This posts a constraint that each robot has to agree on the same gauge convention. Therefore, they have to agree on the measurement of gauge dependent quantities such as Ω. Of courses, because we assume that each particle is able to detect the other particles, such agreements can be enforced. However, this implies that some particles have to estimate the gauge dependent quantities indirectly from their observations. Such indirect estimates may introduce more severe noise than direct observations.

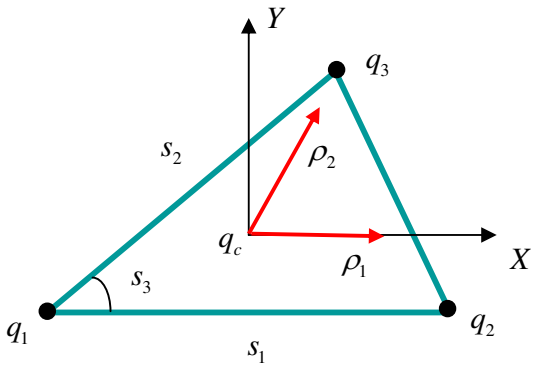

Figure 3.1: *Gauge convention for a triangular formation.*

For example, in the case of a three particle formation, suppose each particle is able to measure the relative positions between itself and the other two particles. If all three particles agree on the gauge convention established in

section 2.4.1, as shown in figure 3.1, then particle 3 has to use the relative position between particle 1 and particle 2 as the estimate for x-axis of the body coordinate system. This estimate incorporates noise from observations of both particle 1 and particle 2.

We now proceed to argue that by transforming (u_g, u_s) into a proper gauge covariant form, we could have a controller design procedure which allows each robot to establish its own gauge convention. In our example above, for particle 3, we may establish the x-axis of the body coordinate system as being aligned with the vector $q_3\vec{q}_1$, which is observed directly by sensors of q_3.

We define the **cooperative control form** to be

$$\begin{aligned} \alpha_g &= u_g \\ \alpha_{sk} &= u_{sk} - \langle u_g, A_k \rangle \end{aligned} \tag{3.90}$$

for $k = 1, 2, ..., 3N-6$. (α_g, α_s) defines a one-form on TF coordinated by $(g, s, g\Upsilon, \dot{s})$ in the following sense

$$\langle \alpha_g, \Upsilon \rangle + \langle \alpha_s, \dot{s} \rangle = \langle u_g, \Omega \rangle + \langle u_s, \dot{s} \rangle \ . \tag{3.91}$$

Then the transform between u_j and (α_g, α_s) is

$$\begin{aligned} \alpha_g &= \sum_{j=1}^{N-1} \rho_j \times u_j \\ \alpha_{sk} &= \sum_{j=1}^{N-1} (\frac{\partial \rho_j}{\partial s_k} - A_k \times \rho_j)^T u_j \ . \end{aligned} \tag{3.92}$$

In order to show that this transform is gauge covariant, we first show that $(\frac{\partial \rho_j}{\partial s_k} - A_k \times \rho_j)$ is gauge covariant. In fact, under a gauge transform such that

$$\begin{aligned} \rho_j &= h(s)\rho_j^1 \\ g^1 &= g\, h(s)\,, \end{aligned} \tag{3.93}$$

we already know that $A_k = h(s)(A_k^1 + \gamma_k)$. Then

$$\begin{aligned} \frac{\partial \rho_j}{\partial s_k} - A_k \times \rho_j &= \frac{\partial h(s)}{\partial s_k}\rho_j - h(s)\frac{\partial \rho_j^1}{\partial s_k} + h(s)((A_k^1 + \gamma_k) \times \rho_j^1) \\ &= h(s)(h^T \frac{\partial h(s)}{\partial s_k}\rho_j - \gamma_k \times \rho_j^1 + \frac{\partial \rho_j^1}{\partial s_k} - A_k^1 \times \rho_j^1) \\ &= h(s)(\frac{\partial \rho_j^1}{\partial s_k} - A_k^1 \times \rho_j^1)\,. \end{aligned} \tag{3.94}$$

This shows that $(\frac{\partial \rho_j}{\partial s_k} - A_k \times \rho_j)$ is gauge covariant. On the other hand, u_j are gauge covariant because

$$u_j = g^{-1}u_{fj} = h(s)(g^1)^{-1}u_{fj} = h(s)u_j^1\,. \tag{3.95}$$

Then

$$\begin{aligned} \alpha_g &= h(s)\sum_{j=1}^{N-1} \rho_j^1 \times u_j^1 = h(s)\alpha_g^1 \\ \alpha_{sk} &= \sum_{j=1}^{N-1}(\frac{\partial \rho_j^1}{\partial s_k} - A_k^1 \times \rho_j^1)^T h^T(s)h(s)u_j^1 = \alpha_{sk}^1 \end{aligned} \tag{3.96}$$

Therefore the transform given by equation (3.92) is a gauge covariant transform.

The cooperative control form allows us to design (α_g, α_s) as gauge covariant quantities. Then the actual forces $\mathbf{f}_\mathrm{i}$ where $i = (1, 2, ..., N)$ can be

computed by each member of the formation in its own coordinate system with its own choice of Jacobi vectors.

Theorem 3.4.1 *Let robot* 1 *and robot* 2 *be two members of a formation governed by the controlled Lagrange equations (3.38),(3.39) and (3.40). Let* ρ^1_{fj} *and* ρ^2_{fj} *where* $j = 1, 2, ..., (N-1)$ *denote the two different sets of Jacobi vectors chosen by the two robots. Suppose the two robots have established two gauge conventions for the formation that are connected by the gauge transform* $g^1 = g^2 h^T(s)$ *for each orientation of the formation. Suppose the cooperative control form* (α^1_g, α^1_s) *computed by robot 1 and* (α^2_g, α^2_s) *computed by robot 2 are gauge covariant, i.e.*

$$(\alpha^1_g, \alpha^1_s) = (h(s)\alpha^2_g, \alpha^2_s) \ , \tag{3.97}$$

and the two robots agree on the same set of shape variables s_k *for* $k = 1, 2, ..., (3N-6)$ *and also agree on the control forces for the center of the formation, which is* u_c*. Then the forces for each robot computed by robot* 1 *are identical to the forces for each robot computed by robot* 2 *i.e.*

$$\mathbf{f}^1_{\mathrm{i}} = \mathbf{f}^2_{\mathrm{i}} \tag{3.98}$$

for $i = 1, 2, ...N$.

Proof

From the definition of (α_g, α_s), we have the following equations

$$\sum_{j=1}^{N-1} \rho^1_j \times u^1_j = h(s) \sum_{j=1}^{N-1} \rho^2_j \times u^2_j$$

$$\sum_{j=1}^{N-1}(\frac{\partial \rho_j^1}{\partial s_k} - A_k^1 \times \rho_j^1)^T u_j^1 = \sum_{j=1}^{N-1}(\frac{\partial \rho_j^2}{\partial s_k} - A_k^2 \times \rho_j^2)^T u_j^2 \ . \tag{3.99}$$

According to democracy property of Jacobi vectors, there exists $\mathbf{h} \in \mathrm{O(N-1)}$ s.t.

$$[\rho_{\mathrm{f1}}^1, \rho_{\mathrm{f2}}^1, ..., \rho_{\mathrm{f}(N-1)}^1] = [\rho_{\mathrm{f1}}^2, \rho_{\mathrm{f2}}^2, ..., \rho_{\mathrm{f}(N-1)}^2]\mathbf{h} \ , \tag{3.100}$$

which implies that

$$g^1[\rho_1^1, \rho_2^1, ..., \rho_{(N-1)}^1] = g^2[\rho_1^2, \rho_2^2, ..., \rho_{(N-1)}^2]\mathbf{h} \ . \tag{3.101}$$

Furthermore, we can write

$$\rho_j^1 = h(s) \sum_{i=1}^{N-1} \mathbf{h}_{ij} \rho_i^2 \ . \tag{3.102}$$

According to the definition of the locked inertia tensor I, we have

$$\begin{aligned} I^1 &= \sum_{j=1}^{N-1}(\| \rho_j^1 \|^2 \mathbf{e} - \rho_j^1 \rho_j^{1T}) \\ &= h(s) \sum_{j=1}^{N-1} \sum_{i,l=1}^{N-1} (\mathbf{h}_{ij}\mathbf{h}_{lj}(\rho_i^{2T}\rho_l^2\mathbf{e} - \rho_i^2\rho_l^{2T}))h^T(s) \\ &= h(s) \sum_{i,l=1}^{N-1} \delta_l^i(\rho_i^{2T}\rho_l^2\mathbf{e} - \rho_i^2\rho_l^{2T})h^T(s) \\ &= h(s) \sum_{i=1}^{N-1} (\rho_i^{2T}\rho_i^2\mathbf{e} - \rho_i^2\rho_i^{2T})h^T(s) \\ &= h(s) I^2 h^T(s) \ , \end{aligned} \tag{3.103}$$

furthermore,

$$A_k^1 = (I^1)^{-1} \sum_{i=1}^{N-1} \rho_i^1 \times \frac{\partial \rho_i^1}{\partial s^k}$$

$$
\begin{aligned}
&= h(s)(I^2)^{-1}h^T(s)h(s)\sum_{i=1}^{N-1}\sum_{j,l=1}^{N-1}\mathbf{h}_{ji}\mathbf{h}_{li}(\rho_j^2\times\left(\frac{\partial\rho_l^2}{\partial s^k}+\gamma_k\times\rho_l^2\right))\\
&= h(s)(I^2)^{-1}\sum_{j,l=1}^{N-1}\delta_l^j(\rho_j^2\times\left(\frac{\partial\rho_l^2}{\partial s^k}+\gamma_k\times\rho_l^2\right))\\
&= h(s)(I^2)^{-1}\sum_{j=1}^{N-1}(\rho_j^2\times\left(\frac{\partial\rho_j^2}{\partial s^k}+\gamma_k\times\rho_j^2\right))\\
&= h(s)(A_k^2+\gamma_k)\ . \qquad (3.104)
\end{aligned}
$$

Therefore,

$$
\begin{aligned}
\sum_{j=1}^{N-1}\rho_j^1\times u_j^1 &= \sum_{j=1}^{N-1}(h(s)\sum_{i=1}^{N-1}\mathbf{h}_{ij}\rho_i^2)\times u_j^1\\
&= h(s)\sum_{i=1}^{N-1}(\sum_{j=1}^{N-1}\rho_i^2\times h^T(s)(\mathbf{h}_{ij}u_j^1))\\
&= h(s)\left(\sum_{i=1}^{N-1}\rho_i^2\times(\sum_{j=1}^{N-1}\mathbf{h}_{ij}h^T(s)u_j^1)\right)\ , \qquad (3.105)
\end{aligned}
$$

and

$$
\begin{aligned}
&\sum_{j=1}^{N-1}(\frac{\partial\rho_j^1}{\partial s_k}-A_k^1\times\rho_j^1)^Tu_j^1\\
=\ &\sum_{j=1}^{N-1}(\sum_{i=1}^{N-1}(\mathbf{h}_{ij}\frac{\partial\rho_i^2}{\partial s_k}+\gamma_k\times\mathbf{h}_{ij}\rho_i^2-(A_k^2+\gamma_k)\times\mathbf{h}_{ij}\rho_i^2)^Th^T(s)u_j^1)\\
=\ &\sum_{i=1}^{N-1}((\frac{\partial\rho_i^2}{\partial s_k}-A_k^2\times\rho_i^2)^T(\sum_{j=1}^{N-1}\mathbf{h}_{ij}h^T(s)u_j^1))\ . \qquad (3.106)
\end{aligned}
$$

Equations (3.105) and (3.106) implies that

$$
u_j^2=h^T(s)\sum_{i=1}^{N-1}\mathbf{h}_{ji}u_i^1 \qquad (3.107)
$$

which can be written in vector form as

$$[u_1^2, u_2^2, ..., u_{(N-1)}^2] = h^T(s)[u_1^1, u_2^1, ..., u_{(N-1)}^1]\mathbf{h}^{\mathrm{T}} \tag{3.108}$$

Therefore, the controls u_{fj}^1 and u_{fj}^2 that corresponding to the Jacobi vectors satisfies

$$[u_{\mathrm{f1}}^1, u_{\mathrm{f2}}^1, ..., u_{\mathrm{f}(N-1)}^1] = [u_{\mathrm{f1}}^2, u_{\mathrm{f2}}^2, ..., u_{\mathrm{f}(N-1)}^2]\mathbf{h} \ . \tag{3.109}$$

Then given $u_c^1 = u_c^2$, this implies that

$$\mathbf{f}_{\mathrm{i}}^1 = \mathbf{f}_{\mathrm{i}}^2 \ , \tag{3.110}$$

for $i = 1, 2, ...N$. ■

In the next session, we will show one such control law which stablize a non-singular formation.

3.5 Gauge covariant control law

Suppose the potential function V is invariant under translation and rotation i.e. V is only a function of the shape variables. Then in the system equations (3.38), (3.39) and (3.40), the equation for q_c is decoupled from the other two. Then we can define a function on the tangent bundle of the pre-shape space as

$$V_L = h_s(s) + \frac{1}{2}(\Omega + A\dot{s})^T I(\Omega + A\dot{s}) + \frac{1}{2}\dot{s}^T G\dot{s} \tag{3.111}$$

where s^0 specifies a desired shape. The derivative of this function along the reduced dynamics (3.39) and (3.40) is

$$\dot{V}_L \ = \ \langle \frac{dh_s}{ds}, \dot{s} \rangle + \langle \Omega, u_g \rangle + \langle \dot{s}, u_s - \frac{\partial V}{\partial s} \rangle$$

$$= \langle \dot{s}, u_s - \frac{\partial V}{\partial s} + \frac{dh_s}{ds} \rangle + \langle \Omega, u_g \rangle \tag{3.112}$$

where we use $\langle\ ,\ \rangle$ to denote the inner product.

In [45], we showed that by letting the control law be

$$\begin{aligned} u_g &= -k_1 \Omega \\ u_s &= \frac{\partial V}{\partial s} - (s - s^0) - \dot{s} \end{aligned} \tag{3.113}$$

where $k_1 > 0$, we have

$$\dot{V}_L = - \parallel \dot{s} \parallel^2 - k_1 \parallel \Omega \parallel^2 \leq 0 \tag{3.114}$$

and the control law will stabilize the shape $s = s^0$ and $\Omega = 0$. However, as we can see here this control law is not gauge covariant.

We now design a new cooperative control law to be

$$\begin{aligned} \alpha_g &= -k \Upsilon \\ \alpha_s &= \frac{\partial V}{\partial s} - \frac{dh_s}{ds} - k\dot{s} \end{aligned} \tag{3.115}$$

which is obviously gauge covariant. The resulting (u_g, u_s) is

$$\begin{aligned} u_g &= -k(\Omega + A\dot{s}) \\ u_s &= \frac{\partial V}{\partial s} - \frac{dh_s}{ds} - k\dot{s} - kA^T(\Omega + A\dot{s}) \ . \end{aligned} \tag{3.116}$$

Then, under such a control law, we have

$$\dot{V}_L = - \parallel \dot{s} \parallel^2 - k \parallel \Omega + A\dot{s} \parallel^2 \leq 0 \tag{3.117}$$

with $\dot{V}_L = 0$ if and only if $\Omega = 0$ and $\dot{s} = 0$

Now we can apply LaSalle's invariance principle to argue that the controlled dynamics converge to the maximal invariant set C_2 within the set M_2 where $\dot{V}_L = 0$. Hence let

$$M_2 = \{(g, s, \Omega, \dot{s}) \in TF | \Omega = 0, \dot{s} = 0\} \tag{3.118}$$

and

$$C_2 = \{(g, s, \Omega, \dot{s}) \in M_2 | \dot{\Omega} = 0, \ddot{s} = 0\} \ . \tag{3.119}$$

In the system equations (3.39) and (3.40), letting $\Omega = 0$ and $\dot{s} = 0$, we have

$$\begin{aligned} I\dot{\Omega} &= u_g = 0 \\ G\ddot{s} + I\dot{\Omega} &= u_s - \frac{\partial V}{\partial s} = 0 \ . \end{aligned} \tag{3.120}$$

Thus on the set C_2, in order for $\dot{\Omega} = 0$ and $\ddot{s} = 0$, we must have $\frac{dh_s}{ds} = 0$. Therefore, we have proved the following theorem

Theorem 3.5.1 *Suppose the potential V is rigid motion invariant. By using the cooperative feedback control law (3.115), the Jacobi shape s^0 is locally asymptotically stabilized.*

Again, by letting $\alpha_g = -k(\Omega + A\dot{s})$, we already made the assumption that Ω can be measured. In fact, all we need is an estimate of the direction of Υ which will ensure $\| \Upsilon \|$ be decreasing.

3.6 Simulations and results

We design simulations to verify the gauge covariant control law and theorem 3.4.1. In MATLAB, we model each robot as a Newtonian particle with unit

mass subject to a control force. We show here the simplest example of a formation of three particles. Since the formation is always triangular, the experiment can be carried out in a plane if we choose the initial velocity for each particle to stay in a plane. The following table shows the initial position and velocity of the three particles.

Particle	Position	Velocity
1	$(0, 0)$	$(2, 1)$
2	$(-2, -3.5)$	$(-1, 1)$
3	$(0.1, -0.5)$	$(-1, 1)$

We choose a set of three shape variables as in section 2.4.1. Let s_1 be the distance between particle 1 and 2. Shape variable s_2 measures distance between particle 1 and 3. Shape variable s_3 measures the angle as shown in Figure 3.1. The desired shape of the formation is an equilateral triangle described by

$$s_1 = s_2 = 2 \ \ , s_3 = \frac{\pi}{3} \, . \tag{3.121}$$

In experiment 1, all particles establish the same gauge frame as in section 2.4.1. They also choose the same set of Jacobi vectors as shown in Figure 3.1. We assume no noise in the measurements of the shape variables. Under the gauge covariant control law (3.115), the formation converges to the desired shape as shown in Figure 3.2. The convergence of the three shape variables are shown in Figure 3.3(a), 3.3(b) and 3.3(c). The rotation speed of the formation are shown in Figure 3.3(d). We see that the formation stops rotating. On the other hand, the center of mass is moving constantly at velocity $(0, 1)$.

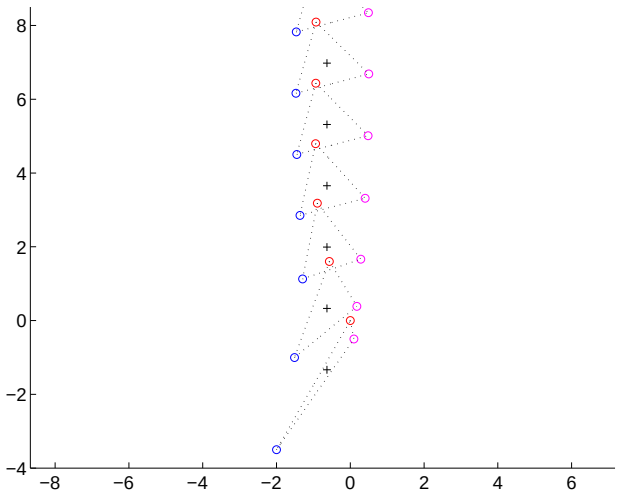

Figure 3.2: *Experiment 1, motion and shape changes of the three robot formation when all robots agree on the same gauge.*

In experiment 2, particle 1 and 2 still use the same gauge frame as in the first experiment. For particle 3 we establish a different gauge frame as shown in Figure 3.4. We also choose a new set of Jacobi vectors, with

$$\begin{aligned} \rho_{\mathrm{f1}} &= \frac{1}{\sqrt{2}}(q_3 - q_2) \\ \rho_{\mathrm{f2}} &= \sqrt{\frac{3}{2}}\,(q_1 - \frac{q_2 + q_3}{2})\,. \end{aligned} \tag{3.122}$$

We use the same gauge covariant control law as in experiment 1. The formation also converges as shown in Figure 3.5. We see there is no difference between Figure 3.5 and 3.2. This is also true when we compare the convergence plots for the shape variables. This validates the claims in theorem 3.4.1.

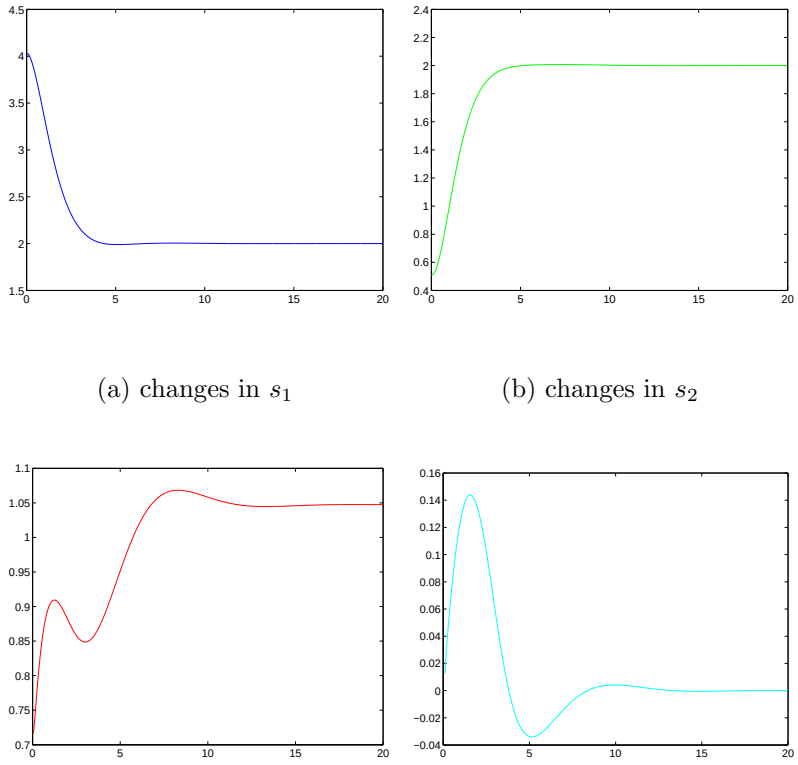

(a) changes in s_1 (b) changes in s_2

(c) changes in s_3 (d) rotation speed

Figure 3.3: *Convergence of shape variables and rotation speed when all robots agree on the same gauge.*

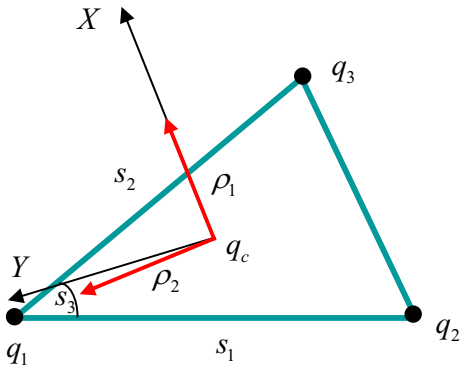

Figure 3.4: *The gauge frame and Jacobi vectors for robot 3.*

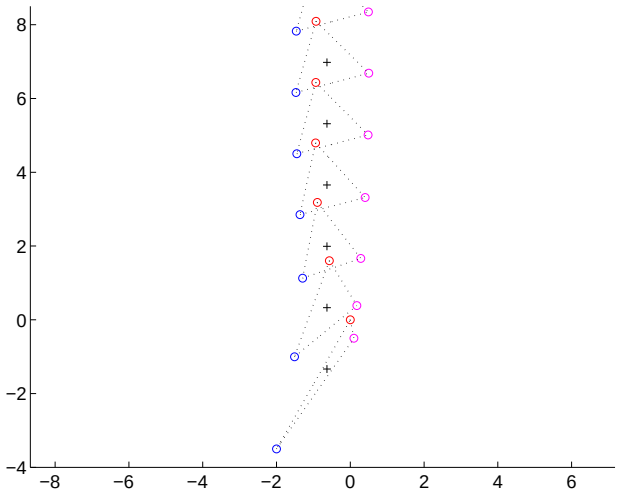

Figure 3.5: *Experiment 2, motion and shape changes of the three robot formation when robot 3 uses different gauge frame from robot 1 and 2.*

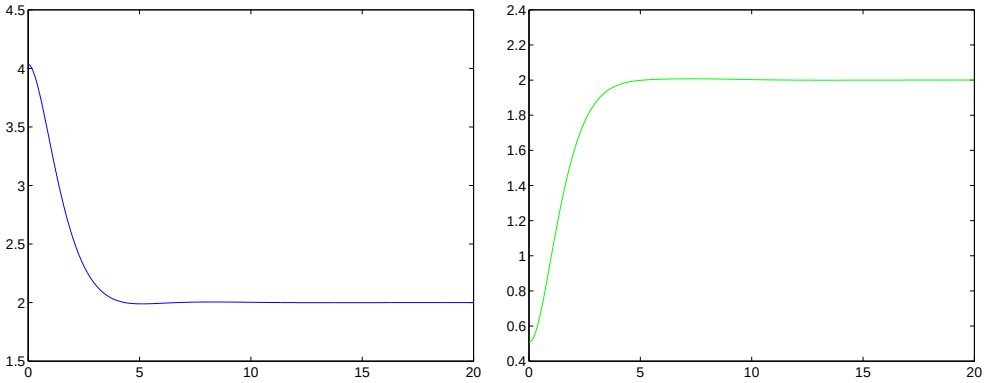

(a) changes in s_1 (b) changes in s_2

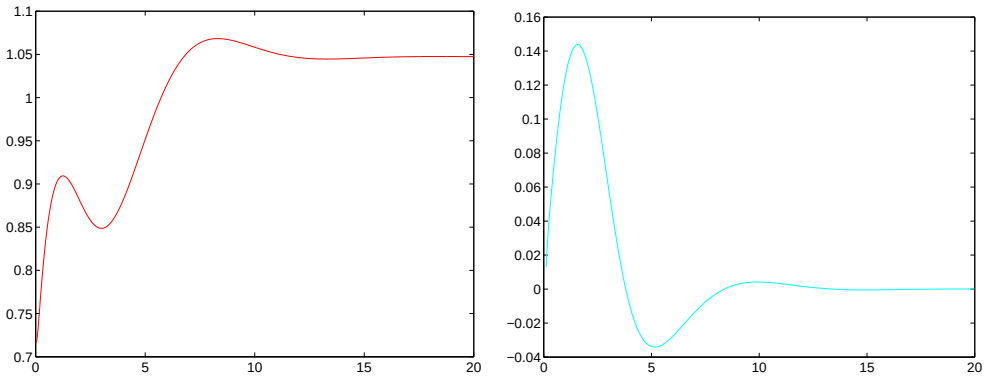

(c) changes in s_3 (d) Rotation speed

Figure 3.6: *Convergence of shape variables and rotation speed when robot 3 uses a special gauge.*

Next, we compare the performance of the gauge covariant control law when there are simulated noise in the shape measurements. In our simulation, each particle is able to determine the relative positions of the other two particles. We add independent Gaussian noise $\mathcal{N}(0, 0.1)$ in the estimates for both the x and y coordinates for the relative positions. Hence noise is introduced in the estimates for the shape variables and the rotational speed. If particle 3 uses the same gauge as particle 1 and 2, it has to estimate vector $q_1\vec{q}_2$ in order to estimate the rotational speed. If particle 3 uses the special gauge as shown in Figure 3.4, it needs to estimate $q_2\vec{q}_3$. The estimate for $q_1\vec{q}_2$ is more noisy than the estimate for $q_2\vec{q}_3$.

To compare the results for the two cases, namely the case of same gauge frames and the case of different gauge frames. We run 100 experiments in each case. We then compare the mean and variance of the values for the shape variables and the rotational speed in the last 1.5 seconds of the simulation when "steady state" is reached. As shown in Figure 3.8, 3.9 and 3.10, using different gauge frames slightly outperforms using same gauge frames. But when its comes to the rotational speed, using different gauge frames has a clear advantage. The variance of the rotational speed when same gauge frames are used is much larger than the variance of the final rotational speed when different gauge frames are used as shown in Figure 3.7.

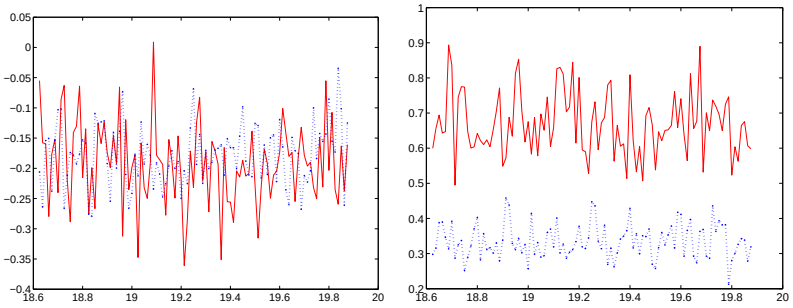

(a) Mean (b) Variance

Figure 3.7: *The mean and variance of the rotation speed in the last* 1.5 *seconds of the simulation. Red solid line represents the case when all robots use the same gauge. Blue dotted line represents the case when robot 3 chooses a special gauge.*

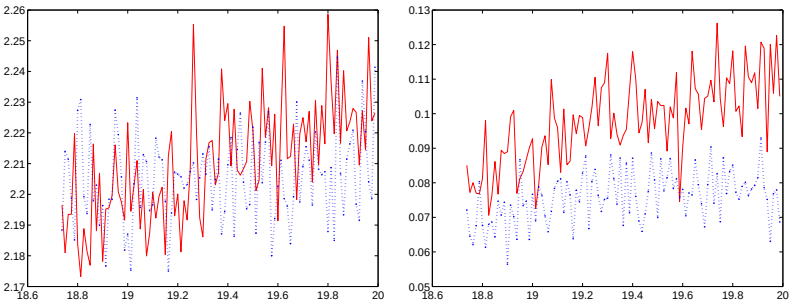

(a) Mean (b) Variance

Figure 3.8: *The mean and variance of* s_1 *in the last* 1.5 *seconds of simulation. Red solid line represents the case when all robots use the same gauge. Blue dotted line represents the case when robot 3 chooses a special gauge.*

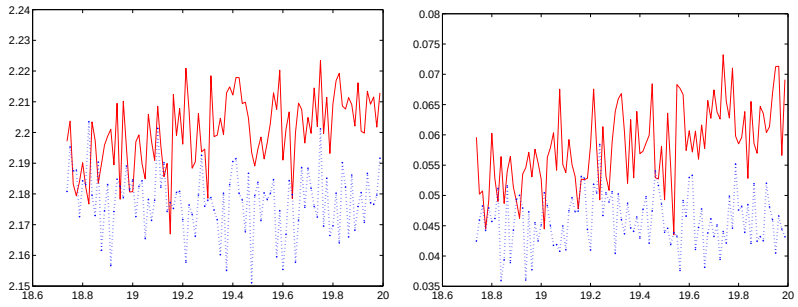

(a) Mean (b) Variance

Figure 3.9: *The mean and variance of s_2 in the last* 1.5 *seconds of simulation. Red solid line represents the case when all robots use the same gauge. Blue dotted line represents the case when robot 3 chooses a special gauge.*

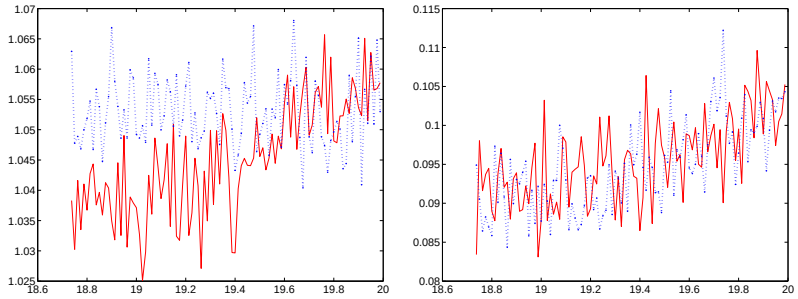

(a) Mean (b) Variance

Figure 3.10: *The mean and variance of s_3 in the last* 1.5 *seconds of simulation. Red solid line represents the case when all robots use the same gauge. Blue dotted line represents the case when robot 3 chooses a special gauge.*

Chapter 4

Navigation in Plane

In an unknown environment, a moving robot has to be able to avoid collision in order to survive. Because the environment might be changing, we install various sensors on the robot so that it is able to observe its surroundings. The behavior of the robot should be designed to react to the observations. An algorithm of such kind, if it enables the robot to arrive at a destination without collision, is called a navigation algorithm. Currently, when a map is unavailable, there are two major categories of navigation algorithms.

The first category is potential function (or navigation function) based algorithms as introduced in [18], [28], [33] and various other papers. A robot follows the gradient vector field generated by some artificial potential function assigned to the workspace. The potential function assumes its minimum at the destination, and detection of new obstacles will cause a recalculation of the function. This approach is computationally efficient and easy to imple-

ment. Furthermore, incorporating dynamic model, the algorithm produces an explicit control law for the robot. But it has two drawbacks. First, the potential function will almost certainly have critical points other than the goal. Instead of always moving toward the goal, the robot might be trapped near such a critical point. Second, the path may be hard to compute and predict. This is due to the complexity of the potential functions, and the difficulty to integrate a gradient vector field.

The second category of navigation algorithms use local path planning, that is, the technique to prescribe a path according to current sensor readings. A typical case is the "bug" family originated from the work of Lumelsky and Stepanov[24], where a robot is instructed to follow boundary curves of obstacles. It is proved that by following the boundary curves until certain conditions are satisfied, and then departing for the goal, a robot is guaranteed to reach the goal without collision. Of course, in addition to navigation, we want the path traveled by the robot to be the shortest. Some interesting results on the optimality of local path planning is addressed in [34]. Comparing to algorithms based on navigation functions, the local path-planning algorithms always predict coherent paths. However, they do not tell the robot how to follow such a path. One has to solve an inverse dynamics problem to find an applicable control law. This process is difficult and a solution is not guaranteed.

Because it is very difficult to avoid the unwanted critical points of the navigation functions, a recent development is to keep the robot at a constant

speed. Control will only be applied to steering. With the constant speed assumption, such a control law has a gyroscopic nature [42]. The authors of [37], [38] and [44] give empirical ways to design steering control laws for obstacle avoidance, but the methods are still in their preliminary stages and are only applied to a limited number of special cases. In [32], the authors proposed a navigation steering law with obstacles treated via potential functions on the space of steering angles. This paper has inspired the group led by Warren to investigate the steering behavior of human beings in a non-static environment, see [9] and see [10] for the latest results. This approach is promising when the obstacles are relatively small compared to the aperture of the range sensors.

We believe boundary curves of the obstacles provide cues for designing steering vector fields. In a plane, an oriented boundary curve is determined by its curvature function in the canonical Frenet-Serret frame [26] together with the location of one point on the curve. The curvature function can be estimated from the range data obtained by sensors such as sonar or laser range finder (ladar). By using such curvature measurements, we have given a systematic way to produce gyroscopic steering vector fields which guarantee avoiding obstacles and reaching the goal. We take advantage of new developments in shape theory [45] and formation control [14]. The essence is that we not only produce a justifiable control law, but also predict paths for the robot.

4.1 Frenet-Serret system for planar curves

With a fixed coordinate system being given in a plane, any point in the plane can be denoted by using a vector $\mathbf{r}$. If a point is chosen as the starting point of a planar curve, then any point on the curve can be represented by $\mathbf{r}(s)$ where s is the length of the curve measured between the starting point and the current point. The derivative $\frac{d\mathbf{r}}{ds}$, if well-defined, is called the tangent vector at s. A *regular curve* is a curve with well-defined tangent vectors for all values of s.

We can then attach a moving coordinate frame to a regular curve. For any point on the curve, we put the origin of the moving frame at the point, the x-axis will be aligned with the tangent vector to the curve and the y-axis will be perpendicular to x-axis but form a right handed coordinate system with it.

To avoid confusion, we denote the axes of the fixed coordinate system as X and Y. We now define vector $\mathbf{x}$ as the unit tangent vector along the x-axis and define vector $\mathbf{y}$ as the unit vector along the y-axis. We can then study the motion of three vectors $\mathbf{r}$, $\mathbf{x}$ and $\mathbf{y}$ in the fixed coordinate frame. Frenet and Serret discovered a slightly different but equivalent version of the following set of equations:

$$\begin{aligned} \frac{d\mathbf{r}}{ds} &= \mathbf{x} \\ \frac{d\mathbf{x}}{ds} &= \kappa(s)\mathbf{y} \\ \frac{d\mathbf{y}}{ds} &= -\kappa(s)\mathbf{x}\ . \end{aligned} \tag{4.1}$$

Here, $\kappa(s)$ is called the *algebraic curvature* of the curve.

Because the vectors $\mathbf{x}$ and $\mathbf{y}$ are orthogonal, if we construct a matrix by

$$g = \begin{bmatrix} \mathbf{x} & \mathbf{y} & \mathbf{r} \\ 0 & 0 & 1 \end{bmatrix}, \tag{4.2}$$

then $g \in SE(2)$. Equation (4.1) now has a simpler representation as

$$\frac{dg}{ds} = g\xi, \tag{4.3}$$

where

$$\xi = \begin{bmatrix} 0 & -\kappa(s) & 1 \\ \kappa(s) & 0 & 0 \\ 0 & 0 & 0 \end{bmatrix} \tag{4.4}$$

and $\xi \in se(2)$, the Lie algebra associated with $SE(2)$. Thus, a regular curve in the plane can be studied as a curve on Lie group $SE(2)$ determined by equation (4.3).

4.2 Bertrand family

There exists a family of straight lines that are parallel to any given straight line in the plane. Choosing one in this family as reference, on each side of the reference, we can determine any family member by knowing its distance to the reference line. As generalization to this well-known setting, for a regular

curve determined by $(g_0(s_0), \kappa_0(s_0))$, where

$$g_0(s_0) = \begin{bmatrix} \mathbf{x}_0(s_0) & \mathbf{y}_0(s_0) & \mathbf{r}_0(s_0) \\ & & \\ 0 & 0 & 1 \end{bmatrix}, \tag{4.5}$$

we may construct a family of curves that are "parallel" to it.

We first find the starting point for each family member. Let $s_0 = 0$. For each value of λ, there exists a unique group element $g_{\lambda 0} \in SE(2)$, satisfying

$$g_0^{-1}(0)(g_{\lambda 0}) = \begin{bmatrix} 1 & 0 & 0 \\ 0 & 1 & \lambda \\ 0 & 0 & 1 \end{bmatrix}. \tag{4.6}$$

We can solve $g_{\lambda 0}$ as

$$g_{\lambda 0} = \begin{bmatrix} \mathbf{x}_0(0) & \mathbf{y}_0(0) & \mathbf{r}_0(0) + \lambda \mathbf{y}_0(0) \\ 0 & 0 & 1 \end{bmatrix}. \tag{4.7}$$

On the next step, we construct one "parallel" curve starting from the initial point given by $g_{\lambda 0}$. Notice that curves starting from those $g_{\lambda 0}$ where $\lambda > 0$ are on one side of curve $g_0(s_0)$ while curves starting from those $g_{\lambda 0}$ where $\lambda < 0$ are on the other side. When $\lambda < 0$ and $\kappa_0 < 0$, we require that

$$\lambda > -\frac{1}{|\kappa_0|}. \tag{4.8}$$

When $\lambda > 0$ and $\kappa_0 > 0$, we require that

$$\lambda < \frac{1}{|\kappa_0|}. \tag{4.9}$$

This is to ensure $1-\kappa_0\lambda > 0$ so that the tangent vector is always well-defined. For each λ, there exists a well defined smooth function $s_\lambda(s_0)$ s.t.

$$\begin{aligned} s_\lambda(0) &= 0 \\ \frac{ds_\lambda}{ds_0} &= 1-\kappa_0\lambda\,. \end{aligned} \tag{4.10}$$

Then since $1-\kappa_0\lambda > 0$, the inverse function exists so that s_0 is also a function of s_λ. Such function s_λ is called a *reparametrization* of the curve. We then let

$$\kappa_\lambda(s_\lambda) = \frac{\kappa_0(s_0)}{1-\kappa_0\lambda}\,. \tag{4.11}$$

A curve on $SE(2)$ can be constructed by the following differential equation

$$\frac{dg_\lambda}{ds_\lambda} = g_\lambda \begin{bmatrix} 0 & -\kappa_\lambda & 1 \\ \kappa_\lambda & 0 & 0 \\ 0 & 0 & 0 \end{bmatrix} \tag{4.12}$$

Definition 4.2.1 *Given a planar curve described by $(g_0(s_0), \kappa_0(s_0))$, for each value of $\lambda > 0$, suppose we can construct a curve $(g_\lambda(s_\lambda), \kappa_\lambda(s_\lambda))$ starting from $g_{\lambda 0}$ and satisfies equation (4.12), with s_λ given by equation (4.10) and κ_λ given by equation (4.11). We define curve $(g_\lambda(s_\lambda), \kappa_\lambda(s_\lambda))$ as a* **Bertrand mate** *to curve $(g_0(s_0), \kappa_0(s_0))$. The two curves form a* **Bertrand pair**. *And the family of all Bertrand mates, indexed by λ, is defined as a* **Bertrand family** *for curve $(g_0(s_0), \kappa_0(s_0))$. We say $(g_0(s_0), \kappa_0(s_0))$ is the* **reference curve** *of its Bertrand family.*

We can re-parametrize all members of a Bertrand family by s_0. By using

the chain rule, from equation (4.12) and equation (4.10), we obtain

$$\begin{aligned} \frac{dg_\lambda}{ds_0} &= \frac{dg_\lambda}{ds_\lambda}\frac{ds_\lambda}{ds_0} \\ &= g_\lambda \begin{bmatrix} 0 & -\kappa_0(s_0) & 1-\kappa_0\lambda \\ \kappa_0(s_0) & 0 & 0 \\ 0 & 0 & 0 \end{bmatrix} . \end{aligned} \tag{4.13}$$

Let

$$\xi(s_0,\lambda) = \begin{bmatrix} 0 & -\kappa_0(s_0) & 1-\kappa_0\lambda \\ \kappa_0(s_0) & 0 & 0 \\ 0 & 0 & 0 \end{bmatrix} . \tag{4.14}$$

Then, any given value of s_0 determines a unique group element $g_\lambda(s_0)$ located on the Bertrand mate indexed by λ. The relative displacement between $g_\lambda(s_0)$ and $g_0(s_0)$ is

$$h_\lambda(s_0) = g_0^{-1}(s_0)g_\lambda(s_0) . \tag{4.15}$$

Theorem 4.2.2 (Bertrand) *$h_\lambda(s_0)$ is a constant group element of $SE(2)$ for all $s_0 \geq 0$ i.e.*

$$h_\lambda(s_0) = \begin{bmatrix} 1 & 0 & 0 \\ 0 & 1 & \lambda \\ 0 & 0 & 1 \end{bmatrix} . \tag{4.16}$$

Proof

According to the definition of Bertrand mate, we know that when $s_0 = 0$, $h_\lambda(0)$ satisfies (4.16) . We now compute the derivative of $h_\lambda(s_0)$ with respect

to s_0.

$$\begin{aligned}\frac{dh_\lambda(s_0)}{ds_0} &= \frac{dg_0^{-1}}{ds_0}g_\lambda + g_0^{-1}\frac{dg_\lambda}{ds_0} \\ &= -g_0^{-1}\frac{dg_0}{ds_0}g_0^{-1}g_\lambda + g_0^{-1}g_\lambda\xi_\lambda \\ &= -\xi_0 h_\lambda + h_\lambda\xi_\lambda \qquad (4.17)\end{aligned}$$

If $h_\lambda(s_0)$ takes the form in equation (4.16) , then by direct calculation we can show

$$\frac{dh_\lambda(s_0)}{ds_0} = 0\ . \qquad (4.18)$$

Because this is true for all values of s_0 we conclude that $h_\lambda(s_0) = h_\lambda(0)$ for all values of s_0. ■

The following corollary is obtained by studying the components of the matrix representation of h_λ.

Corollary 4.2.3 *The following properties hold for all values of* s_0*:*

1. $\mathbf{x}_0 \cdot \mathbf{y}_\lambda = 0$ *and* $\mathbf{x}_0 \cdot \mathbf{x}_\lambda = 1$.
2. $\mathbf{r}_\lambda - \mathbf{r}_0 = \lambda \mathbf{y}_0$.
3. $\| \mathbf{r}_0 - \mathbf{r}_\lambda \| = \lambda$.

The purpose for us to study these properties is to apply them to formation control and navigation for particles with constant speed.

4.3 Shape space for particles with constant speed

In many applications, formation members are required to move at constant speed. For example, for unmanned aerial vehicles (UAVs) and high speed ground vehicles, keeping constant speed improves fuel efficiency and dynamic stability. We call a particle with constant speed a *vehicle*.

From now on, we assume that all our particles have unit mass. In a plane, the motion of a Newtonian particle $\mathbf{r} \in R^2$ can be described as $\ddot{\mathbf{r}} = \mathbf{f}$. If the particle has speed ν and wants to keep the constant speed, we require

$$\begin{aligned} \dot{r}_x^2 + \dot{r}_y^2 &= \nu^2 \\ \mathrm{f}_x \, \dot{r}_x + \mathrm{f}_y \, \dot{r}_y &= 0 \, . \end{aligned} \tag{4.19}$$

By introducing a new variable θ and defining $u = \dot{\theta}$, we can write down the solution as

$$\begin{aligned} \dot{r}_x &= \nu \cos\theta \\ \dot{r}_y &= \nu \sin\theta \\ \dot{\theta} &= u \, . \end{aligned} \tag{4.20}$$

And we must let $\mathbf{f}$ be

$$\begin{aligned} \mathrm{f}_x &= -\dot{r}_y \, u \\ \mathrm{f}_y &= \dot{r}_x \, u \, . \end{aligned} \tag{4.21}$$

Notice that $\mathbf{f}$ is always perpendicular to the velocity vector $\dot{\mathbf{r}}$. Therefore, it will not change the kinetic energy of the particle. We say the force is *gyroscopic*. Under such a force, the particle lives on a submanifold of its phase space where kinetic energy is constant. This submanifold is $SE(2)$. On this submanifold, The states of the particle can be represented by (r_x, r_y, θ) and the force can be simplified to a *steering control* which is represented by u.

Jacobi shape theory is difficult to be applied to vehicles without modification and extension. We establish a shape theoretic approach for formation control, which is based on [14]. This theory will then be applied to create boundary following behaviors for vehicles.

Given $(N+1)$ vehicles, for $i = 0, 1, 2, ..., N$, define

$$\begin{aligned} \mathbf{x_i} &= \begin{bmatrix} \cos\theta_i \\ \sin\theta_i \end{bmatrix}, \ \mathbf{y_i} = \begin{bmatrix} -\sin\theta_i \\ \cos\theta_i \end{bmatrix} \\ \mathbf{r_i} &= \begin{bmatrix} x_i \\ y_i \end{bmatrix}. \end{aligned} \tag{4.22}$$

Then define

$$g_i = \begin{bmatrix} \mathbf{x_i} & \mathbf{y_i} & \mathbf{r_i} \\ 0 & 0 & 1 \end{bmatrix} \tag{4.23}$$

$\mathbf{x_i}$ and $\mathbf{y_i}$ define a frame carried by particle i. The motion of particle can now be expressed as

$$\dot{\mathbf{r}}_\mathbf{i} = \nu_i \, \mathbf{x_i}$$

$$\begin{aligned} \dot{\mathbf{x}}_\mathbf{i} &= \nu_i \, \mathbf{y}_\mathbf{i} \, u_i \\ \dot{\mathbf{y}}_\mathbf{i} &= \nu_i \, \mathbf{x}_\mathbf{i} \, u_i \ . \end{aligned} \tag{4.24}$$

Comparing equation (4.24) with equation (4.1), we notice that the motion description of a unit speed particle is the same as a planar curve, with the curvature κ replaced by the steering control u_i. Similarly, the vehicle motion can also be described by

$$\dot{g}_i = g_i \xi_i \tag{4.25}$$

where

$$\xi_i = \begin{bmatrix} 0 & -\nu_i \, u_i & \nu_i \\ \nu_i \, u_i & 0 & 0 \\ 0 & 0 & 0 \end{bmatrix} . \tag{4.26}$$

We select the vehicle g_0 as the reference vehicle, then define the *shape variables* to be $h_i = g_0^{-1} g_i$ for $i = 1, 2, ..., N$. The space of each h_i is $SE(2)$. The *shape space of* $N + 1$ *vehicles* is the product of N copies of $SE(2)$.

In this section, we extend these ideas so that they are able to be applied to controller design for boundary following. We only require the reference vehicle to travel at constant speed. For other particles, their speed ν_i are not constant. Later we will see that in the boundary following problem, ν_i depend on u_0, the steering control of the reference vehicle.

The *shape dynamics* is described by the system equations for the shape variables h_i. We compute the shape dynamics as

$$\dot{h}_i = \dot{g}_0^{-1} g_i + g_0^{-1} \dot{g}_i$$

$$
\begin{aligned}
&= -g_0^{-1}\dot{g}_0 g_0^{-1} g_i + g_0^{-1} g_i \xi_i \\
&= -\xi_0 h_i + h_i \xi_i \ . \qquad (4.27)
\end{aligned}
$$

We would then like to characterize the equilibria of the shape dynamics. The following theorem tells us that a relative equilibrium of the shape dynamics of a pair of particles, one traveling at constant speed and the other one not, produces trajectories that form a Bertrand pair.

Theorem 4.3.1 *Let $g_1(t)$ and $g_0(t)$ describe the motion of two particles in the plane parametrized by t satisfying*

$$
\begin{aligned}
\dot{g}_1 &= g_1 \xi_1 \\
\dot{g}_0 &= g_0 \xi_0 \ . \qquad (4.28)
\end{aligned}
$$

Suppose vehicle described by g_0 travels at unit speed. Let $h_1(t) = g_0^{-1}(t) g_1(t)$. Then $h_1(t)$ satisfies the differential equation

$$
\dot{h}_1 = -\xi_0 h_1 + h_1 \xi_1 \ . \qquad (4.29)
$$

Furthermore, if this shape dynamics has equilibria, then we have the following conclusions:

1. *$h_1(t) = h_e(t) = h_\lambda$ are equilibria of the shape dynamics, where h_λ are constant group elements given in equation (4.16).*

2. *If the steering control of $g_0(t)$ is not a constant, then $h_1(t) = h_e(t) = h_\lambda$ are the only possible equilibria of the shape dynamics.*

3. *For a given value of* λ, $g_1(t) = g_e(t) = g_0(t)h_\lambda$ *is a relative equilibrium for the system (4.28) under the left action of group* $SE(2)$.

4. *Let* $g_\lambda(t)$ *be the Bertrand mate of curve* $g_0(t)$ *indexed by* λ. *Then* $g_1(t) = g_e(t) = g_\lambda(t)$.

Proof

We have shown that the shape dynamics satisfies equation (4.29). We know that ξ_0 and ξ_1 can be written in the following form

$$\begin{aligned} \xi_0 &= \begin{bmatrix} 0 & -u_0 & 1 \\ u_0 & 0 & 0 \\ 0 & 0 & 0 \end{bmatrix} \\ \xi_1 &= \begin{bmatrix} 0 & -\nu_1 u_1 & \nu_1 \\ \nu_1 u_1 & 0 & 0 \\ 0 & 0 & 0 \end{bmatrix}, \end{aligned} \tag{4.30}$$

where u_0 and u_1 are steering controls, ν_1 is the speed for vehicle 1. If there exists h_e s.t.

$$-\xi_0 h_e + h_e \xi_1(t) = 0\ . \tag{4.31}$$

We may write $h_e(t)$ as

$$h_e(t) = \begin{bmatrix} \cos\theta & -\sin\theta & x \\ \sin\theta & \cos\theta & y \\ 0 & 0 & 1 \end{bmatrix} \tag{4.32}$$

and then solve for θ, x and y. Notice that because h_e is an equilibrium, then θ, x and y assumes constant values.

We then compute

$$\xi_0 h_e = \begin{bmatrix} -u_0 \sin\theta & -u_0 \cos\theta & 1 - u_0 y \\ u_0 \cos\theta & -u_0 \sin\theta & u_0 x \\ 0 & 0 & 0 \end{bmatrix}, \tag{4.33}$$

and

$$h_e \xi_1 = \begin{bmatrix} -\nu_1 u_1 \sin\theta & -\nu_1 u_1 \cos\theta & \nu_1 \cos\theta \\ \nu_1 u_1 \cos\theta & -\nu_1 u_1 \sin\theta & \nu_1 \sin\theta \\ 0 & 0 & 0 \end{bmatrix}. \tag{4.34}$$

Therefore, the following set of equations are used to solve for h_e:

$$\begin{aligned} (u_0 - \nu_1 u_1)\sin\theta &= 0 \\ (u_0 - \nu_1 u_1)\cos\theta &= 0 \end{aligned} \tag{4.35}$$

$$\begin{aligned} \nu_1 \cos\theta + u_0 y - 1 &= 0 \\ \nu_1 \sin\theta - u_0 x &= 0\,. \end{aligned} \tag{4.36}$$

Obviously, if $\sin\theta = 0$, then the solutions are $x = 0$, $y = \lambda$ and $\nu_1 = 1 - u_0\lambda$. This solution is h_λ. We have proved the first claim that $h_e = h_\lambda$ are equilibria.

To prove there are no other equilibria if u_0 is not constant, we assume that $\sin\theta \neq 0$. Then

$$\nu_1 = \frac{u_0 x}{\sin\theta} = \frac{1 - u_0 y}{\cos\theta} \tag{4.37}$$

which implies

$$u_0(x\cos\theta + y\sin\theta) = 1 \tag{4.38}$$

which further implies that u_0 has to be a constant. Therefore, there is no solution other than letting $\sin\theta = 0$.

Let $g_a \in SE(2)$ denote an arbitrary group element of $SE(2)$. Then the left action of g_a on $(g_1, g_0) \in SE(2) \times SE(2)$ is defined as:

$$\Phi_{g_a}[g_1, g_0] = (g_a g_1,\ g_a g_0)\ . \tag{4.39}$$

The lifted action on $(\dot{g}_1, \dot{g}_0)$ which belongs to the tangent space of $SE(2) \times SE(2)$ is

$$T\Phi_{g_a}[\dot{g}_1, \dot{g}_0] = (g_a g_1 \xi_1, g_a g_0 \xi_0). \tag{4.40}$$

The action Φ_{g_a} leaves h invariant because

$$\Phi_{g_a}[h_1] = (\Phi_{g_a}[g_0])^{-1}(\Phi_{g_a}[g_1]) = g_0^{-1} g_a^{-1} g_a g_1 = g_0^{-1} g_1 = h_1\ . \tag{4.41}$$

The lifted action $T\Phi_{g_a}$ leaves $\dot{h}_1$ invariant because

$$\begin{aligned} T\Phi_{g_a}[\dot{h}_1] &= \frac{d(\Phi_{g_a}[g_0])^{-1}}{dt}\Phi_{g_a}[g_1] + (\Phi_{g_a}[g_0])^{-1}\frac{d\Phi_{g_a}[g_1]}{dt} \\ &= -g_0^{-1}\frac{dg_0}{dt}g_0^{-1}g_a^{-1}g_a g_1 + g_0^{-1}g_a^{-1}g_a g_1 \xi_1 \\ &= -\xi_0 h_1 + h_1 \xi_1 \\ &= \dot{h}_1 \end{aligned} \tag{4.42}$$

Therefore, equation (4.29) is the reduced dynamics for equation (4.28) under the left action of symmetry group $SE(2)$.

If $h_e(t) = h_\lambda$ is an equilibrium for equation (4.29), then from

$$-\xi_0 h_e + h_e \xi_1 = 0 \tag{4.43}$$

we obtain the solution for ξ_e as

$$\xi_e = \begin{bmatrix} 0 & -u_0(t) & 1-u_0\lambda \\ u_0(t) & 0 & 0 \\ 0 & 0 & 0 \end{bmatrix} \tag{4.44}$$

Corresponding to $h_e(t) = h_\lambda$, we have $g_e(t) = g_0 h_\lambda$. Such $g_e(t)$ satisfies

$$\begin{aligned} \dot{g}_e &= g_e \xi_e \\ &= g_e \begin{bmatrix} 0 & -u_0(t) & 1-u_0\lambda \\ u_0(t) & 0 & 0 \\ 0 & 0 & 0 \end{bmatrix}. \end{aligned} \tag{4.45}$$

We notice that $\xi_e = \xi_\lambda$. From the definition of Bertrand family, we see $g_e(t) = g_\lambda(t)$, which is a Bertrand mate for $g_0(t)$.

To show that $g_e(t)$ and $g_0(t)$ form a relative equilibria, we shall find out $\eta \in se(2)$ s.t. the infinitesimal generator of such η is equal to the vector field at (g_e, g_0). The infinitesimal generator is

$$\eta_G(g_e, g_0) = (\eta\, g_e,\ \eta\, g_0). \tag{4.46}$$

Then we shall see whether we can solve η from the equation

$$(\eta\, g_e,\ \eta\, g_0) = (g_e\xi_e, g_0\xi_0) \tag{4.47}$$

when $g_e = g_\lambda$ and $\xi_e = \xi_\lambda$. Because we already know

$$\xi_0 = h_e \xi_e h_e^{-1}\,, \tag{4.48}$$

we have

$$g_0\xi_0 g_0^{-1} = g_0 h_e \xi_e (g_0 h_e)^{-1} = g_e \xi_e g_e^{-1} \ . \tag{4.49}$$

Thus equation (4.47) does have a unique solution

$$\eta = g_0\xi_0 g_0^{-1} = g_e \xi_e g_e^{-1} \ . \tag{4.50}$$

This proves that (g_e, g_0) is a relative equilibrium for the system given by equation (4.28). We then conclude that in the relative equilibrium state, the trajectory curves traveled by the two particles form a Bertrand pair. ■

We noticed that the vector field of $(\dot{g}_1, \dot{g}_0)$ is non-autonomous because ξ_0 and ξ_1 depend explicitly on time. Therefore, a Bertrand pair is an example of a relative equilibrium for non-autonomous systems.

4.4 Controlled motion of the closest point

In the planar setting, consider a vehicle moving at unit speed in the presence of a single obstacle, that is, the region enclosed by a simple closed regular curve. Suppose that at each instant of time, the point on the obstacle boundary which is closest to the moving vehicle is unique. This point, which we will call the "closest point" (or "shadow point"), moves along the boundary curve. We assume uniqueness of the closest point in order to streamline the discussion and bring out the key ideas. Of course, in dealing with real-world obstacles, non-uniqueness of the closest point is an important issue.

In terms of the arc-length parametrization, the boundary curve can be

described by

$$\begin{aligned}
\frac{d\mathbf{r}_1}{ds} &= \mathbf{x}_1, \\
\frac{d\mathbf{x}_1}{ds} &= \mathbf{y}_1\kappa_1, \\
\frac{d\mathbf{y}_1}{ds} &= -\mathbf{x}_1\kappa_1,
\end{aligned} \tag{4.51}$$

where κ_1 is the plane curvature function for the boundary curve. Using the chain rule, we can express the time-evolution of the closest point as

$$\begin{aligned}
\dot{\mathbf{r}}_1 &= \nu_1\mathbf{x}_1, \\
\dot{\mathbf{x}}_1 &= \mathbf{y}_1\nu_1\kappa_1, \\
\dot{\mathbf{y}}_1 &= -\mathbf{x}_1\nu_1\kappa_1,
\end{aligned} \tag{4.52}$$

where

$$\nu_1 = \frac{ds}{dt}, \tag{4.53}$$

with s denoting the arc-length parameter. Because the closest point depends on the motion of the moving vehicle, ν_1 depends on both the boundary curve and on the trajectory of the moving vehicle.

Letting $\mathbf{r}_2$ denote the position of the moving vehicle, $\mathbf{x}_2$ the unit tangent vector, $\mathbf{y}_2$ the unit normal vector, and u_2 the steering control, we have the following system of equations for the "formation" consisting of the moving vehicle and the closest point:

$$\begin{aligned}
\dot{\mathbf{r}}_1 &= \nu_1\mathbf{x}_1, & \dot{\mathbf{r}}_2 &= \mathbf{x}_2, \\
\dot{\mathbf{x}}_1 &= \mathbf{y}_1\nu_1\kappa_1, & \dot{\mathbf{x}}_2 &= \mathbf{y}_2u_2, \\
\dot{\mathbf{y}}_1 &= -\mathbf{x}_1\nu_1\kappa_1, & \dot{\mathbf{y}}_2 &= -\mathbf{x}_2u_2,
\end{aligned} \tag{4.54}$$

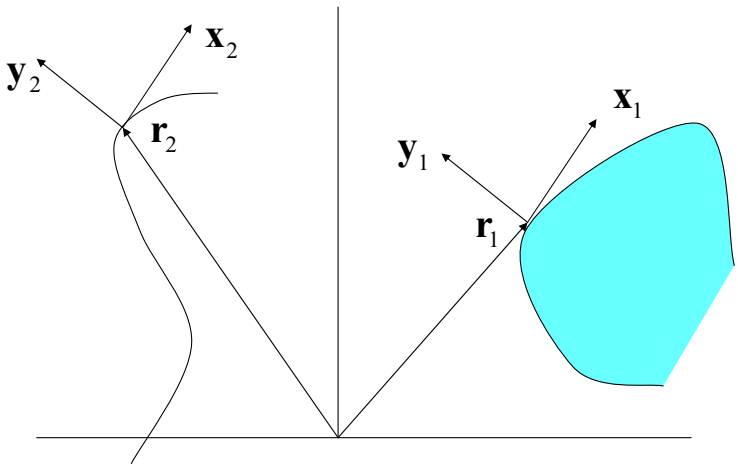

Figure 4.1: *Positions and frames for the trajectory of the moving vehicle ($\mathbf{r}_2$, $\mathbf{x}_2$, and $\mathbf{y}_2$) and for the closest point on the boundary curve ($\mathbf{r}_1$, $\mathbf{x}_1$, and $\mathbf{y}_1$).*

where κ_1 may be considered given (in practice, κ_1 is derived from sensor data, e.g., from a laser range finder); ν_1 is a deterministic function of $(\mathbf{r}_1, \mathbf{x}_1, \mathbf{y}_1)$, $(\mathbf{r}_2, \mathbf{x}_2, \mathbf{y}_2)$, and κ_1; and u_2 is the control input we apply to avoid colliding with the obstacle and to achieve boundary following. Our objective is to determine u_2, as a feedback function of $(\mathbf{r}_1, \mathbf{x}_1, \mathbf{y}_1)$, $(\mathbf{r}_2, \mathbf{x}_2, \mathbf{y}_2)$, and κ_1, such that we can prove analytically that collision avoidance and boundary following are achieved.

Figure 4.1 illustrates the frames for the trajectories of the moving vehicle and the closest point on the boundary curve.

4.4.1 Boundary-curve frame convention

We define

$$\mathbf{r} = \mathbf{r}_2 - \mathbf{r}_1, \tag{4.55}$$

to be the vector from the closest point on the boundary curve to the moving vehicle. We assume that initially

$$|\mathbf{r}| > 0, \tag{4.56}$$

and we will prove that under this assumption as well as other appropriate hypotheses, our boundary-following control law guarantees (4.56) for all future time. Then

$$\begin{aligned} \frac{d}{dt}|\mathbf{r}| &= \frac{\mathbf{r}\cdot\dot{\mathbf{r}}}{|\mathbf{r}|} = \frac{\mathbf{r}}{|\mathbf{r}|}\cdot(\mathbf{x}_2 - \nu_1\mathbf{x}_1) \\ &= \left(\frac{\mathbf{r}}{|\mathbf{r}|}\cdot\mathbf{x}_2\right) - \nu_1\left(\frac{\mathbf{r}}{|\mathbf{r}|}\cdot\mathbf{x}_1\right). \end{aligned} \tag{4.57}$$

The first-order necessary conditions for the closest point to be an extremum of the Euclidean distance from the moving vehicle to the curve are

$$\mathbf{r}\cdot\mathbf{x}_1 = 0, \tag{4.58}$$

and

$$\mathbf{y}_1 = \pm\frac{\mathbf{r}}{|\mathbf{r}|}, \tag{4.59}$$

where the correct choice of sign depends on whether the boundary curve is to the right or left of the moving vehicle, and on what convention is chosen for the positive direction along the boundary curve.

Using (4.57) with (4.58) and (4.59), we obtain

$$\frac{d}{dt}|\mathbf{r}| = \left(\frac{\mathbf{r}}{|\mathbf{r}|}\cdot\mathbf{x}_2\right) = \mathrm{sgn}(\mathbf{r}\cdot\mathbf{y}_1)\mathbf{y}_1\cdot\mathbf{x}_2 = -\mathrm{sgn}(\mathbf{r}\cdot\mathbf{y}_1)\mathbf{x}_1\cdot\mathbf{y}_2\ , \tag{4.60}$$

where the function $\mathrm{sgn}(z)$ is

$$\begin{aligned} \mathrm{sgn}(z) = 1 \quad &\text{for} \quad z > 0 \\ \mathrm{sgn}(z) = 0 \quad &\text{for} \quad z = 0 \\ \mathrm{sgn}(z) = -1 \quad &\text{for} \quad z < 0\ . \end{aligned} \tag{4.61}$$

We can derive an expression for ν_1 by differentiating (4.58) with respect to time, to obtain

$$\begin{aligned} \frac{d}{dt}\left(\mathbf{r}\cdot\mathbf{x}_1\right) &= \dot{\mathbf{r}}\cdot\mathbf{x}_1 + \mathbf{r}\cdot\dot{\mathbf{x}}_1 \\ &= \left(\mathbf{x}_2 - \nu_1\mathbf{x}_1\right)\cdot\mathbf{x}_1 + \left(\frac{\mathbf{r}}{|\mathbf{r}|}\cdot\mathbf{y}_1\right)|\mathbf{r}|\nu_1\kappa_1 \\ &= \mathbf{x}_1\cdot\mathbf{x}_2 - \nu_1 + \mathrm{sgn}(\mathbf{r}\cdot\mathbf{y}_1)|\mathbf{r}|\nu_1\kappa_1 \\ &= 0, \end{aligned} \tag{4.62}$$

where we have used equations (4.58) and (4.59). We then have

$$\left(1 - \mathrm{sgn}(\mathbf{r}\cdot\mathbf{y}_1)|\mathbf{r}|\kappa_1\right)\nu_1 = \mathbf{x}_1\cdot\mathbf{x}_2, \tag{4.63}$$

and for simplicity we replace $-\mathrm{sgn}(\mathbf{r}\cdot\mathbf{y}_1)\kappa_1$ with $\pm|\kappa_1|$, leading, finally, to

$$\nu_1 = \frac{\mathbf{x}_1\cdot\mathbf{x}_2}{1 \pm |\kappa_1||\mathbf{r}|} > 0. \tag{4.64}$$

In (4.64), the plus sign is used when the boundary curves away from the moving vehicle, and the minus sign is used when the boundary curves inward

toward the moving vehicle. For example, if the boundary curve is a circle, then we use the plus sign when the vehicle is outside the circle and use the minus sign when the vehicle is inside the circle. In the latter case, we note that there is a singularity in the expression for ν_1 when $|\mathbf{r}| = 1/|\kappa_1|$ and the boundary curves inward toward the moving vehicle. Later we will see that this convention for determine the sign for curvature agrees with the convention we use in section 4.2 for a Bertrand family.

4.4.2 Shape variables

We would like to treat the moving vehicle and the closest point on the boundary as two interacting "vehicles" - one moving at unit speed, and the other not necessarily moving at unit speed - and then demonstrate analytically that the motion of the two "vehicles" converges to a steady-state "formation." This approach is easiest to describe if appropriate "shape variables," which depend only on the relative positions and orientations of the vehicles, can be identified. The formation is then an equilibrium for the shape dynamics, and is therefore a relative equilibrium for the dynamics in configuration space. However, in order to reduce the dynamics from configuration space to shape space, the control law must possess the symmetry group $SE(2)$.

In the proof for theorem 4.3.1, we showed that h_λ is invariant under the left action of symmetry group $SE(2)$. Hence as components for h_λ, the shape variables $|\mathbf{r}|$ and $\mathbf{x}_1 \cdot \mathbf{y}_2$ are invariant under the left action of symmetry group

$SE(2)$. Note that we can define the angle variable ϕ according to

$$\mathbf{x}_1 \cdot \mathbf{y}_2 = \sin\phi, \tag{4.65}$$

let $\rho = |\mathbf{r}|$, and instead use (ρ, ϕ) as shape variables.

We can express the shape dynamics as follows. From (4.60) we have

$$\dot{\rho} = -\mathrm{sgn}(\mathbf{r} \cdot \mathbf{y}_1) \sin\phi, \tag{4.66}$$

where $\mathrm{sgn}(\mathbf{r} \cdot \mathbf{y}_1)$ is constant on a segment of smooth curve.

Differentiating $\mathbf{x}_1 \cdot \mathbf{y}_2$ with respect to time gives

$$\begin{aligned}
\frac{d}{dt}(\mathbf{x}_1 \cdot \mathbf{y}_2) &= \dot{\mathbf{x}}_1 \cdot \mathbf{y}_2 + \mathbf{x}_1 \cdot \dot{\mathbf{y}}_2 \\
&= \nu_1\kappa_1(\mathbf{y}_1 \cdot \mathbf{y}_2) - u_2(\mathbf{x}_1 \cdot \mathbf{x}_2) \\
&= \left[\left(\frac{\mathbf{x}_1 \cdot \mathbf{x}_2}{1 \pm |\kappa_1||\mathbf{r}|}\right)\kappa_1 - u_2\right](\mathbf{x}_1 \cdot \mathbf{x}_2) \\
&= \left[\left(\frac{\kappa_1}{1 \pm |\kappa_1|\rho}\right)\cos\phi - u_2\right]\cos\phi,
\end{aligned} \tag{4.67}$$

where we have used (4.64). Since we also have

$$\frac{d}{dt}(\mathbf{x}_1 \cdot \mathbf{y}_2) = \frac{d}{dt}(\sin\phi) = (\cos\phi)\dot{\phi}, \tag{4.68}$$

we obtain

$$\dot{\phi} = \left(\frac{\kappa_1}{1 \pm |\kappa_1|\rho}\right)\cos\phi - u_2. \tag{4.69}$$

Thus, provided $u_2 = u_2(\rho, \phi)$, we see that the shape dynamics are self-contained.

4.4.3 System equations on $SE(2)$

The motion of both the vehicle and the closest point can be described on $SE(2)$. Let

$$g_1 = \begin{bmatrix} \mathbf{x}_1 & \mathbf{y}_1 & \mathbf{r}_1 \\ 0 & 0 & 1 \end{bmatrix}, \tag{4.70}$$

and

$$g_2 = \begin{bmatrix} \mathbf{x}_2 & \mathbf{y}_2 & \mathbf{r}_2 \\ 0 & 0 & 1 \end{bmatrix}. \tag{4.71}$$

Then the dynamics on $SE(2)$ can be written as

$$\begin{aligned} \frac{dg_1}{dt} &= g_1\xi_1 \\ \frac{dg_2}{dt} &= g_2\xi_2 \end{aligned} \tag{4.72}$$

where

$$\xi_1 = \begin{bmatrix} 0 & -\nu_1\kappa_1 & \nu_1 \\ \nu_1\kappa_1 & 0 & 0 \\ 0 & 0 & 0 \end{bmatrix}, \tag{4.73}$$

and

$$\xi_2 = \begin{bmatrix} 0 & -u_2 & 1 \\ u_2 & 0 & 0 \\ 0 & 0 & 0 \end{bmatrix}. \tag{4.74}$$

We note that this system is a time-varying system because ν_1 and κ_1 depend on time.

Next, we use $h = g_1^{-1} g_2$ to represent the shape of the formation formed by the vehicle and the closest point. Then

$$h = \begin{bmatrix} \mathbf{x}_1 \cdot \mathbf{x}_2 & \mathbf{x}_1 \cdot \mathbf{y}_2 & \mathbf{x}_1 \cdot (\mathbf{r}_2 - \mathbf{r}_1) \\ \mathbf{y}_1 \cdot \mathbf{x}_2 & \mathbf{y}_1 \cdot \mathbf{y}_2 & \mathbf{y}_1 \cdot (\mathbf{r}_2 - \mathbf{r}_1) \\ 0 & 0 & 1 \end{bmatrix} , \tag{4.75}$$

and the controlled system equation for the shape is

$$\frac{dh}{dt} = -\xi_1 h + h\xi_2 \, . \tag{4.76}$$

If u_2 is designed as a feedback law for the shape variables, then system (4.76) can be viewed as the shape dynamic equations for system (4.72).

4.5 Tracking of boundary curves

We want to understand what is a boundary tracking behavior for the vehicle. We say a vehicle *tracks* a boundary curve with separation r_c if the trajectory of the vehicle is a Bertrand mate of the boundary curve with $\lambda = r_c$. To produce such behavior, we propose two control laws. Under these control laws, the trajectory of the vehicle converges to a Bertrand mate of the boundary curve asymptotically.

4.5.1 The first control law and convergence proof

Let $f(\rho)$ be a smooth monotone increasing function on $(0, +\infty)$ such that

$$f(\rho) \;\; = \;\; 0 \;\; \text{when} \;\; \rho = r_c$$

$$
\begin{aligned}
-\frac{k_1}{2(1+k\,k_1)} < f(\rho) &< 0 \text{ when } 0<\rho<r_c \\
0 < f(\rho) &< \frac{k_1}{2(1+k\,k_1)} \text{ when } \rho > r_c\,.
\end{aligned} \tag{4.77}
$$

and

$$
f(\rho) \to \frac{k_1}{2(1+k\,k_1)} \text{ as } \rho \to +\infty\,, \tag{4.78}
$$

$$
|\int_0^{r_c} f(\rho)d\rho| < \infty\,, \tag{4.79}
$$

where $k>0$ and $k_1>0$. An example of such a function is

$$
f(\rho) = \frac{k_1}{\pi(1+k\,k_1)}\arctan(\rho - r_c)\,. \tag{4.80}
$$

We define

$$
l = \mathrm{sgn}(\mathbf{r}\cdot\mathbf{y}_1)\sin(\phi) - kf(\rho)\,. \tag{4.81}
$$

where $k>0$. Then by using the shape dynamics (4.66) and (4.69), and notice that $\mathrm{sgn}(\mathbf{r}\cdot\mathbf{y}_1)$ is constant, we have the following

$$
\begin{aligned}
\dot{l} &= \mathrm{sgn}(\mathbf{r}\cdot\mathbf{y}_1)\cos(\phi)\dot{\phi} - k\frac{df}{d\rho}\dot{\rho} \\
&= -\mathrm{sgn}(\mathbf{r}\cdot\mathbf{y}_1)\cos(\phi)u_2 + \mathrm{sgn}(\mathbf{r}\cdot\mathbf{y}_1)\frac{\kappa_1\,\cos^2(\phi)}{1\pm|\kappa_1|\rho} + \mathrm{sgn}(\mathbf{r}\cdot\mathbf{y}_1)k\frac{df}{d\rho}\,\sin(\phi) \\
\dot{\rho} &= -k\,f(\rho) - l\,.
\end{aligned} \tag{4.82}
$$

Proposition 4.5.1 *Given the control law*

$$
u_2 = \frac{1}{\cos(\phi)}\left(\frac{\kappa_1\,\cos^2(\phi)}{1\pm|\kappa_1|\rho} + k\frac{df}{d\rho}\sin(\phi) - \mathrm{sgn}(\mathbf{r}\cdot\mathbf{y}_1)(f(\rho)-k_1 l)\right) \tag{4.83}
$$

where the choice of $+$ or $-$ sign is determined by the shape of the curve and the position of the robot. Suppose all the curve segments which result in the

choice of $-$ sign have curvature bounded by a constant κ_c i.e. $|\kappa_1| \leq \kappa_c$. Furthermore, let

$$V(\rho, \phi) = \int_0^{\rho} f(z)dz + \frac{1}{2}l^2. \tag{4.84}$$

If the initial condition for the robot is such that $|cos(\phi(t_0))| \neq 0$ and

$$V(\rho(t_0), \phi(t_0)) < \min\{0, \int_0^{\frac{1}{\kappa_c}} f(z)dz\} \ , \tag{4.85}$$

then u_2 produces converging shape dynamics s.t. $\sin(\phi(t)) \to 0$ and $\rho(t) \to r_c$ as $t \to \infty$. In addition, the robot will not collide with the boundary curve segment where the closest point belongs.

Proof

We first prove that if the initial condition is such that $2n\pi \leq \phi(t_0) < 2n\pi + \pi/2$ where n is an integer, then $\phi(t) < 2n\pi + \pi/2$ for all $t > t_0$. In fact, under the proposed control law, one has

$$\begin{aligned} \dot{\phi} &= \frac{\kappa_1 \cos(\phi)}{1 \pm |\kappa_1|\rho} - u_2 \\ &= \frac{1}{\cos(\phi)} \left(-(k\frac{df}{d\rho} + k_1)\sin(\phi) + \text{sgn}(\mathbf{r} \cdot \mathbf{y}_1)(1 + k\, k_1) f(\rho) \right) \\ &< \frac{1}{\cos(\phi)} \left(-(k\frac{df}{d\rho} + k_1)\sin(\phi) + \frac{k_1}{2} \right). \end{aligned} \tag{4.86}$$

Because $df/d\rho > 0$, if $\phi(t) \in (2n\pi, 2n\pi + \pi/2)$, then

$$(k\frac{df}{d\rho} + k_1)\sin(\phi) > 0 \ . \tag{4.87}$$

Furthermore, for a given ρ, there exists $\epsilon(\rho, \delta) > 0$ such that if $\phi(t) \in (2n\pi + \pi/2 - \epsilon, 2n\pi + \pi/2)$, then

$$(k\frac{df}{d\rho} + k_1)\sin(\phi) > \frac{k_1}{2} \ . \tag{4.88}$$

Therefore, it is clear that $\dot{\phi}(t) < 0$ if $\phi(t) \in (2n\pi + \pi/2 - \epsilon, 2n\pi + \pi/2)$. We deduce that $\phi(t) < 2n\pi + \pi/2$ for all $t > t_0$ given $2n\pi \leq \phi(t_0) < 2n\pi + \pi/2$.

Next, we prove that if the initial condition is such that $2n\pi - \pi/2 < \phi(t_0) \leq 2n\pi$, then $\phi(t) > 2n\pi - \pi/2$ for all $t > t_0$.

In fact, under the proposed control law, one has

$$\begin{aligned} \dot{\phi} &= \frac{\kappa_1 \cos(\phi)}{1 \pm |\kappa_1|\rho} - u_2 \\ &= \frac{1}{\cos(\phi)} \left(-(k\frac{df}{d\rho} + k_1)\sin(\phi) + \mathrm{sgn}(\mathbf{r} \cdot \mathbf{y}_1)(1 + k\,k_1) f(\rho) \right) \\ &> \frac{1}{\cos(\phi)} \left(-(k\frac{df}{d\rho} + k_1)\sin(\phi) - \frac{k_1}{2} \right). \end{aligned} \tag{4.89}$$

Because $df/d\rho > 0$, if $\phi(t) \in (2n\pi - \pi/2, 2n\pi)$, then

$$(k\frac{df}{d\rho} + k_1)\sin(\phi) < 0\ . \tag{4.90}$$

Furthermore, for a given ρ, there exists $\epsilon'(\rho, \delta) > 0$ such that if $\phi(t) \in (2n\pi - \pi/2, 2n\pi - \pi/2 + \epsilon')$, then

$$-(k\frac{df}{d\rho} + k_1)\sin(\phi) > \frac{k_1}{2}\ . \tag{4.91}$$

Therefore, it is clear that $\dot{\phi}(t) > 0$ if $\phi(t) \in (2n\pi - \pi/2, 2n\pi - \pi/2 + \epsilon')$. We deduce that $\phi(t) > 2n\pi - \pi/2$ for all $t > t_0$ given $2n\pi - \pi/2 < \phi(t_0) \leq 2n\pi$.

By similar argument, we can show that $\phi(t) \in (2n\pi + \pi/2, 2n\pi + 3\pi/2)$ for all $t > t_0$ given $2n\pi + \pi/2 < \phi(t_0) \leq 2n\pi + 3\pi/2$. Therefore, our control law is well defined for all $t > t_0$, if initially $\cos(\phi(t_0)) \neq 0$. This statement also confirms that $\mathrm{sgn}(\mathbf{r} \cdot \mathbf{y}_1)$ is a constant under the controlled dynamics.

Let a candidate Lyapunov function be $V = \int_0^{\rho} f(z)dz + \frac{1}{2}l^2$.This function is bounded below by $\int_0^{r_c} f(z)dz$. Then

$$\begin{aligned}
\dot{V} &= f(\rho)(-kf(\rho) - l) \\
&+ l(-\text{sgn}(\mathbf{r}\cdot\mathbf{y}_1)\cos(\phi)u_2 + \text{sgn}(\mathbf{r}\cdot\mathbf{y}_1)\frac{\kappa\cos^2(\phi)}{1 \pm |\kappa|\rho} + \text{sgn}(\mathbf{r}\cdot\mathbf{y}_1)k\frac{df}{d\rho}\sin(\phi)) \\
&= f(\rho)(-kf(\rho) - l) + l(f(\rho) - k_1 l) \\
&= -k\, f^2(\rho) - k_1 l^2 \leq 0 \qquad (4.92)
\end{aligned}$$

with $\dot{V} = 0$ iff $\rho = r_c$ and $l = 0$. Therefore, by Lyapunov stability theory, $l \to 0$ and $\rho \to r_c$ as $t \to \infty$. This further implies that $\sin(\phi) \to 0$.

If during the convergent process $\rho = 0$, then the robot collides with the obstacle. Notice that when $\rho = 0$, the minimum value for the Lyapunov function V is 0. Therefore, if the initial condition for the robot satisfies

$$V(\rho(t_0), \phi(t_0)) < 0\ , \qquad (4.93)$$

then because along the controlled robot dynamics V is decreasing, the robot will not assumes the state where $\rho = 0$. Thus the whole path is collision free.

On the other hand, the condition $V(\rho(t_0), \phi(t_0)) < \int_0^{\frac{1}{\kappa_c}} f(z)dz$ guarantees that on the trajectory of the robot, if the $-$ sign is chosen in u_2, then the control u_2 does not go to infinity. ■

The limiting case $\sin(\phi) = 0$ has two possible solutions: $\phi = 2n\pi$ or $\phi = 2n\pi + \pi$. Which solution is achieved depends on the initial value $\phi(t_0)$, which is determined by the choice of positive direction of the boundary curve. If the positive direction of the curve is chosen so that $\mathbf{x}_1(t_0)\cdot\mathbf{x}_2(t_0) > 0$, then

$\phi(t_0) \in (2n\pi - \pi/2, 2n\pi + \pi/2)$ so that $\phi \to 2n\pi$. The vehicle moves to the same direction as the positive direction of the curve. If $\mathbf{x}_1(t_0) \cdot \mathbf{x}_2(t_0) < 0$, then $\phi(t_0) \in (2n\pi + \pi/2, 2n\pi + 3\pi/2)$ so that $\phi \to 2n\pi + \pi$. The vehicle moves against the positive direction of the curve. Comparing the two cases, we conclude that the direction of the limiting vehicle motion is independent of the choice of the positive direction of the boundary curve. Therefore, for simplicity, we may assign positive direction to a boundary curve by always requiring $\mathbf{x}_1(t_0) \cdot \mathbf{x}_2(t_0) > 0$. Therefore the limiting motion of the vehicle always achieves $\phi \to 2n\pi$.

4.5.2 Stabilized relative equilibrium

As $t \to \infty$, because $\phi(t) \to 2n\pi$, we have

$$h_0 = \lim_{t\to\infty} h(t) = \lim_{t\to\infty} g_1^{-1} g_2 = \begin{bmatrix} 1 & 0 & 0 \\ 0 & 1 & \pm r_c \\ 0 & 0 & 1 \end{bmatrix} , \tag{4.94}$$

$$u_2(t) \to \frac{\kappa_1}{1 \pm |\kappa_1| r_c} \tag{4.95}$$

and

$$\nu_1(t) \to \frac{1}{1 \pm |\kappa_1| r_c} . \tag{4.96}$$

Then

$$\xi_1(t) \to \begin{bmatrix} 0 & -\frac{\kappa_1}{1\pm|\kappa_1|r_c} & \frac{1}{1\pm|\kappa_1|r_c} \\ \frac{\kappa_1}{1\pm|\kappa_1|r_c} & 0 & 0 \\ 0 & 0 & 0 \end{bmatrix} \tag{4.97}$$

and

$$\xi_2(t) \to \begin{bmatrix} 0 & -\frac{\kappa_1}{1\pm|\kappa_1|r_c} & 1 \\ \frac{\kappa_1}{1\pm|\kappa_1|r_c} & 0 & 0 \\ 0 & 0 & 0 \end{bmatrix}. \tag{4.98}$$

The limiting vehicle trajectory is a Bertrand mate to the boundary curve. To see this, we denote the limiting trajectory as $(g_\infty(t), \kappa_\infty(t))$ and its corresponding Lie algebra as ξ_∞ i.e. $\xi_2(t) \to \xi_\infty(t)$. This curve satisfies the following differential equation on $SE(2)$

$$\begin{aligned} \dot{g}_\infty &= g_\infty \xi_\infty \\ &= g_\infty \begin{bmatrix} 0 & -\kappa_\infty & 1 \\ \kappa_\infty & 0 & 0 \\ 0 & 0 & 0 \end{bmatrix}. \end{aligned} \tag{4.99}$$

We use this limiting trajectory as the reference curve. Comparing equation (4.98) with equation (4.99), it is clear that

$$\frac{\kappa_1}{1 \pm |\kappa_1| r_c} = \kappa_\infty \tag{4.100}$$

hence

$$\kappa_1 = \frac{\kappa_\infty}{1 + \mathrm{sgn}(\mathbf{r} \cdot \mathbf{y}_1)\kappa_\infty r_c} \tag{4.101}$$

Then if we use t as parameter, the boundary curve $(g_1(t), \kappa_1(t))$ satisfies

$$\dot{g}_1 = g_1 \begin{bmatrix} 0 & -\kappa_\infty & 1 + \mathrm{sgn}(\mathbf{r} \cdot \mathbf{y}_1)\kappa_\infty r_c \\ \kappa_\infty & 0 & 0 \\ 0 & 0 & 0 \end{bmatrix}. \tag{4.102}$$

We can rewrite

$$1 + \text{sgn}(\mathbf{r} \cdot \mathbf{y}_1)\kappa_\infty r_c = 1 - \kappa_\infty \lambda \tag{4.103}$$

if we let $\lambda = -\text{sgn}(\mathbf{r} \cdot \mathbf{y}_1)r_c$. Comparing to the definition for Bertrand mate in section 4.2, we immediately see that in the steady state, $g_1(t)$ and $g_\infty(t)$ form a Bertrand pair with $g_\infty(t)$ serving as the reference curve.

Proposition 4.5.1 tells us that the relative equilibrium $h(t) = h_0$ is asymptotically stable for initial values $h(0) \in SE(2)$ except for the ones with $\cos(\phi(0)) = 0$. Starting with $h(0)$, the trajectory of the vehicle converges to a Bertrand mate of the boundary curve. On the other hand, the initial condition $\cos(\phi(0)) = 0$ is unstable. Therefore, due to existence of noise, the vehicle will not adhere to this condition.

4.5.3 Tracking piece-wise smooth curves

In reality, instead of being regular, almost all boundary curves are only piecewise regular. For example, obstacles with polygonal shape appear everywhere. We say a point on the boundary is a *vertex* if the tangent vector at this point is not well-defined. Suppose a vertex appears when $s = s_0$. Then if a tangent vector on each side of the vertex is well defined, i.e. $\lim_{s \to s_0^+} d\mathbf{r}/ds$ and $\lim_{s \to s_0^-} d\mathbf{r}/ds$ exists, we say the vertex is of *type one*. At a type one vertex, there is a sudden change in the direction of the curve.

There are possibilities that the closest point may be a vertex. If this

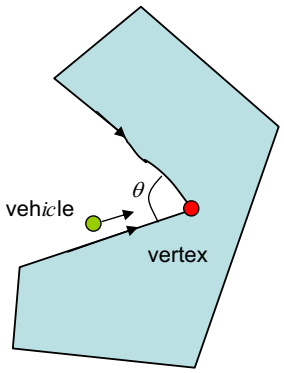

Figure 4.2: *A crack with a type one vertex. Under the first control law, the vehicle will crash with the vertex.*

happens, we assign a unit tangent vector $\mathbf{x}_1$ to the vertex such that

$$\mathbf{r} \cdot \mathbf{x}_1 = 0 \tag{4.104}$$

is still enforced. We may also let $\kappa_1 = 0$ at the vertex. As long as there are only finitely many vertices, and the curve segments between vertices are sufficient long, then the vehicle may use our first control law to track the regular boundary curve segments. Near the vertices, the vehicle will be disturbed by the discontinuity in the direction of tangent vector and in curvature. It will deviate from the Bertrand mate of the regular boundary curve segments. However, since the discontinuity only happens at the vertex, the vehicle will come back to follow the Bertrand mate under the first control law.

A more severe problem caused by vertices is the possible existence of a

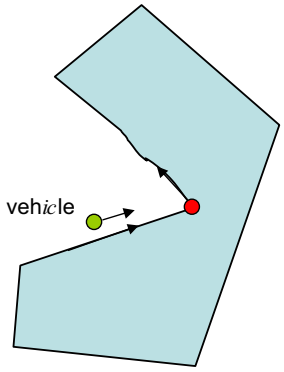

Figure 4.3: *A crack with new convention for the direction of the curve. Under the second control law, the vehicle will track the boundary in given direction.*

crack, that is, two segments of boundary near a type one vertex shown in Figure 4.2. When the direction of the boundary curve is chosen as shown, the angle θ is less than or equal to $\pi/2$. If a vehicle moves in the crack i.e. the space between the two curve segments near the vertex, then under our first control law, the vehicle will be guided toward the vertex and eventually collide with the obstacle, as shown in Figure 4.2.

To solve this problem, a new convention is needed. When the vehicle detects a crack, we assign the clock-wise or counter clock-wise direction as the positive direction for all the detected curve segments that form the crack. Therefore, the closest point detected by the vehicle in the crack may result in $\phi \in (-\pi, +\pi)$, instead of $(-\pi/2, \pi/2)$ restricted by the previous convention. This new convention is shown in Figure 4.3.

We also need a new boundary tracking control law, which enables the

vehicle to track boundary curves in an assigned positive direction. Such a control law would complement the first control law which perform the tracking in a direction that is independent of the direction of a boundary curve. We follow the similar process in deriving the first control law by starting from the shape dynamics

$$\begin{aligned} \dot{\rho} &= -\text{sgn}(\mathbf{r}\cdot\mathbf{y}_1)\sin(\phi) \\ \dot{\phi} &= \left(\frac{\kappa_1}{1\pm|\kappa_1|\rho}\right)\cos\phi - u_2. \end{aligned} \tag{4.105}$$

Let $\widetilde{f}(\rho)$ be a smooth monotone increasing function on $(0,+\infty)$, with $\widetilde{f}(\rho) = 0$ if and only if $\rho = r_c$. Define

$$l = \text{sgn}(\mathbf{r}\cdot\mathbf{y}_1)2\sin(\phi/2) - k\widetilde{f}(\rho)\ . \tag{4.106}$$

Then

$$\begin{aligned} \dot{\rho} &= -\cos(\frac{\phi}{2})k\,\widetilde{f}(\rho) - \cos(\frac{\phi}{2})\,l \\ \dot{l} &= -\text{sgn}(\mathbf{r}\cdot\mathbf{y}_1)\cos(\frac{\phi}{2})u_2 + \text{sgn}(\mathbf{r}\cdot\mathbf{y}_1)\frac{\kappa_1\cos(\phi)\cos(\frac{\phi}{2})}{1\pm|\kappa_1|\rho} \\ &\quad +\text{sgn}(\mathbf{r}\cdot\mathbf{y}_1)k\frac{d\widetilde{f}}{d\rho}\sin(\phi). \end{aligned} \tag{4.107}$$

The control law u_2 is designed as

$$u_2 = \frac{\kappa_1\cos(\phi)}{1\pm|\kappa_1|\rho} + 2k\frac{d\widetilde{f}}{d\rho}\sin(\phi/2) - \text{sgn}(\mathbf{r}\cdot\mathbf{y}_1)\left(\widetilde{f}(\rho) - k_1 l\right) \tag{4.108}$$

so that

$$\dot{l} = \cos(\frac{\phi}{2})\,(\widetilde{f}(\rho) - k_1 l) \tag{4.109}$$

where $k_1 > 0$.

We now prove the convergence of the controlled dynamics. The Lyapunov candidate function is

$$V = \hbar(\rho) + \frac{1}{2} l^2 \ . \tag{4.110}$$

where $\hbar(\cdot)$ is continuously differentiable and satisfies the following hypotheses.

(A1) $d\hbar/d\rho = \widetilde{f}(\rho)$, where $\widetilde{f}(\rho)$ is a smooth monotone increasing function on $(0, \infty)$, so that $\hbar(\rho)$ is continuously differentiable on $(0, \infty)$;

(A2) $\widetilde{f}(r_c) = 0$ and $\widetilde{f}(\rho) \neq 0$ if $\rho \neq r_c$;

(A3) $\frac{d\widetilde{f}}{d\rho} > \frac{1+k_1 k}{k} |\widetilde{f}(\rho)| - \frac{k_1}{k}$;

(A4) $\lim_{\rho \to 0} \hbar(\rho) = \infty$, $\lim_{\rho \to \infty} \hbar(\rho) = \infty$, and $\exists \widetilde{\rho}$ such that $\hbar(\widetilde{\rho}) = 0$.

With control u_2 given, we now compute its derivative as

$$\begin{aligned} \dot{V} &= \widetilde{f}(\rho)\dot{\rho} + l\,\dot{l} \\ &= \widetilde{f}(\rho)(-\cos(\frac{\phi}{2}) k\, \widetilde{f}(\rho) - \cos(\frac{\phi}{2})\, l) + l(\cos(\frac{\phi}{2})\widetilde{f}(\rho) - \cos(\frac{\phi}{2}) k_1 l) \\ &= -\cos(\frac{\phi}{2})\, k\, \widetilde{f}^2(\rho) - \cos(\frac{\phi}{2})\, k_1\, l^2 \leq 0 \ . \end{aligned} \tag{4.111}$$

If $\phi(t) \in (-\pi, +\pi)$, then $\dot{V} = 0$ if and only if $\widetilde{f}(\rho) = 0$ and $l = 0$. While $\widetilde{f}(\rho) = 0$ implies that $\rho = r_c$, $l = 0$ is used to conclude $\sin(\frac{\phi}{2}) = 0$, which gives one unique answer $\phi = 0$. Therefore, by Lyapunov stability theorem, the system dynamics under control law u_2 converges asymptotically to the equilibrium $\rho = r_c$ and $\phi = 0$.

When $\rho \to 0$, the function $V \to \infty$. Then if the robot start with a state $\rho \neq 0$, the value of V is finite. Along the controlled dynamics V will decrease. Therefore, the robot will not collide with any obstacle.

We notice that the configuration when $\phi = \pm\pi$ is unstable. Because of condition (A3), by similar analysis for the first control law, we know that slight perturbation of the angle ϕ will cause the vehicle converging to $\phi = 0$. In reality, since ϕ is measured by noisy sensors, we almost never can get $\phi = \pm\pi$ exactly. Therefore, we consider this as a problem that can be omitted. In summary, we have proved the following proposition.

Proposition 4.5.2 *Given control law u_2 as in equation (4.108). Suppose all the curve segments which result in the choice of $-$ sign in u_2 have curvature bounded by a constant κ_c i.e. $|\kappa_1| \leq \kappa_c$. If the initial condition $\phi(t_0) \in (-\pi, \pi)$ and*

$$V(\rho(t_0), \phi(t_0)) < \hbar(\frac{1}{\kappa_c}) \,, \tag{4.112}$$

then the control law given by (4.108) produces converging shape dynamics s.t. $\phi(t) \to 0$ and $\rho(t) \to r_c$ as $t \to \infty$. Furthermore, the robot will not collide with the boundary curve where the closest point belongs.

We point out that there exists functions $\widetilde{f}(\rho)$ and $\hbar(\rho)$ which satisfy the conditions (A1)-(A4). We let

$$\widetilde{f}(\rho) = \frac{k_1}{1 + k_1\, k}(1 - \frac{r_c}{\rho}) \,. \tag{4.113}$$

This function is clearly monotone increasing with $\widetilde{f}(\rho) = 0$ if and only if $\rho = r_c$. We then need to verify condition (A3). First, we noticed that if

$\rho \geq r_c$, then because

$$0 \leq \widetilde{f}(\rho) < \frac{k_1}{1 + kk_1} \, , \tag{4.114}$$

it is true that

$$\frac{d\widetilde{f}}{d\rho} > 0 > \frac{1 + k_1 k}{k} \, \widetilde{f}(\rho) - \frac{k_1}{k} \, . \tag{4.115}$$

Next, when $\rho < r_c$, we want to show

$$\frac{k_1}{1 + k_1 \, k} \frac{r_c}{\rho^2} > -\frac{k_1}{k}(1 - \frac{r_c}{\rho}) - \frac{k_1}{k} \, , \tag{4.116}$$

which is equivalent to show

$$2\rho^2 - r_c \rho + \frac{k}{1 + k_1 k} r_c > 0 \, . \tag{4.117}$$

Suppose we select the value of k and k_1 so that

$$r_c < \frac{8 \, k}{1 + k_1 \, k} \, . \tag{4.118}$$

Then the inequality (4.117) is satisfied. Therefore, the condition (A3) is satisfied. Then an $\hbar(\rho)$ that satisfies condition (A4) is

$$\hbar(\rho) = \frac{k_1}{1 + k_1 \, k} \left(\rho - r_c \log(\rho) - r_c + r_c \log(r_c) \right) \tag{4.119}$$

with $\hbar(r_c) = 0$.

4.6 Simulation results of boundary tracking

In this section we present simulation results verifying the two boundary tracking control laws. Our simulated robot is equipped with 32 range sensors

evenly distributed across the 360 degree perimeter of the robot. Since the angle between two sensor rays are not arbitrarily small, the movement of the closest point could be discontinuous. We will see this effect in the results.

To test the first control law, we use an elliptic obstacle with smooth boundary curve. The trajectories are shown in figure 4.6, the initial condition of the robot determines the direction of the trajectory circling the obstacle.

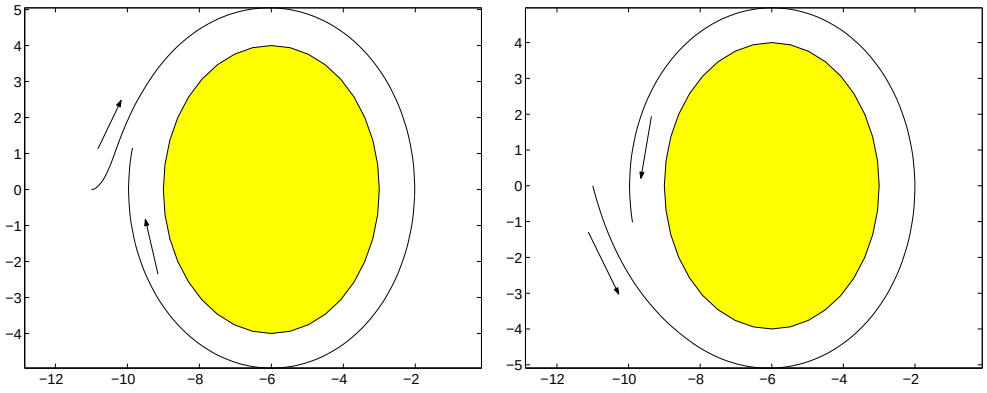

(a) $\phi(0) < 0$ (b) $\phi(0) > 0$

Figure 4.4: *Trajectories of boundary tracking of an elliptic obstacle.*

The shape variables ϕ and ρ are plotted in figure 4.5(a) and 4.5(b). One can see the averaged value for the angle ϕ converges to 0. The averaged value for ρ converges to 0.95 which is very close to 1, the designated separation. The curvature value at the closest point is plotted in 4.5(c). We see oscillations in all these data. This is because there are limited number of sensor rays, therefore the detected closest point could be jumping from one ray to another,

causing discontinuities.

We then use a nonconvex polygon as the obstacle to test the first tracking control law. The trajectories are shown in figure 4.6. Again, the direction of the trajectories are determined by the initial orientation of the robot.

The shape variables ϕ and ρ corresponding to figure 4.6(a) are plotted in figure 4.7(a) and 4.7(b). We see clearly that vertices cause large disturbances in ϕ and ρ. Here the designated value for ρ is 0.6. One can see that after each vertex the control law tries to control ϕ and ρ back to the desired value. But from the data of ϕ and ρ it is difficult to recognize when a vertex is detected.

The curvature value at the closest point is plotted in figure 4.7(c). We discovered that the upward and downward spikes in this curvature plot has clearly indicated where the vertices are. The eight spikes in the curvature plot correspond to the eight vertices of the obstacle.

Under the second control law, the robot always circling the obstacle in the same direction. For the elliptic obstacle, the trajectory is plotted in figure 4.6.

The shape variables ϕ and ρ for figure 4.8(a) are plotted in figure 4.9(a) and 4.9(b). The curvature value at the closest point is plotted in figure 4.9(c). The plots are quite similar to those of the first tracking control law.

We then used a polygon with a crack to test the boundary tracking ability of the second control law. The trajectory is shown in figure 4.6. We see that the tracking is successful.

The shape variables ϕ and ρ are plotted in 4.10(a) and 4.10(b). Again

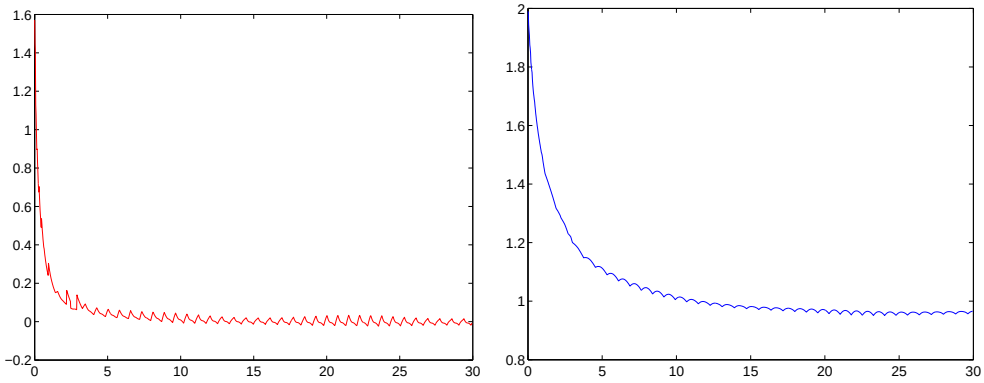

(a) $\phi(t)$ (b) $\rho(t)$

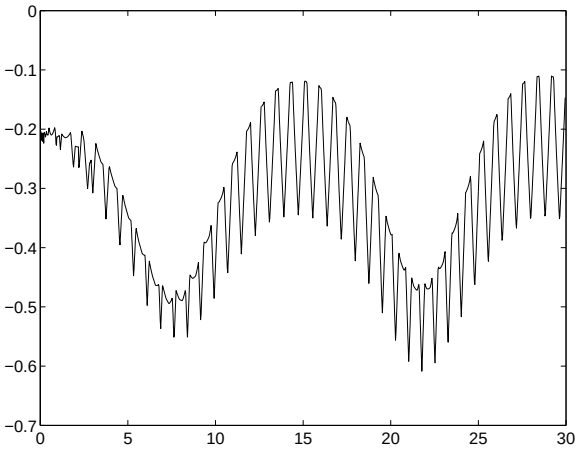

(c) $\kappa_1(t)$

Figure 4.5: *Shape variables and curvature measured at the closest point when tracking an elliptic obstacle.*

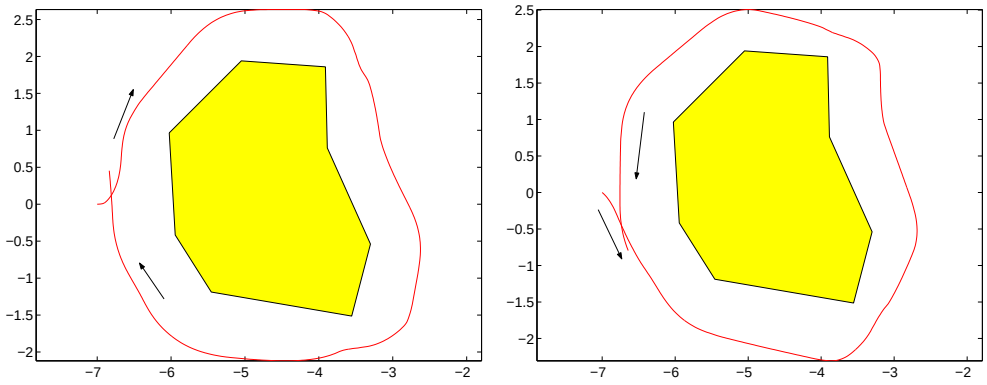

(a) $\phi(0) < 0$ (b) $\phi(0) > 0$

Figure 4.6: *Trajectories of boundary tracking of a nonconvex polygon.*

we see big disturbances caused by the vertices. The curvature value at the closest point is plotted in 4.10(c). The spikes in the curvature measurements correspond to the vertices with one exception. The vertex that serves as the peak of the crack is never a closest point to the robot. Therefore, there is no corresponding spike in the curvature plot.

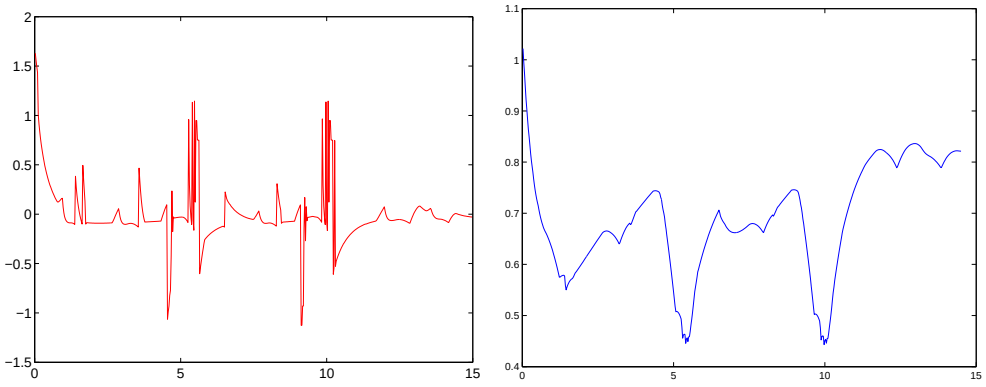

(a) $\phi(t)$ (b) $\rho(t)$

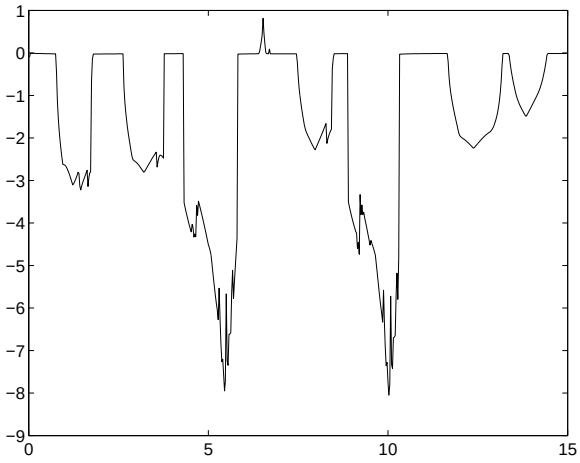

(c) $\kappa_1(t)$

Figure 4.7: *Shape variables and curvature measured at the closest point when tracking a nonconvex polygon.*

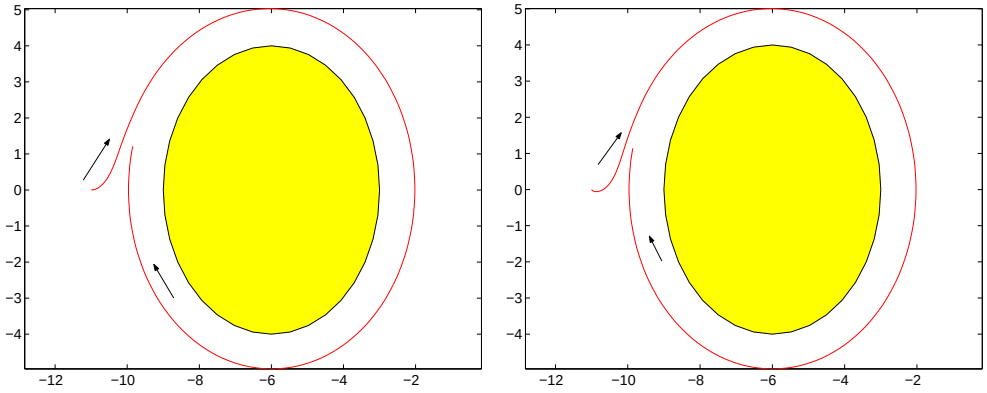

(a) $\phi(0) < 0$ (b) $\phi(0) > 0$

Figure 4.8: *Trajectories of boundary tracking of an elliptic obstacle, using the second control law.*

4.7 Navigation using boundary tracking behaviors

We consider a plane with finitely many static obstacles, each one is modeled as a simply connected compact set with a smooth boundary curve with bounded curvature. A moving vehicle on this plane has the ability to detect a fixed point target located at the origin of a right handed coordinate system with the direction of the X-axis arbitrarily chosen. Furthermore, we assume that for each obstacle, there exists a cone with its apex located at the origin such that the obstacle is contained in the cone. Notice that the cones mentioned here all have open angles less than π.

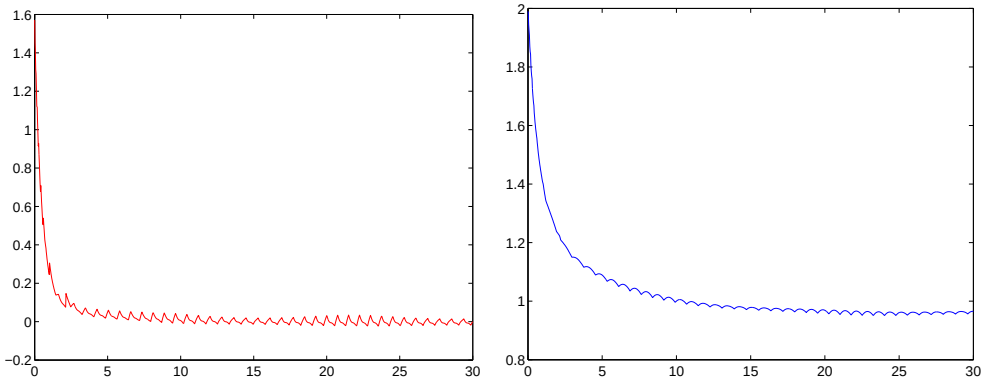

(a) $\phi(t)$ (b) $\rho(t)$

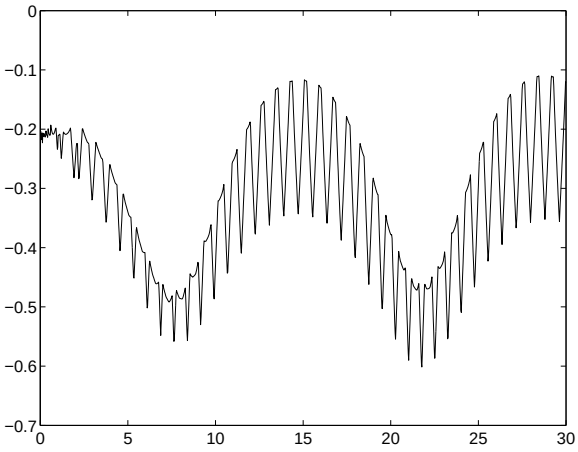

(c) $\kappa_1(t)$

Figure 4.9: *Shape variables and curvature measured at the closest point when tracking an elliptic obstacle, using the second control law.*

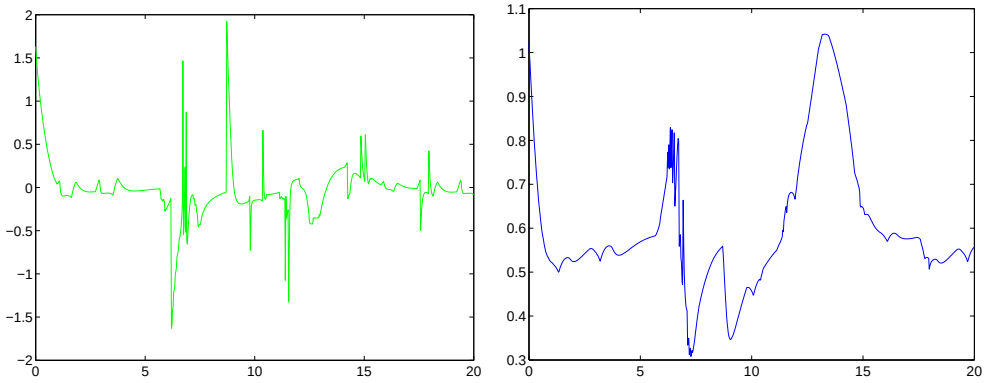

(a) $\phi(t)$ (b) $\rho(t)$

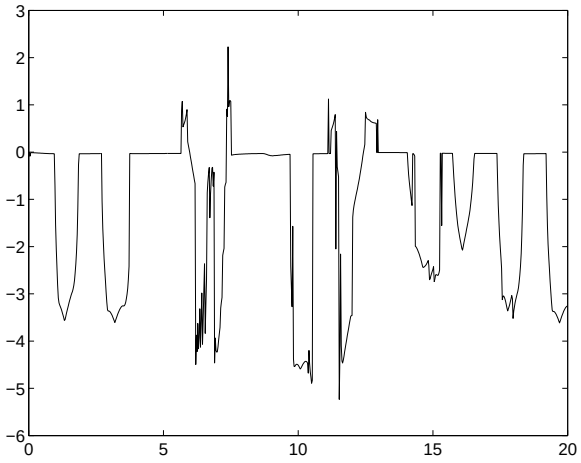

(c) $\kappa_1(t)$

Figure 4.10: *Shape variables and curvature measured at the closest point when tracking a nonconvex polygon, using the second control law.*

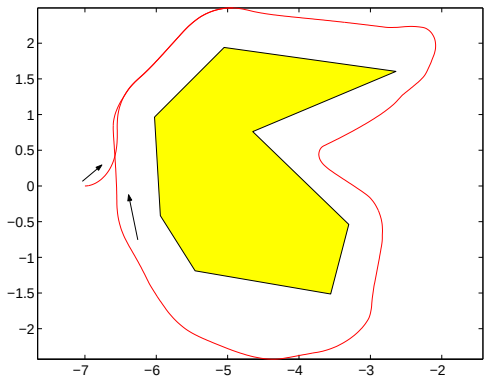

Figure 4.11: *Trajectories of boundary tracking of a nonconvex polygon, using the second control law.*

The vehicle is able to detect segments of the boundary curves of obstacles by using sensor rays and is able to estimate the tangent vector and curvature of the boundary curve at any detected point. As an idealization, we suppose that each sensor ray has infinite range of detection. Furthermore, the vehicle has enough sensor rays that are able to scan a full 360 degree view. Our goal is to design a control law which enables the vehicle to get within a small neighborhood of the target without colliding with any of the obstacles.

4.7.1 Virtual boundary segments

For each obstacle denoted by Ob_j where $(j = 1, 2, 3, ..., N)$, we define a set H_j to be the set of all line segments connecting points of the set Ob_j and the target $\mathbf{o}$.

$$H_j = \{\mathbf{q}(x, y) | \mathbf{q} = t\mathbf{o} + (1 - t)\mathbf{b}, t \in [0, 1], \mathbf{b} \in Ob_j\} \tag{4.120}$$

For convenience of discussion, we denote the boundary curve of Ob_j by Γ_j, denote the boundary curve of H_j by Λ_j, as shown in Figure 4.12. We want to know the structure of Λ_j.

From figure 4.12, it is intuitive that Λ_j contains two straight line segments $\mathbf{o\bar{w}}_1$ and $\mathbf{o\bar{w}}_2$ and part of Γ_j. We shall rigorously prove this.

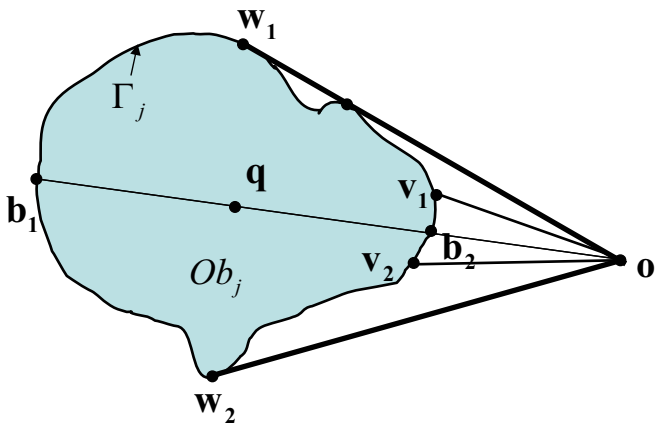

Figure 4.12: *The construction of virtual boundary curve segments.*

Claim 4.7.1 *H_j can be constructed as the collection of all line segments that connect points of Γ_j and* $\mathbf{o}$

Proof

Let

$$H_j^1 = \{\mathbf{q_1}(x,y) | \mathbf{q_1} = t_1\mathbf{o} + (1-t_1)\mathbf{b}_1, t_1 \in [0,1], \mathbf{b}_1 \in \Gamma_j\} \tag{4.121}$$

For any $\mathbf{q}_1 \in H_j^1$, because $\mathbf{b}_1 \in \Gamma_j \subset Ob_j$, we know $\mathbf{q}_1 \in H_j$. Hence $H_j^1 \subset H_j$. On the other hand, for any $\mathbf{q} \in H_j$, if $\mathbf{b} \in \text{int}(Ob_j)$, one can extend the ray $\vec{\mathbf{ob}}$

so that this ray intersects with Γ_j at point $\mathbf{b}_1$. One can do this because Ob_j is compact. Then a reparametrization shows $\mathbf{q} \in H_j^1$. Therefore $H_j \subset H_j^1$.

■

Claim 4.7.2 *The boundary curve of H_j passes through $\mathbf{o}$ i.e. $\mathbf{o} \in \Lambda_j$.*

Proof

Use proof by contradiction. We assume that $\mathbf{o}$ is in the interior of H_j i.e. $\mathbf{o} \in \text{int}(H_j)$. Then consider a ray emit from $\mathbf{o}$. The ray intersects Γ_j at some point $\mathbf{b}_1$. When the ray sweeps 360 degree the intersection point traces a closed curve that encircles $\mathbf{o}$. This contradicts with the assumption that Ob_j is contained in a cone with its peak point at $\mathbf{o}$. ■

Claim 4.7.3 *The boundary curve of H_j contains two segments of straight lines $\mathbf{ow}_1$ and $\mathbf{ow}_2$ where $\mathbf{w}_1, \mathbf{w}_2 \in \Gamma_j$. The extensions of the straight line segments beyond $\mathbf{w}_1$ and $\mathbf{w}_2$ have no more intersection with Ob_j.*

Proof

Because Ob_j is compact, each straight line segment that connects $\mathbf{o}$ with a point on Γ_j must has a intersection $\mathbf{b}_1$ with Γ_j such that the distance between $\mathbf{o}$ and $\mathbf{b}_1$ is the maximum among all the intersections between Ob_j and the straight line. If the line segment $\mathbf{ob}_1$ has another intersection $\mathbf{b}_2$ with Γ_j such that the line segment $\mathbf{b}_1\mathbf{b}_2 \in Ob_j$, then the boundary curve Γ_j is partitioned into two parts with each part lying on one side of the line $\mathbf{b}_1\mathbf{b}_2$, as shown in Figure 4.12. Hence at the point $\mathbf{b}_2$, we can find a small boundary segment with its points on both sides of $\mathbf{b}_1\mathbf{b}_2$. Connecting the two end points of such

segments, $\mathbf{v}_1$ and $\mathbf{v}_2$ with $\mathbf{o}$, we can see that $\mathbf{ov}_1 \in H_j$ and $\mathbf{ov}_2 \in H_j$. We observe that there exists a small enough neighborhood of $\mathbf{b}_2$ with radius less than $\| \mathbf{b}_2\mathbf{v}_1 \|$ and $\| \mathbf{b}_2\mathbf{v}_2 \|$ that is entirely contained in H_j. Therefore, $\mathbf{b}_2$ is not on the boundary of H_j. This implies that $\mathbf{ob}_2$ is not part of the boundary of H_j. Thus for $\mathbf{ob}_1$ to be part of the boundary curve of H_j, $\mathbf{b}_1$ and all the intersections between $\mathbf{ob}_1$ and Ob_j must be tangent points. Therefore, $\mathbf{ob}_1$ must be a tangent line of the boundary of Ob_j.

Because Ob_j can be contained in a cone with its apex at $\mathbf{o}$, there exists tangent lines like $\mathbf{ob}_1$. We can only have two such tangent lines because if there is a third one, one line must lie between the other two, hence fails to be a segment of the boundary curve. Therefore, we can find points $\mathbf{w}_1$ and $\mathbf{w}_2$ on Γ_j where $\mathbf{ow}_1$ and $\mathbf{ow}_2$ are tangent to the boundary curve Γ_j so that $\mathbf{ow}_1$ and $\mathbf{ow}_2$ are boundary segments of H_j. We name the tangent points with maximum distance to $\mathbf{o}$ along the lines as $\mathbf{w}_1$ and $\mathbf{w}_2$. ■

Definition 4.7.4 *We define the two straight line segments* $\mathbf{ow}_1$ *and* $\mathbf{ow}_2$ *as* **virtual boundary segments** *of the set* H_j.

Claim 4.7.5 *For any point* $\mathbf{w} \in \Gamma_j$, Ob_j *lies entirely on one side of a line obtained by extending the segment* $\mathbf{ow}$, *if and only if* $\mathbf{ow} \subset \mathbf{ow}_1 \cup \mathbf{ow}_2$.

Proof

If $\mathbf{ow} \subset \mathbf{ow}_1 \cup \mathbf{ow}_2$, without loss of generality, suppose $\mathbf{ow}$ is aligned with $\mathbf{ow}_1$. Then by definition, all points in this line that belongs to Ob_j are tangent points. Now, suppose there are points belong to Ob_j on both sides of the

extended line $\mathbf{ow}_1$. Because Ob_j is simply connected, there exists a path that connect these two points and lies entirely within int(Ob_j). Such path must intersect $\mathbf{ow}_1$ and the intersection point can not be a tangent point because it is not a boundary point of Ob_j. Therefore, by contradiction, we proved that Ob_j is located on one side of the extended line.

If we know Ob_j is located on one side of the extended line $\mathbf{ow}$, $\mathbf{w}$ must be a tangent point and all possible intersections between the extended line and Ob_j must be tangent points, because otherwise there will be boundary points of Ob_j on both sides of the line. Therefore, $\mathbf{ow}$ is a virtual segment that passes through $\mathbf{o}$. As mentioned before, the only two possible lines are $\mathbf{ow}_1$ and $\mathbf{ow}_2$. Hence $\mathbf{ow} \subset \mathbf{ow}_1 \cup \mathbf{ow}_2$. ■

4.7.2 Detection of virtual boundary

We already developed a boundary following control law. Is it possible to use such a control law to allow the vehicle to move towards the target? One answer may be to enable the robot to follow the virtual boundary segments instead of the true boundary curve in certain context, taking advantage of the two virtual segments which pass through the target. Since the virtual boundary segments do not exist physically, we must provide an algorithm for the moving vehicle to construct the virtual segments based on its sensor readings. A simple algorithm exists: to construct one virtual boundary segment, the vehicle only need to detect the tangent point $\mathbf{w}_1$ or $\mathbf{w}_2$ on the true

boundary curve Γ_j. Because the vehicle knows where the target is, knowing a tangent point is enough to determine a virtual segment.

We assume that the sensor rays of the moving vehicle have infinite detection range. Then, if there is only one obstacle Ob_1, one possibility for the vehicle to fail to detect $\mathbf{w}_1$ is when $\mathbf{w}_1$ is *invisible* to $\mathbf{r}$, that is, the line connecting the vehicle $\mathbf{r}$ and $\mathbf{w}_1$ intersect Γ_1 at some point other than $\mathbf{w}_1$. We can apply the same argument to $\mathbf{w}_2$. The two cases when both $\mathbf{w}_1$ and $\mathbf{w}_2$ are invisible are shown in Figure 4.13 and 4.14.

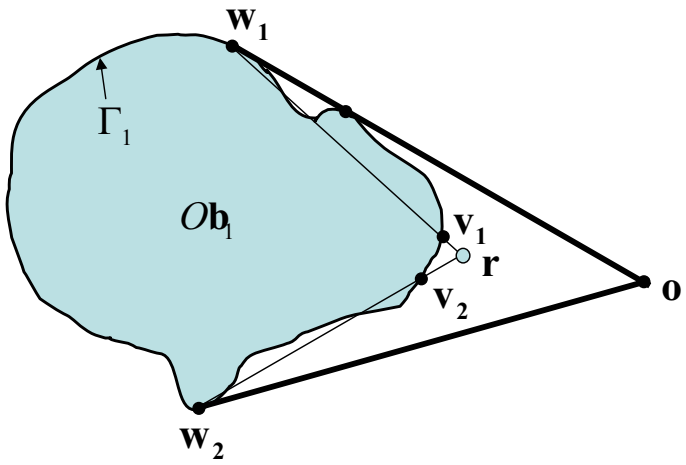

Figure 4.13: *The vehicle lies inside the cone formed by* $\mathbf{ow}_1$ *and* $\mathbf{ow}_2$. *Both* $\mathbf{w}_1$ *and* $\mathbf{w}_2$ *are invisible by the moving vehicle.*

Claim 4.7.6 *Either* $\mathbf{w}_1$ *or* $\mathbf{w}_2$ *is visible to* $\mathbf{r}$, *if* $\mathbf{r}$ *lies outside the cone formed by rays* $\mathbf{ow}_1$ *and* $\mathbf{ow}_2$ *that contains* Ob_1.

Proof

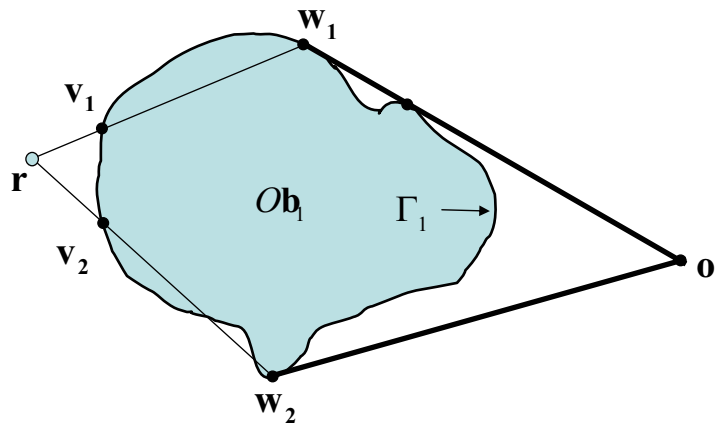

Figure 4.14: *Another case where the vehicle lies inside the cone formed by* $\mathbf{ow}_1$ *and* $\mathbf{ow}_2$*, both* $\mathbf{w}_1$ *and* $\mathbf{w}_2$ *are invisible. However, the vehicle is able to detect a segment of* Γ_1 *which is also a segment of* Λ_1*.*

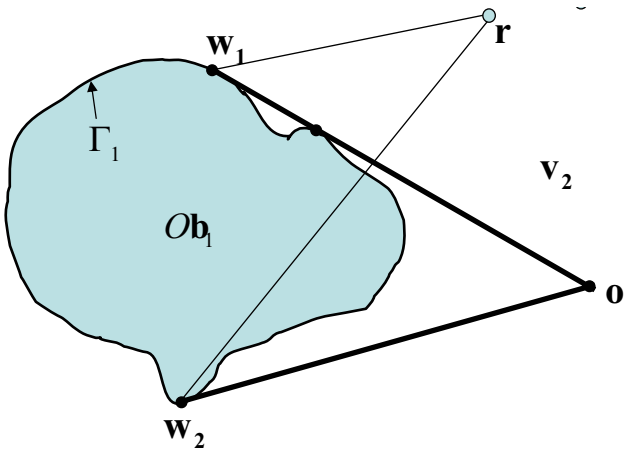

Figure 4.15: *When the vehicle lies outside the cone, either* $\mathbf{w}_1$ *or* $\mathbf{w}_2$ *can be detected.*

The obstacle Ob_1 lies between the rays $\mathbf{ow}_1$ and $\mathbf{ow}_2$. If $\mathbf{r}$ lies outside this cone, then $\mathbf{r} \notin H_1$.

We now prove by contradiction. Suppose neither $\mathbf{w}_1$ nor $\mathbf{w}_2$ are visible by the vehicle at $\mathbf{r}$. Then the line segments $\mathbf{rw}_1$ and $\mathbf{rw}_2$ must intersect the boundary curve of Ob_1 at points $\mathbf{v}_1$ and $\mathbf{v}_2$. We know $\mathbf{v}_1 \in H_1$ and $\mathbf{v}_2 \in H_1$.

Because $\mathbf{r}$ is outside the cone that contains the obstacle, we know that both line segments $\mathbf{rv}_1$ and $\mathbf{rv}_2$ must intersect with the cone boundary which consists of two extended rays, $\mathbf{ow}_1$ and $\mathbf{ow}_2$. There are three possible configurations.

First, suppose both $\mathbf{rv}_1$ and $\mathbf{rv}_2$ intersect with $\mathbf{ow}_2$ or its extension, as shown in Figure 4.16. Denote the intersection points as $\mathbf{v}_3$ and $\mathbf{v}_4$. Then we observe that there are two distinct intersections, $\mathbf{v}_4$ and $\mathbf{w}_2$, between two straight lines $\mathbf{ow}_2$ and $\mathbf{rw}_2$. Therefore, this is impossible.

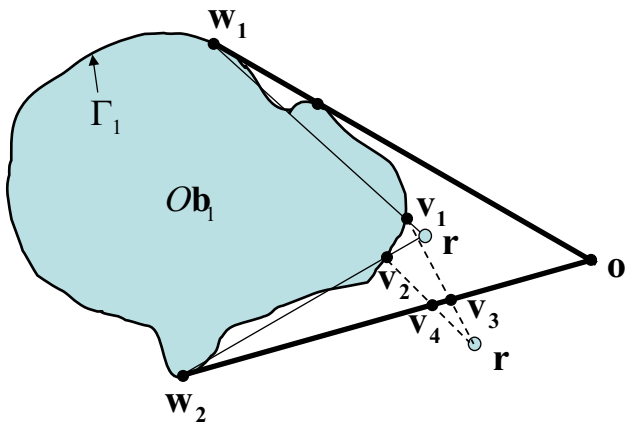

Figure 4.16: *The first impossible case.*

Second, suppose both $\mathbf{rv}_1$ and $\mathbf{rv}_2$ intersect with $\mathbf{ow}_1$ or its extension. By the similar argument as the previous case, we claim that this can not happen.

Third, suppose $\mathbf{rv}_1$ intersect with $\mathbf{ow}_2$ at $\mathbf{v}_3$ and $\mathbf{rv}_2$ intersect with $\mathbf{ow}_1$ at $\mathbf{v}_4$. Then as shown in Figure 4.17, $\mathbf{w}_1\mathbf{v}_3$ and $\mathbf{w}_2\mathbf{v}_4$ are diagonal lines for a quadrangle, which implies that their intersection lies within the quadrangle. However, since we assume that they have another intersection $\mathbf{r}$ outside the cone, we obtain a contradiction.

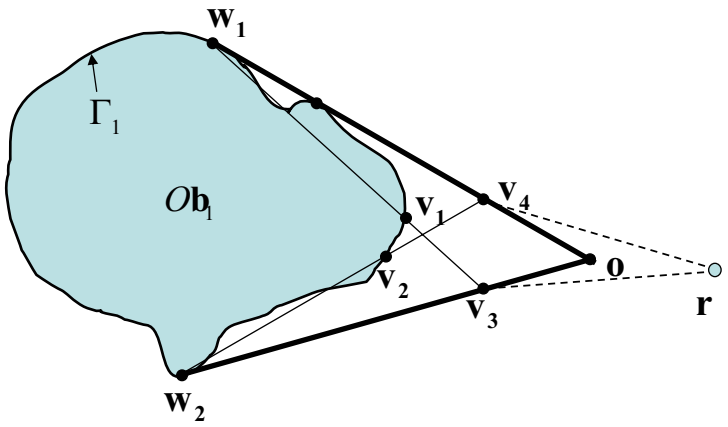

Figure 4.17: *The third impossible configuration.*

As a summary, when $\mathbf{r}$ lies outside the cone, either $\mathbf{w}_1$ or $\mathbf{w}_2$ must be visible to $\mathbf{r}$. ■

When either $\mathbf{w}_1$ or $\mathbf{w}_2$ is visible, the vehicle has to distinguish them from all detected points. A candidate $\mathbf{w}$ for $\mathbf{w}_1$ or $\mathbf{w}_2$ satisfies the following necessary conditions: (1) the tangent vector to Γ_1 at $\mathbf{w}$ is aligned with $\mathbf{ow}$;

(2) all detected points are located on one side of the line **ow**, with **r** lying on the other side. The first condition can be easily verified because the tangent vector at **w** and the line **ow** are known. As declared by Claim 4.7.5, the second condition is a sufficient condition for $\mathbf{w} \in \mathbf{ow}_1$ or $\mathbf{w} \in \mathbf{ow}_2$ when there is only one obstacle with the assumption that it is contained in a cone. Therefore, an algorithm to construct $\mathbf{ow}_1$ and $\mathbf{ow}_2$ is:

Algorithm 4.7.7 *Let* **w** *be a detected point. For any other detected point* **z**, *let* $\mathbf{z}_1$ *be the intersection between the extended ray* $\mathbf{o}\vec{\mathbf{w}}$ *and the extended ray* $\mathbf{r}\vec{\mathbf{z}}$, *as shown in Figure 4.18. Then if* $\| \mathbf{rz} \| \geq \| \mathbf{rz}_1 \|$ *for all* **z**, *then* **w** *is either on the line segment* $\mathbf{ow}_1$ *or on the line segment* $\mathbf{ow}_2$. **ow** *is the virtual line segment we want to construct.*

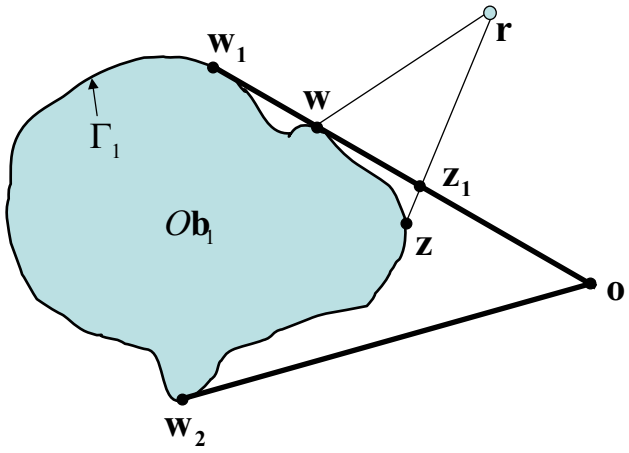

Figure 4.18: *An algorithm to detect virtual boundary* $\mathbf{ow}_1$.

Claim 4.7.8 *A vehicle can always detect a segment of Λ_1, the boundary curve of H_1, if its position* $\mathbf{r}$ *satisfies* $\mathbf{r} \notin H_1$.

Proof

When $\mathbf{r}$ is outside the cone formed by $\mathbf{ow}_1$ and $\mathbf{ow}_2$, we know that it can detect either the virtual boundary $\mathbf{ow}_1$ or $\mathbf{ow}_2$. When $\mathbf{r}$ is inside the cone but does not belong to H_1, it can detect a boundary segment of Ob_1 which is also a boundary segment of H_1. The statement is proved. ■

Theorem 4.7.9 *Suppose a vehicle satisfies the following conditions:*

1. *The initial position of the vehicle does not belong to H_1.*
2. *The vehicle is able to detect virtual boundary segments using for example, algorithm 4.7.7.*
3. *The vehicle is under a control law which enable it to follow a detected boundary with a given distance in unit speed. One such control law may be the second control law in the boundary following section.*

Then the vehicle is able to follow the boundary of H_1 at a given distance. Furthermore, for any $\delta > 0$, there exists $\epsilon > 0$ s.t. by following the boundary of H_1 at distance ϵ, the vehicle is able to get within the δ neighborhood of $\mathbf{o}$ *in finite time.*

Proof

Starting outside the set H_1, the vehicle is always able to detect the boundary curve of H_1. Because the vehicle is able to follow a detected boundary, it

is able to follow the virtual boundary segments too. Since the boundary curve of H_1 has finite length and the vehicle has unit speed, by following the boundary of H_1 at distance small enough, the vehicle will be able to reach the δ neighborhood of any point on the boundary curve Λ_1 in finite time. Since $\mathbf{o} \in \Lambda_1$, the statement is proved. ■

4.7.3 Navigation through many obstacles

Adding a second obstacle to the environment causes several difficulties. The biggest challenge of all is how to segment the detected points, that is, to determine whether two detected points belong to the same obstacle or two obstacles. Because of the complexity of the shape of each obstacle and the many possibilities for the relative position between the vehicle and the obstacles, we have not found one general algorithm which is successful for all cases. However, in many cases, this task can be performed by combining several methods. Therefore, it is reasonable to *assume* that segmentation can be successfully achieved.

Denote the obstacles by Ob_1 and Ob_2. Under the assumption that we know to which obstacle a detected point belongs, we may use Algorithm 4.7.7 to determine the tangent points $\mathbf{w}_{11}$,$\mathbf{w}_{12}$ for Ob_1 and $\mathbf{w}_{21}$,$\mathbf{w}_{22}$ for Ob_2 depending on whether one or more of them are visible . Then we may construct one or more of the virtual boundary segments $\mathbf{ow}_{ij}$ for $i, j = 1, 2$, therefore partly construct H_1 and H_2.

Suppose the position of the vehicle $\mathbf{r}$ lies outside the set H_1 and H_2. Then by Claim 4.7.8, the vehicle is always able to detect a boundary segment. We may answer two questions. Is the vehicle still able to follow the boundary of $H_1 \cup H_2$? And, will the vehicle be able to enter a small neighborhood of the target by following the boundary?

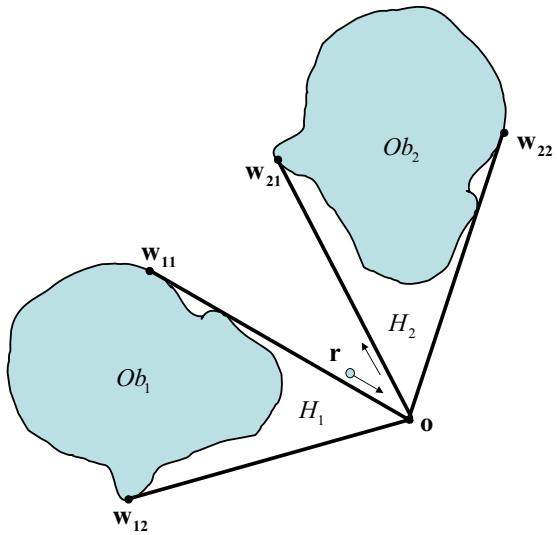

Figure 4.19: *The case when* $H_1 \cap H_2 = \{\mathbf{o}\}$*, two virtual boundary segments* $\mathbf{ow}_{11}$ *and* $\mathbf{ow}_{21}$ *form a crack.*

In order to understand the behavior of the vehicle, we need to study the following cases:

1. $H_1 \subset H_2$, this case is no different than the single obstacle case.

2. $H_1 \cap H_2 = \{\mathbf{o}\}$. In this case, the virtual boundaries intersect at target $\mathbf{o}$ and may form a crack, as shown in Figure 4.19. The vehicle is able to follow the combined boundary of $H_1 \cup H_2$. By following the boundary, the

vehicle will visit a neighborhood of the target and then departure from it to come back again later.

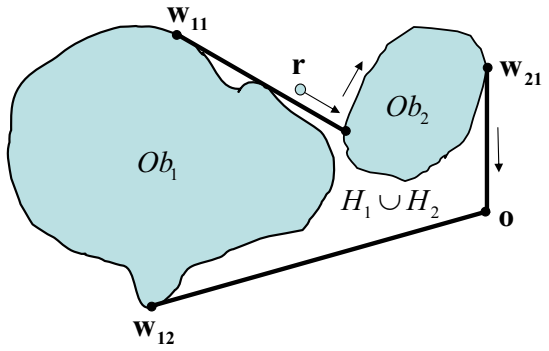

Figure 4.20: *The case when one virtual boundary segment* $\mathbf{ow}_{11}$ *intersects with a true boundary segment. We choose the direction of the true boundary so that the boundary of* $H_1 \cup H_2$ *can be followed.*

3. $H_1 \cap H_2 \neq \emptyset$ with case 1 and 2 excluded. In this case, at least one virtual boundary segments of one obstacle intersects a true boundary segment of the other obstacle. In order to follow the combined boundary for $H_1 \cup H_2$, at the intersection point, the vehicle determines the direction of the true boundary curve so that there is no conflict at the intersection point. Then the combination of the virtual boundary and the true boundary becomes one segment of the boundary curve for $H_1 \cup H_2$, as shown in Figure 4.20. The vehicle will be able to follow the combined boundary. Furthermore, since $\mathbf{o}$ belongs to the boundary of the set $H_1 \cup H_2$, then by following this boundary, the vehicle will arrive in a small neighborhood of the target in finite time.

When there are more than two obstacles, depends on the shape of the

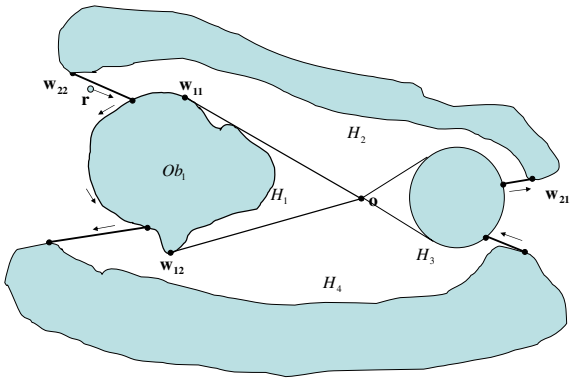

Figure 4.21: *The case when the boundary of the set* $\bigcup_i H_i$ *does not contain the target* **o**.

obstacles, there does exist possibility that **o** becomes a interior point of the combined set, as shown in Figure 4.21. In this case the vehicle will not get close to the target by following the combined boundary. This difficulty is under investigation and might be solved by different ways of constructing virtual boundary segments.

Based on the discussions for two obstacles, the following theorem states some facts about the case when there are more than two obstacles.

Theorem 4.7.10 *Suppose the following conditions are satisfied:*

1. *There exist finitely many obstacles* Ob_i, $i = 1, 2, ..., N$ *satisfying the assumptions given in the beginning paragraph of this section.*

2. *For each* Ob_i, *the vehicle is able to detect boundary segments of* H_i *by using algorithm 4.7.7.*

3. *The vehicle is able to track boundary curve of H_i for each i with any given distance using , for example, the second boundary following law.*

Then starting from a position $\mathbf{r}(t_0) \notin \bigcup_{i=1}^{N} H_i$, the vehicle is able to follow the boundary curve of the set $\bigcup_{i=1}^{N} H_i$. Furthermore, if the target $\mathbf{o}$ lies on the boundary of $\bigcup_{i=1}^{N} H_i$, then given $\delta > 0$, there exists $\epsilon > 0$ s.t. the δ neighborhood of the target can be reached by the vehicle in finite time if the tracking distance between the vehicle and the boundary cure is less than ϵ.

Proof

We have shown the case for two obstacles. We shall use the method of proof by induction to prove the general case. We suppose the statements are true when there are $N-1$ obstacles and use this as the induction hypothesis.

When there are N obstacles, we view this case as adding one more obstacle to the case of $N-1$ obstacles. We may construct the set H_N. Very similar to the case when there are only two obstacles, we can find three possibilities:

1. $H_N \subset \bigcup_{i=1}^{N-1} H_i$ or $\bigcup_{i=1}^{N-1} H_i \subset H_N$. Then there is no difference from the case of $N-1$ obstacles or the case of just one obstacles. The statements hold by the induction hypothesis.

2. $H_N \cap \bigcup_{i=1}^{N-1} H_i = \{\mathbf{o}\}$. This case is similar to the case of two obstacles. The boundary of H_N will be appended to the boundaries of $\bigcup_{i=1}^{N-1} H_i$. Because the vehicle will visit the δ neighborhood of the target in finite time by following the boundary of H_N with distance less than ϵ_N, we know that by following the boundaries of the set $H_N \cup \bigcup_{i=1}^{N-1} H_i = \{\mathbf{o}\}$ with distance

less than

$$\epsilon = min\{\epsilon_1, \epsilon_2, \ldots, \epsilon_N\} \ , \tag{4.122}$$

the vehicle will visit the δ-neighborhood of the target in finite time.

3. $H_1 \cap \bigcup_{i=1}^{N-1} H_i \neq \emptyset$, but case 1 and 2 is excluded. In this case, intersections of virtual boundary segment and real boundary segment exist. By similar argument of the case of two obstacles, we are able to determine the direction of the true boundary so that the combination of the virtual boundary and the true boundary becomes one part of the boundary curve for $H_N \cup \bigcup_{i=1}^{N-1} H_i$. If $\mathbf{o}$ lies on the boundary of $\bigcup_{i=1}^{N} H_i$, by following this boundary, the vehicle will arrive in a neighborhood of the target in finite time.

Chapter 5

Coordinated Orbit Transfer of Satellite Clusters

There is increasing interest in the behaviors of a cluster of relatively small satellites in space. Such satellites are usually inter-connected by wireless radio or laser links for communication. By keeping a cluster of such satellites in a certain geometrical form, one can acquire benefits for scientific observations. The information sharing across the cluster will allow the satellites to work cooperatively to perform tasks impossible or difficult for a single satellite. Compared to a single satellite providing the functionality of a cluster, a member of a cluster can be smaller/lighter. Building and launching costs will then be reduced. In addition, A cluster can also be reconfigured according to different mission goals or in the case that a member of the cluster fails.

The size and shape of a cluster or formation are usually determined by

the required functionality of the formation. With J_2 and higher order terms of the earth's gravitational field ignored, the solution of the Kepler problem tells us that a satellite will track an elliptical or circular orbit. To determine the orbit of each satellite in a cluster such that the size and shape of the cluster is kept unchanged over sufficiently long period is not a trivial problem. Because the amount of fuel on board is limited for each satellite, one needs to find a set of orbits that demand the minimum control effort. This problem becomes more challenging when the effect of J_2 and other disturbances are considered. In [13] the authors proposed a ring of evenly distributed satellites on the same circular orbit for communication purpose. The stability of such ring is proved in [19]. In [6] and [29] the investigations of Clohessy-Wiltshire equations revealed possible formations with constant apparent distributions. The effects of perturbations are calculated and possible station keeping strategy are proposed. In [31], the authors proposed that in the presence of J_2, a set of constraints on the orbital elements shall be satisfied to prevent the orbits from drifting apart. However, extra station keeping is still necessary due to the complicated nature of the disturbances. The adjustment can be performed periodically when the drifting error exceeds certain threshold.

The initialization of a formation is another important problem. The whole cluster can be launched together by a space shuttle or rocket. Satellites will be first placed in a parking orbit before transferring to the final orbits where desired formation will be achieved. The orbital transfer can be performed individually using a control law based on a Lyapunov function which achieves

its minimum when correct orbit is reached. In [30], the Lyapunov function is expressed as a quadratic function of the differences of orbital elements between current orbit and the destination orbit. In [5], the authors proved that an elliptic orbit can be represented uniquely as a point on the linear space formed by the angular momentum vectors and Laplace vectors. A Lyapunov function was built naturally from the Euclidean metric on this space. It has been suggested that compared to Hohmann transfer, this approach will consume less fuel.

The problem we are interested in is a cooperative orbit transfer alogorithm to achieve a satellite formation. What we want to consider here is the case when members of the formation have been placed relatively far apart. They have to use their on-board thrusters to get to the desired orbits to form the desired formation. A similar case is when the whole formation has to be restructured for mission-related reasons. We want the formation to be maintained to some extent during the transfer and be re-established after the transfer.

In section 5.1, we develop formulas used in the proofs of our theorems. In section 5.3, a brief summary of results in [5] and [47] are given.We introduce the definition of periodic satellite formations in section 5.4. Our main results and proofs about orbit transfer of periodic formations are presented in section 5.5. Simulation results are shown in section 5.7.

5.1 Control osculating elements

If the mass of a satellite is small compared to the mass of the earth, the Kepler two body problem can be approximated by a one-center problem as:

$$m\ddot{q} = -\nabla V_G + u \tag{5.1}$$

where $q \in \mathcal{R}^3$ is the position vector of the satellite relative to the center of the earth, m is the mass of the satellite, V_G is the gravitational potential of the earth, u is the control force plus other disturbances. Without considering higher order terms, V_G takes the form

$$V_G = -m\frac{\mu}{\| q \|} \tag{5.2}$$

where μ is the gravitational constant. Let $p = m\dot{q}$ be the momentum vector of the satellite. **For simplicity we assume that all the satellites considered in this chapter have unit mass.**

Let us make the following definitions:

$$\begin{aligned} l(t) &= q(t) \times p(t) \\ A(t) &= p(t) \times l(t) - \mu\frac{q(t)}{\| q(t) \|} \\ e(t) &= \frac{\| A(t) \|}{\mu} \\ a(t) &= \frac{h(t)^2}{\mu(1 - e(t)^2)} \\ \cos(E(t)) &= \frac{1}{e(t)}(1 - \frac{r(t)}{a(t)}) \\ M(t) &= E(t) - e(t)\sin(E(t)) \end{aligned} \tag{5.3}$$

where $h(t) = \| l(t) \|$ and $r(t) = \| q(t) \|$. These formulas can be found in textbooks on celestial mechanics [8]. l is the angular momentum vector. A is called the Laplace vector. They are conserved if $u(t) \equiv 0$. a is the length of the semi-major axis and e is the eccentricity. E is the eccentric anomaly and M is the mean anomaly. The last equation is Kepler's equation. When $e(t) = 0$, the eccentric anomaly $E(t)$ is defined to be $M(t)$ which is measured from the line of ascending node. For now, we will assume that $e(t) \neq 0$.

Notice that these formulas are valid for all t and all the elements are differentiable on $\mathcal{R}^3 \times \mathcal{R}^3 - \{0\}$. So we can take derivative on both sides of equations (5.3). By using the property that l, A, a and e are conserved when $u(t) \equiv 0$, we have

$$\begin{aligned} \dot{l}(t) &= \frac{\partial l}{\partial q}\dot{q} + \frac{\partial l}{\partial p}\dot{p} \\ &= \frac{\partial l}{\partial q}\dot{q} + \frac{\partial l}{\partial p}(-\nabla V_G + u) \\ &= \dot{l}|_{u=0} + \frac{\partial l}{\partial p}u(t) \\ &= \frac{\partial l}{\partial p}u(t) \ . \end{aligned} \tag{5.4}$$

Similarly, we have

$$\dot{A}(t) = \frac{\partial A}{\partial p}u(t) \ . \tag{5.5}$$

We derive the perturbation equations for the orbital elements used in our control algorithm. The control forces are continuous functions of time. Hence the derivatives are taken along the *controlled* dynamics of a satellite. Part of the orbital elements are shown in figure 5.1.

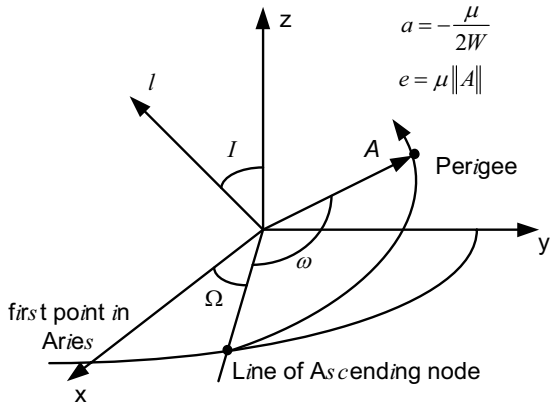

Figure 5.1: *The illustration of the vectors l, A and orbital elements a, e, i, Ω and ω.*

Starting with the eccentricity, we have

$$\begin{aligned} \dot{e}(t) &= \frac{A \cdot \dot{A}}{\mu \parallel A \parallel} = \frac{A}{\mu \parallel A \parallel} \cdot \frac{\partial A}{\partial p} u(t) \\ &= \frac{1}{\mu} (\frac{\partial A}{\partial p})^T \widetilde{A} \cdot u(t) \end{aligned} \tag{5.6}$$

where $\widetilde{A}$ is the unit vector along the direction of A. We also have

$$\dot{h}(t) = \frac{l \cdot \dot{l}}{\parallel l \parallel} = \frac{1}{h} (\frac{\partial l}{\partial p})^T l \cdot u(t) \tag{5.7}$$

$$\begin{aligned} \dot{a}(t) &= \frac{1}{\mu(1-e^2)} (2h\dot{h} + 2\mu a e \dot{e}) \\ &= \frac{2}{\mu(1-e^2)} (\frac{\partial l}{\partial p})^T l \cdot u(t) \\ &\quad + \frac{2ae}{\mu(1-e^2)} (\frac{\partial A}{\partial p})^T \widetilde{A} \cdot u(t) \ . \end{aligned} \tag{5.8}$$

We now derive the formulas for $\dot{M}$. Since $r^2 = q \cdot q$, we have $r\dot{r} = q \cdot p$.

Hence

$$\begin{aligned} h^2 &= l \cdot l = (q \times p) \cdot (q \times p) \\ &= (q \cdot q)(p \cdot p) - (q \cdot p)(q \cdot p) \\ &= r^2\mu(\frac{2}{r} - \frac{1}{a}) - r^2\dot{r}^2 \ . \end{aligned} \tag{5.9}$$

On the other hand

$$h^2 = \mu a(1 - e^2) \ . \tag{5.10}$$

Thus

$$\dot{r}^2 = -\frac{\mu a(1 - e^2)}{r} + \mu(\frac{2}{r} - \frac{1}{a}) \ . \tag{5.11}$$

Apply $r = a(1 - e\ \cos(E))$. After simplification, we have

$$\dot{r} = \sqrt{\mu a}\frac{e\ \sin(E)}{r} \ . \tag{5.12}$$

Taking derivatives on both sides of $r = a(1 - e\ \cos(E))$, we have

$$\dot{r} = \dot{a}(1 - e\ \cos(E)) + a(\dot{e}\ \cos(E) - e\ \sin(E)\dot{E}) \ . \tag{5.13}$$

Thus,

$$\begin{aligned} \dot{E} &= \frac{\dot{r}}{ae\ \sin(E)} - \frac{r}{a^2 e\ \sin(E)}\dot{a} + \frac{a\ \cos(E)}{ae\ \sin(E)}\dot{e} \\ &= \sqrt{\frac{\mu}{a}}\frac{1}{r} + \frac{\cos(E)}{e\ \sin(E)}\dot{e} - \frac{r}{a^2 e\ \sin(E)}\dot{a} \ . \end{aligned} \tag{5.14}$$

On the other hand, taking derivative on both sides of $M = E - e\ \sin(E)$, we get

$$\dot{M} = \dot{E} - \dot{e}\ \sin(E) - e\ \cos(E)\dot{E}$$

$$= \quad (1 - e\,\cos(E))\dot{E} - \dot{e}\,\sin(E)\;. \tag{5.15}$$

Combining this equation with equation (5.14),(5.8)and (5.6), we have

$$\begin{aligned}
\dot{M} &= (1 - e\,\cos(E))\sqrt{\frac{\mu}{a}}\frac{1}{r} + (\frac{\cos(E)(1 - e\,\cos(E))}{e\,\sin(E)} \\
&\quad - \sin(E))\dot{e} - \frac{r(1 - e\,\cos(E))}{a^2 e\,\sin(E)}\dot{a} \\
&= \sqrt{\frac{\mu}{a^3}} + \frac{\cos(E) - e}{e\,\sin(E)}\dot{e} - \frac{(1 - e\,\cos(E))^2}{ae\,\sin(E)}\dot{a} \\
&= n + \eta(\frac{\partial A}{\partial p})^T \widetilde{A} \cdot u(t) + \xi(\frac{\partial l}{\partial p})^T l \cdot u(t)\;,
\end{aligned} \tag{5.16}$$

where $n = \sqrt{\frac{\mu}{a^3}}$ and

$$\begin{aligned}
\xi(l, A, E) &= -\frac{2(1 - e\,\cos(E))^2}{\mu a e(1 - e^2)\sin(E)} \\
\eta(l, A, E) &= \frac{\cos(E) - e}{\mu e\,\sin(E)} - \frac{2(1 - e\,\cos(E))^2}{\mu(1 - e^2)\sin(E)}\;.
\end{aligned} \tag{5.17}$$

Notice that ξ and η will be ∞ if $\sin(E) = 0$. Physically it means that when the satellite is passing perigee or apogee, the control can cause a sudden jump of the mean and eccentric anomalies. In order to prevent this from happening in our control laws, we will turn off the control when $\sin(E) = 0$.

The inclination I is defined as the angle between the z-axis and the angular momentum vector l. It can be determined by

$$\cos(I) = \frac{l_z}{h}\;. \tag{5.18}$$

Taking derivatives on both sides we get

$$-\sin(I)\,\dot{I} \;=\; -\frac{l_z l_x \dot{l}_x + l_z l_y \dot{l}_y - (l_x^2 + l_y^2)\dot{l}_z}{h^3}$$

$$= -\frac{\sin(I)}{h}[\cos(I)\ \sin(\Omega), -\cos(I)\ \cos(\Omega), -\sin(I)]\ \dot{l}, \quad (5.19)$$

because

$$\cos(\Omega) = \frac{-l_y}{\sqrt{l_x^2 + l_y^2}} = \frac{-l_y}{h\ \sin(I)}\ . \quad (5.20)$$

Thus

$$\dot{I} = \frac{1}{h}[\cos(I)\ \sin(\Omega), -\cos(I)\ \cos(\Omega), -\sin(I)](\frac{\partial l}{\partial p})u\ . \quad (5.21)$$

The argument of the ascending node Ω is defined as the angle between the x- axis and the ascending node. It can be determined by

$$\tan(\Omega) = -\frac{l_x}{l_y}\ . \quad (5.22)$$

By taking derivatives on both sides of equation (5.22), we have

$$\begin{aligned} \frac{1}{\cos^2(\Omega)}\dot{\Omega} &= -\frac{l_y\dot{l}_x - l_x\dot{l}_y}{l_y^2} \\ &= -\frac{1}{l_y^2}[l_y, -l_x, 0]\ \frac{\partial l}{\partial p}u\ . \end{aligned} \quad (5.23)$$

Let $\widetilde{n} = \frac{1}{\sqrt{l_x^2+l_y^2}}[-l_y, l_x, 0]^T$, we have

$$\begin{aligned} \dot{\Omega} &= \frac{h\ \sin(I)\cos^2(\Omega)}{l_y^2}(\frac{\partial l}{\partial p})^T\widetilde{n}\cdot u \\ &= \frac{1}{h\ \sin(I)}(\frac{\partial l}{\partial p})^T\widetilde{n}\cdot u\ . \end{aligned} \quad (5.24)$$

Notice that this $\widetilde{n}$ is the unit vector pointing to the ascending node.

The argument of the perigee ω is defined as the angle between the vector $\widetilde{n}$ and $\widetilde{A}$. It can be determined by

$$\cos(\omega) = \widetilde{n}\cdot\widetilde{A}\ . \quad (5.25)$$

By taking derivatives on both sides, we get

$$\dot{\omega} = -\frac{1}{\sin(\omega)}(\dot{\widetilde{n}} \cdot \widetilde{A} + \dot{\widetilde{A}} \cdot \widetilde{n}) \ . \tag{5.26}$$

Because

$$\dot{\widetilde{A}} = \frac{1}{\mu\, e}(\mathrm{I_d} - \widetilde{A}\widetilde{A}^T)\dot{A} \tag{5.27}$$

and

$$\dot{\widetilde{n}} = \frac{1}{h\, \sin(I)}(\mathrm{I_d} - \widetilde{n}\widetilde{n}^T)\dot{n} \tag{5.28}$$

where $\mathrm{I_d}$ represents the identity matrix, one can verify that

$$\dot{\widetilde{n}} \cdot \widetilde{A} = \dot{\Omega} \cos(I) \sin(\omega) \tag{5.29}$$

and

$$\dot{\widetilde{A}} \cdot \widetilde{n} = \frac{1}{\mu\, e}(\widetilde{n} - \cos(\omega)\widetilde{A}) \cdot \dot{A} = \frac{1}{\mu\, e} \sin(\omega)\widetilde{A}_\perp \cdot \dot{A} \tag{5.30}$$

where $\widetilde{A}_\perp$ is the unit vector perpendicular to $\widetilde{A}$ and l forming an acute angle with $\widetilde{n}$. The derivative of ω is

$$\dot{\omega} = -\frac{\cos(I)}{h\, \sin(I)}(\frac{\partial l}{\partial p})^T \widetilde{n} \cdot u - \frac{1}{\mu\, e}(\frac{\partial A}{\partial p})^T \widetilde{A}_\perp \cdot u \tag{5.31}$$

The longitude parameter θ is used in stead of the true anomaly when the orbit is circular. To determine θ, we have the following

$$q \cdot \widetilde{n} = q_x \ \cos(\Omega) + q_y \ \sin(\Omega) = r \ \cos(\theta) \ . \tag{5.32}$$

Hence

$$\cos(\theta) = \frac{x}{r} \ \cos(\Omega) + \frac{y}{r} \ \sin(\Omega) \ . \tag{5.33}$$

On the other hand,

$$-q \times \widetilde{n} = r \, \sin(\theta) \, \frac{l}{h} \, . \tag{5.34}$$

This gives the following set of equations:

$$\begin{aligned} \sin(\theta) \, \frac{l_x}{h} &= \frac{z}{r} \, \sin(\Omega) \\ \sin(\theta) \, \frac{l_y}{h} &= -\frac{z}{r} \, \cos(\Omega) \\ \sin(\theta) \, \frac{l_z}{h} &= -\frac{x}{r} \, \sin(\Omega) + \frac{y}{r} \, \cos(\Omega) \, . \end{aligned} \tag{5.35}$$

Thus, θ can be uniquely determined by using equation (5.33) and any one of equation (5.35).

We now calculate the derivative of θ which contains two parts. The first part is due to the orbital motion of the satellite and the second part is due to the perturbation of the line of ascending node i.e.

$$\dot{\theta} = \frac{h}{r^2} - \frac{\cos(I)}{h \, \sin(I)} (\frac{\partial l}{\partial p})^T \widetilde{n} \cdot u \, . \tag{5.36}$$

We will now derive equation (5.120) for $\dot{M}_\theta$. We start from the cosine relationship between the true anomaly f and the eccentric anomaly E

$$\cos(E) = \frac{e + \cos(f)}{1 + e \, \cos(f)} \, . \tag{5.37}$$

Taking derivatives on both sides yields

$$-\sin(E) \, \dot{E} = \frac{(e^2 - 1) \, \sin(f)}{(1 + e \, \cos(f))^2} \dot{f} + \frac{\sin^2(f)}{(1 + e \, \cos(f))^2} \dot{e} \, . \tag{5.38}$$

Because

$$\sin(E) = \frac{\sqrt{1 - e^2} \, \sin(f)}{1 + e \, \cos(f)} \, , \tag{5.39}$$

we have

$$\begin{aligned}\dot{E} &= \frac{\sqrt{1-e^2}}{1+e\,\cos(f)}\dot{f} - \frac{\sin(E)}{1-e^2}\dot{e} \\ &= \frac{1-e\,\cos(E)}{\sqrt{1-e^2}}\dot{f} - \frac{\sin(E)}{1-e^2}\dot{e}\,. \end{aligned} \tag{5.40}$$

We know

$$f = \theta - \omega\,. \tag{5.41}$$

The true anomaly of the ascending node is $(-\omega)$. Let E_ω be the eccentric anomaly of the ascending node. Its derivative is

$$\dot{E}_\omega = \frac{1-e\,\cos(E_\omega)}{\sqrt{1-e^2}}(-\dot{w}) - \frac{\sin(E_\omega)}{1-e^2}\dot{e}\,. \tag{5.42}$$

Let M_θ be the mean anomaly measured from the line of ascending node. By using the Kepler's equation, it is easy to see that

$$M_\theta = E - e\,\sin(E) - (E_\omega - e\,\sin(E_\omega))\,. \tag{5.43}$$

Thus the derivative

$$\begin{aligned}\dot{M}_\theta &= (1-e\,\cos(E))\dot{E} - (1-e\,\cos(E_\omega))\dot{E}_\omega - \dot{e}\,(\sin(E)-\sin(E_\omega)) \\ &= \frac{(1-e\,\cos(E))^2}{\sqrt{1-e^2}}\dot{\theta} - \dot{e}\,(\sin(E)-\sin(E_\omega)) \\ &\quad -\dot{e}(\frac{\sin(E)(1-e\,\cos(E))}{1-e^2} - \frac{\sin(E_\omega)(1-e\,\cos(E_\omega))}{1-e^2}) \\ &\quad -\frac{(1-e\,\cos(E))^2-(1-e\,\cos(E_\omega))^2}{\sqrt{1-e^2}}\dot{\omega}\,. \end{aligned} \tag{5.44}$$

We know that

$$(1-e\,\cos(E)) = \frac{r}{a}\,. \tag{5.45}$$

Therefore,

$$\frac{(1-e\,\cos(E))^2-(1-e\,\cos(E_\omega))^2}{\sqrt{1-e^2}}=\frac{r^2-r_w^2}{a^2\sqrt{1-e^2}}\;. \tag{5.46}$$

Because of equation (5.31), we have

$$\begin{aligned}\frac{r^2-r_w^2}{a^2\sqrt{1-e^2}}\dot{\omega} &= -\frac{r^2-r_w^2}{\mu\,a^2\,e\,\sqrt{1-e^2}}((\frac{\partial A}{\partial p})^T\widetilde{A}_\perp\cdot u)\\ &\quad -\frac{r^2-r_w^2}{a^2\sqrt{1-e^2}}\frac{\cos(I)}{h\,\sin(I)}(\frac{\partial l}{\partial p})^T\widetilde{n}\cdot u\;.\end{aligned} \tag{5.47}$$

Since we already know that

$$\begin{aligned}\dot{\theta} &= \frac{h}{r^2}-\dot{\Omega}\cos(I)\\ \dot{e} &= \frac{1}{\mu}(\frac{\partial A}{\partial p})^T\widetilde{A}\cdot u(t)\;,\end{aligned} \tag{5.48}$$

substitute the derivatives in equation (5.44) by equations (5.47) and (5.48), we obtain

$$\begin{aligned}\dot{M}_\theta &= n-\frac{r^2}{a^2\,\sqrt{1-e^2}}\frac{\cos(I)}{h\,\sin(I)}(\frac{\partial l}{\partial p})^T\widetilde{n}\cdot u\\ &\quad -(\sin(E)-\sin(E_\omega)+\frac{r\,\sin(E)-r_\omega\,\sin(E_\omega)}{a(1-e^2)})\frac{1}{\mu}(\frac{\partial A}{\partial p})^T\widetilde{A}\cdot u\\ &\quad +\frac{r^2-r_w^2}{\mu\,a^2\,e\,\sqrt{1-e^2}}((\frac{\partial A}{\partial p})^T\widetilde{A}_\perp\cdot u)\\ &\quad +\frac{r^2-r_w^2}{a^2\sqrt{1-e^2}}\frac{\cos(I)}{h\,\sin(I)}(\frac{\partial l}{\partial p})^T\widetilde{n}\cdot u\;,\end{aligned} \tag{5.49}$$

which simplifies to

$$\begin{aligned}\dot{M}_\theta &= n-\frac{r_w^2}{a^2\,\sqrt{1-e^2}}\frac{\cos(I)}{h\,\sin(I)}(\frac{\partial l}{\partial p})^T\widetilde{n}\cdot u\\ &\quad -(\sin(E)-\sin(E_\omega)+\frac{r\,\sin(E)-r_\omega\,\sin(E_\omega)}{a(1-e^2)})\frac{1}{\mu}(\frac{\partial A}{\partial p})^T\widetilde{A}\cdot u\\ &\quad +\frac{r^2-r_w^2}{\mu\,a^2\,e\,\sqrt{1-e^2}}((\frac{\partial A}{\partial p})^T\widetilde{A}_\perp\cdot u)\;.\end{aligned} \tag{5.50}$$

5.2 Shape space for satellite formations

The Jacobi and Kendall shape space can be certainly applied to study the problems of satellite formations. However, for a satellite formation near an elliptic orbit, we find that it is more convenient to use another way of describing the shape of satellite formations.

For a system of two small satellites, one can make the following assumptions: (a) The gravitational attraction between the satellites can be omitted. (b) The total mass of the satellites satisfies $m_1 + m_2 \ll M$ where M is the mass of the Earth. Under these assumptions, the three body system can be approximated by two uncoupled two body problems. Each of the two body problems can be further simplified to a one center problem with the center of Earth being the center of mass.

Let $p = m\dot{q}$ be the momentum of the satellite. The angular momentum $\mathbf{l} = q \times p$ and the energy $W = \frac{1}{2}m\|\dot{q}\|^2 + V$ are integrals of motion (i.e. they are conserved). The Laplace vector $A = p \times l - m^2\mu\frac{q}{\|q\|}$ is also conserved given $q(t) \neq 0$ for all $t > 0$.

Knowing l , W and A, we have seven integrals for the two-body problem. They are not all independent because there are two relations connecting them. They are:

$$\begin{aligned} A \cdot l &= 0 \\ \| A \|^2 &= m^4\mu^2 + 2mW \| l \|^2 \ . \end{aligned} \tag{5.51}$$

The space of ordered pairs (l, A) is $R^3 \times R^3$ on which we define the metric:

$$d((l_1, A_1), (l_2, A_2)) = (\| l_1 - l_2 \|^2 + \| A_1 - A_2 \|^2)^{\frac{1}{2}} . \tag{5.52}$$

Let P denote the phase space of the satellite, define a mapping $\pi : P \to R^3 \times R^3$, $(q, p) \mapsto (l, A)$. Let the set Σ_e be defined as

$$\Sigma_e = \{(q, p) \in P \,|\, W(q, p) < 0, l \neq 0\} \tag{5.53}$$

and let the set D be defined as

$$D = \{(l, A) \in R^3 \times R^3 \,|\, A \cdot l = 0, l \neq 0, \| A \| < m^2\mu\} . \tag{5.54}$$

In [5], the authors proved the following results:

Theorem 5.2.1 *(Chang-Chichka-Marsden)The following hold:*

1. Σ_e *is the union of all elliptic Keplerian orbits.*

2. $\pi(\Sigma_e) = D$ *and* $\Sigma_e = \pi^{-1}(D)$.

3. The fiber $\pi^{-1}(l, A)$ *is a unique (oriented) elliptic Keplerian orbit for each* $(l, A) \in D$.

The mapping π is a continuous mapping because l and A are continuous with respect to (q, p). Furthermore, the following corollary hold.

Corollary 5.2.2 $\pi^{-1}(K)$ *is compact for any compact set* $K \subset D$.

In the case of two satellites, let $(l_i, A_i, P_i, \Sigma_{ei}, D_i, \pi_i, d_i)$ denote the corresponding objects defined for the ith satellite. Let $\bar{P} = P_1 \times P_2$, $\bar{q}(t) =$

$(q_1(t), q_2(t))$, $\bar{p}(t)) = (p_1(t), p_2(t))$. Let $\bar{\Sigma}_e = \Sigma_{e1} \times \Sigma_{e2}$. Let $\bar{D} = D_1 \times D_2$ and $\bar{l} = (l_1, l_2)$, $\bar{A} = (A_1, A_2)$. Let

$$\bar{d}((\bar{l}_1, \bar{A}_1), (\bar{l}_2, \bar{A}_2)) = \sqrt{d_1^2 + d_2^2} \tag{5.55}$$

and $\bar{\pi} = \pi_1 \times \pi_2$. We define *the space of elliptic Keplerian orbits* to be the set $\bar{D}$ with the distance function $\bar{d}$.

Proposition 5.2.3 *The following hold:*

1. $\bar{\Sigma}_e$ *is the union of all pairs of elliptic Keplerian orbits.*

2. $\bar{\pi}(\bar{\Sigma}_e) = \bar{D}$ *and* $\bar{\Sigma}_e = \bar{\pi}^{-1}(\bar{D})$.

3. The fiber $\bar{\pi}^{-1}(\bar{l}, \bar{A})$ *is a unique pair of (oriented) elliptic Keplerian orbit for each* $(\bar{l}, \bar{A}) \in \bar{D}$.

4. $\bar{\pi}^{-1}(\bar{K})$ *is compact for any compact set* $\bar{K} \subset \bar{D}$.

5.3 Orbit transfer of single satellite

For a single satellite on an elliptic orbit, the set D of ordered pairs (l, A) is a subset of $\mathcal{R}^3 \times \mathcal{R}^3$ with Euclidean norm,

$$D = \{(l, A) \in \mathcal{R}^3 \times \mathcal{R}^3 \mid A \cdot l = 0, l \neq 0, \| A \| < m^2\mu\} \ . \tag{5.56}$$

To control the orbit transfer of a single satellite, one considers a Lyapunov function from [5]

$$V(q, p) = \frac{1}{2}(\| l - l_d \|^2 + \| A - A_d \|^2) \tag{5.57}$$

where (l_d, A_d) is the pair of the angular momentum vector and Laplace vector of the target elliptic(circular) orbit. The derivative of V along the integral curve of the system is

$$\begin{aligned}\dot{V} &= (l - l_d) \cdot \dot{l} + (A - A_d) \cdot \dot{A} \\ &= (l - l_d) \cdot \frac{\partial l}{\partial p} u + (A - A_d) \cdot \frac{\partial A}{\partial p} u \\ &= [(l - l_d) \times q + \\ &\quad l \times (A - A_d) + (A - A_d) \times p \times q] \cdot u \ . \end{aligned} \tag{5.58}$$

If we let the control to be

$$u = -[(l - l_d) \times q + l \times (A - A_d) + ((A - A_d) \times p) \times q] \ , \tag{5.59}$$

then $\dot{V} \leq 0$ along the trajectory of the closed loop system. The following lemma is proved in [47].

Lemma 5.3.1 *Suppose a single satellite has external control $u(t) \equiv 0$. Let x, y be time invariant unknown vectors. Suppose $(q(t), p(t)) \in \Sigma_e$, the solution of equation*

$$x \times q + l \times y + (y \times p) \times q \equiv 0 \tag{5.60}$$

is

$$x = \alpha A \quad y = \alpha l \tag{5.61}$$

For some $\alpha \in R$

We will give a proof of the following theorem by Chang, Chichka and Marsden [5]:

Theorem 5.3.2 (Chang-Chichka-Marsden) *There exists $c > 0$ such that if $V(q_0, p_0) \leq c$, by applying the control law as in equation (5.59), the trajectory of the closed loop system starting at (q_0, p_0) will asymptotically converge to the target orbit $\pi^{-1}((l_d, A_d))$*

Proof Let

$$Q = \{(l, A) \in \mathcal{R}^3 \times \mathcal{R}^3 | l \cdot A = 0\} \ . \tag{5.62}$$

Recall that the set of (l, A) pairs for elliptic orbits is

$$D = \{(l, A) \in \mathcal{R}^3 \times \mathcal{R}^3 | l \cdot A = 0, l \neq 0, \| A \| < m^2 \mu\} \ . \tag{5.63}$$

It is easy to see that Q is a closed subset of $\mathcal{R}^3 \times \mathcal{R}^3$ and D is a subset of Q with nonempty interior. The set

$$B = \{(l, A) \in \mathcal{R}^3 \times \mathcal{R}^3 | V \leq c\} \tag{5.64}$$

is a closed ball in $\mathcal{R}^3 \times \mathcal{R}^3$. This tells us that the set $B \cap Q$ is a compact subset of $\mathcal{R}^3 \times \mathcal{R}^3$. If c small enough, we have $B \cap Q \subset D$, then by corollary 5.2.2, the set $\pi^{-1}(B \cap Q)$ will be a compact subset of Σ_e.

The condition $V(q_0, p_0) \leq c$ tells us that $(q_0, p_0) \in \pi^{-1}(B \cap Q)$. By applying LaSalle's invariance principle,we conclude that the trajectory of the closed loop system will converge to the maximal invariant set within the subset of $B \cap Q$ where $\dot{V} = 0$. In [47], we showed that the maximal invariant set is the set where $u(t) = 0$ for all t.

According to lemma 5.3.1, the solution to

$$(l - l_d) \times q + l \times (A - A_d) + ((A - A_d) \times p \times q) = 0 \tag{5.65}$$

is

$$\begin{aligned} l - l_d &= \alpha A \\ A - A_d &= \alpha l \ . \end{aligned} \tag{5.66}$$

Since $l_d \cdot A_d = 0$ and $l \cdot A = 0$, we have

$$\alpha(\| l \|^2 + \| A \|^2) = 0 \ . \tag{5.67}$$

If we further assumed that

$$c < \frac{1}{2}(\| l_d \|^2 + \| A_d \|^2) \ . \tag{5.68}$$

The closed loop system will not reach the set where $l = 0$ and $A = 0$. Thus the only possibility for equation (5.67) to be true is to have $\alpha = 0$. So the solution is

$$\begin{aligned} l &= l_d \\ A &= A_d \ . \end{aligned} \tag{5.69}$$

■

The authors of [5] do not give an explicit upper bound for the value of c. This upper bound can be calculated by solving a constrained maximization problem as below:

$$\sup\{\frac{1}{2}(\| l - l_d \|^2 + \| A - A_d \|^2)\} \tag{5.70}$$

under constraints

$$(l, A) \in Q, \ \ l \neq 0 \ \text{ and } \ \| A \| < m^2\mu \tag{5.71}$$

First, we need to calculate the supremum of the unconstrained maximization problem. It is easy to see that this value is ∞. Then, we need to calculate the minimum value subject to $l = 0$. The result is $0.5 \| l_d \|^2$ achieved when $A = A_d$. We should also calculate the minimum value subject to $\| A \| = m^2\mu$, by applying the Lagrange multiplier method we found this value to be $0.5(m^2\mu - \| A_d \|)^2$. Hence, for theorem 5.3.2 to be valid, we must have

$$c < \min\{0.5 \| l_d \|^2, 0.5(m^2\mu - \| A_d \|)^2\} \tag{5.72}$$

which guarantees (5.68).

5.4 Periodic formation

Suppose we have a formation consisting of m satellites. Let O_j denote the orbit of the jth satellite. The orbit O_j and the position of the satellite on O_j can be described either by the six orbital elements $(a_j, e_j, I_j, \Omega_j, \omega_j, \tau_j)$ or by (l_j, A_j, τ_j) where a denotes the length of semi-major axis, e is the eccentricity, I is the inclination, Ω is the longitude of the ascending node, ω is the argument of the perigee and τ is the perigee passage time. If O_j is elliptic or circular, except for some singular cases when some of the orbital elements are not well defined, theorem 5.2.1 tells us that the two expressions are equivalent. Among all possible formations, we are interested in formations with periodic shape changes. We can make the following definition:

Definition 5.4.1 *A formation is periodic when a_j, the length of semi-major axis of orbit O_j, satisfies $a_j = a > 0$ for all $j = 1, 2, ...m$.*

This definition is valid since all the satellites in a periodic formation will have the same orbital period

$$T = \frac{2\pi\sqrt{a^3}}{\sqrt{\mu}} \ . \tag{5.73}$$

Thus although the shape of the formation is varying, it is varying periodically.

On the other hand, given a set of orbits with the identical length of semi-major axis, there are infinitely many possible periodic formations. We need to specify their relative positions on the orbits to determine a specific formation. The difficulty is that the relative positions are complicated functions of time. However, the differences between the perigee passage times, $(\tau_i - \tau_j)$, are constants. Because the mean anomaly is

$$M_i = n_i(t - \tau_i) \tag{5.74}$$

where $n_i = 2\pi/T$, then $(M_i - M_j)$ are constants. By specifying the values of $(\tau_i - \tau_j)$ or $(M_i - M_j)$ for all i and j, a periodic formation can be uniquely determined.

5.5 Transfer of satellite formations between elliptic orbits

With all the tools we need developed, we are now ready to determine our control laws. To illustrate our ideas, we will show the calculations for two

satellites. A control law for more than two satellites can be developed based on the two-satellite case in a natural way.

To set up a periodic formation of two satellites, one can control each satellite separately to transfer to its target orbit. However, this will not assure the correct values of $(\tau_i - \tau_j)$ or $(M_i - M_j)$. In order to do that, extra terms involving $(\tau_i - \tau_j)$ or $(M_i - M_j)$ should be added in the summation of the Lyapunov functions for single satellites. This extension will result in a cooperative orbit transfer of multiple satellites.

We introduce a variable Υ_i which is defined as

$$\begin{aligned} \Upsilon_i &= \sqrt{\frac{a_i^3}{a_d^3}} M_i, \quad \text{if } E_i \in (-\epsilon, \pi + \epsilon) \\ \Upsilon_i &= \sqrt{\frac{a_i^3}{a_d^3}} (2\pi - M_i), \text{if } E_i \in (\pi - \epsilon, 2\pi + \epsilon) \end{aligned} \tag{5.75}$$

for $i = 1, 2$, where a_d is the common length of the semi-major axes for the destination orbits.

Here, the trouble of using different expressions for the cases $E_i \in (-\epsilon, \pi + \epsilon)$ and $E_i \in (\pi - \epsilon, 2\pi + \epsilon)$ is caused by the fact that $E_i \in S^1$. Two coordinate charts are required on S^1. Here we pick the charts to be

$$\begin{aligned} &\psi_1 : (-\epsilon, \pi + \epsilon) \to (-\epsilon, \pi + \epsilon) \text{ s.t. } E_i \mapsto E_i \\ &\psi_2 : (\pi - \epsilon, 2\pi + \epsilon) \to (-\epsilon, \pi + \epsilon) \text{ s.t.} E_i \mapsto (2\pi - E_i) \, . \end{aligned} \tag{5.76}$$

Here, the value of ϵ is chosen so that the two satellites will always be in the same chart. Because in a satellite formation the angular separations between satellites are usually small, the value of ϵ is small.

For $E_i \in (-\epsilon, \pi + \epsilon)$, we have

$$\begin{aligned}
\dot{\Upsilon}_i &= \sqrt{\frac{a_i^3}{a_d^3}}\dot{M}_i + \frac{3}{2}\sqrt{\frac{a_i}{a_d^3}}\dot{a}_i M_i \\
&= \sqrt{\frac{\mu}{a_d^3}} + \rho(l_i, A_i, E_i)(\frac{\partial A_i}{\partial p_i})^T \widetilde{A}_i \cdot u_i(t) \\
&\quad + \zeta(l_i, A_i, E_i)(\frac{\partial l_i}{\partial p_i})^T l_i \cdot u_i(t)
\end{aligned} \tag{5.77}$$

where

$$\begin{aligned}
\zeta &= \sqrt{\frac{a_i^3}{a_d^3}}\xi(l_i, A_i, E_i) + \frac{3}{2}\sqrt{\frac{a_i}{a_d^3}}\frac{2}{\mu(1-e_i^2)}M_i \\
\rho &= \sqrt{\frac{a_i^3}{a_d^3}}\eta(l_i, A_i, E_i) + \frac{3}{2}\sqrt{\frac{a_i}{a_d^3}}\frac{2a_i e_i}{\mu(1-e_i^2)}M_i \ .
\end{aligned} \tag{5.78}$$

For $E_i \in (\pi - \epsilon, 2\pi + \epsilon)$,

$$\begin{aligned}
\dot{\Upsilon}_i &= -\sqrt{\frac{a_i^3}{a_d^3}}\dot{M}_i + \frac{3}{2}\sqrt{\frac{a_i}{a_d^3}}\dot{a}_i(2\pi - M_i) \\
&= -\sqrt{\frac{\mu}{a_d^3}} + \rho(l_i, A_i, E_i)(\frac{\partial A_i}{\partial p_i})^T \widetilde{A}_i \cdot u_i(t) \\
&\quad + \zeta(l_i, A_i, E_i)(\frac{\partial l_i}{\partial p_i})^T l_i \cdot u_i(t)
\end{aligned} \tag{5.79}$$

where

$$\begin{aligned}
\zeta &= -\sqrt{\frac{a_i^3}{a_d^3}}\xi(l_i, A_i, E_i) + \frac{3}{2}\sqrt{\frac{a_i}{a_d^3}}\frac{2}{\mu(1-e_i^2)}(2\pi - M_i) \\
\rho &= -\sqrt{\frac{a_i^3}{a_d^3}}\eta(l_i, A_i, E_i) + \frac{3}{2}\sqrt{\frac{a_i}{a_d^3}}\frac{2a_i e_i}{\mu(1-e_i^2)}(2\pi - M_i) \ .
\end{aligned} \tag{5.80}$$

Notice that we have terms that explicitly contain M_i. If not handled well, these terms will cause discontinuity in our control algorithm when the satellites enter a new chart. The reason for us to pick the particular charts

(ψ_1, ψ_2) is to reduce the discontinuities in the derivatives of Υ_i caused by changing charts.

We will design a Lyapunov function on the phase space of the two satellites. This one function will have different expressions in different charts. The Lyapunov function is

$$\begin{aligned} V &= V_1 + V_2 + 4\sin(\frac{\Upsilon_1 - \Upsilon_2 - \phi}{4})^2 \\ &\quad \text{if } E_i \in (-\epsilon, \pi + \epsilon) \\ V &= V_1 + V_2 + 4\sin(\frac{\Upsilon_1 - \Upsilon_2 + \phi}{4})^2 \\ &\quad \text{if } E_i \in (\pi - \epsilon, 2\pi + \epsilon) \end{aligned} \tag{5.81}$$

where

$$\begin{aligned} V_1 &= \frac{1}{2}(\| l_1 - l_{d1} \|^2 + \| A_1 - A_{d1} \|^2) \\ V_2 &= \frac{1}{2}(\| l_2 - l_{d2} \|^2 + \| A_2 - A_{d2} \|^2) \ . \end{aligned} \tag{5.82}$$

Here, (l_{d1}, A_{d1}) and (l_{d2}, A_{d2}) specify the orbits in a two-satellite periodic formation and ϕ specifies the desired $(M_1 - M_2)$ on these orbits.

We can calculate the derivative of V as

$$\dot{V} = \dot{V}_1 + \dot{V}_2 + \sin(\frac{\Upsilon_1 - \Upsilon_2 \mp \phi}{2})(\dot{\Upsilon}_1 - \dot{\Upsilon}_2) \ . \tag{5.83}$$

The choice of $-$ or $+$ depends on the value of E_i as in the definition of V. By the calculations performed in the single satellite case,

$$\begin{aligned} \dot{V}_i &= [(l_i - l_{di}) \times q_i + l_i \times (A_i - A_{di}) \\ &\quad + ((A_i - A_{di}) \times p_i) \times q_i] \cdot u_i \end{aligned} \tag{5.84}$$

for $i = 1, 2$. Thus

$$\begin{aligned}
\dot{V} &= [(l_1 - l_{d1} + \zeta_1 \sin(\frac{\Upsilon_1 - \Upsilon_2 \mp \phi}{2})l_1) \times q_1 + \\
&\quad l_1 \times (A_1 - A_{d1} + \rho_1 \sin(\frac{\Upsilon_1 - \Upsilon_2 \mp \phi}{2})\widetilde{A}_1) + \\
&\quad ((A_1 - A_{d1} + \rho_1 \sin(\frac{\Upsilon_1 - \Upsilon_2 \mp \phi}{2})\widetilde{A}_1) \times p_1) \times q_1] \cdot u_1 \\
&\quad + [(l_2 - l_{d2} - \zeta_2 \sin(\frac{\Upsilon_1 - \Upsilon_2 \mp \phi}{2})l_2) \times q_2 + \\
&\quad l_2 \times (A_2 - A_{d2} - \rho_2 \sin(\frac{\Upsilon_1 - \Upsilon_2 \mp \phi}{2})\widetilde{A}_2) + \\
&\quad ((A_2 - A_{d2} - \rho_2 \sin(\frac{\Upsilon_1 - \Upsilon_2 \mp \phi}{2})\widetilde{A}_2) \times p_2) \times q_2] \cdot u_2 \ . \qquad (5.85)
\end{aligned}$$

In order to get $\dot{V} \leq 0$, we let

$$\begin{aligned}
u_1 &= -\sin^2(E_1)[(l_1 - l_{d1} + \zeta_1 \sin(\tfrac{\Upsilon_1 - \Upsilon_2 \mp \phi}{2})l_1) \times q_1 + \\
&\quad l_1 \times (A_1 - A_{d1} + \rho_1 \sin(\tfrac{\Upsilon_1 - \Upsilon_2 \mp \phi}{2})\widetilde{A}_1) + \\
&\quad ((A_1 - A_{d1} + \rho_1 \sin(\tfrac{\Upsilon_1 - \Upsilon_2 \mp \phi}{2})\widetilde{A}_1) \times p_1) \times q_1] \\
u_2 &= -\sin^2(E_2)[(l_2 - l_{d2} - \zeta_2 \sin(\tfrac{\Upsilon_1 - \Upsilon_2 \mp \phi}{2})l_2) \times q_2 + \\
&\quad l_2 \times (A_2 - A_{d2} - \rho_2 \sin(\tfrac{\Upsilon_1 - \Upsilon_2 \mp \phi}{2})\widetilde{A}_2) + \\
&\quad ((A_2 - A_{d2} - \rho_2 \sin(\tfrac{\Upsilon_1 - \Upsilon_2 \mp \phi}{2})\widetilde{A}_2) \times p_2) \times q_2] \ . \qquad (5.86)
\end{aligned}$$

Notice that the factors $\sin^2(E_i)$ cancel the term $\sin(E_i)$ in the denominators of ζ_i and ρ_i. This will result in a continuous control law which will be 0 when $E_i = 0, \pi$.

Another issue is that when $e_i = 0$, E_i is not well defined. So we should not allow $A_{di} = 0$. Furthermore, we should choose our initial value of function V

s.t. the subset of the space $\Sigma_{e1} \times \Sigma_{e2}$ where $A_i = 0$ will not be reached by the controlled dynamics.

Let $z = (q_1, p_1, q_2, p_2)$. We now proceed to find the initial condition $z_0 = (q_1(0), p_1(0), q_2(2), p_2(0))$ for z s.t. the set

$$S_M = \{z | V(z) \leq V(z_0)\} \tag{5.87}$$

is a compact subset of $\Sigma_{e1} \times \Sigma_{e2} - \{z | A_1 = 0 \; or \; A_2 = 0\}$. This is a necessary step because we want to apply LaSalle's invariance principle to prove our main result.

Lemma 5.5.1 *Let*

$$c < \min\{c_1, c_2\} \tag{5.88}$$

where

$$c_i = \min\{\frac{1}{2} \parallel A_{di} \parallel^2, \frac{1}{2} \parallel l_{di} \parallel^2, \frac{1}{2}(\mu - \parallel A_{di} \parallel)^2\} \tag{5.89}$$

for $i = 1, 2$. *Then the set*

$$S_M = \{z | V(z) \leq c\} \tag{5.90}$$

is a compact subset of $\Sigma_{e1} \times \Sigma_{e2} - \{z | A_1 = 0 \; or \; A_2 = 0\}$.

Proof The first observation is that the set

$$S_1 = \{(q_1, p_1) | V(q_1, p_1) \leq c^*, c^* < c_1\} \tag{5.91}$$

is a subset of Σ_{e1} i.e. $S_1 \cap \Sigma_{e1} = S_1$.

In fact, c_1 is the supremum of $V_1(q_1, p_1)$ on the set $\Sigma_{e1} - \{(q_1, p_1)|A_1 = 0\}$. To see this, we solve a constrained maximization problem as below:

$$\sup\{\frac{1}{2}(\| l_1 - l_{d1} \|^2 + \| A_1 - A_{d1} \|^2)\} \tag{5.92}$$

under the constraints

$$A_1 \cdot l_1 = 0 \;\; l_1 \neq 0 \;\; A_1 \neq 0 \;\text{ and }\; \| A_1 \| < \mu \; . \tag{5.93}$$

First, we need to calculate the supremum of the unconstrained maximization problem. It is easy to see that this value is ∞. Then, we need to calculate the minimum value subject to $l_1 = 0$. The result is $\frac{1}{2} \| l_d \|^2$ achieved when $A = A_d$. Similarly, the minimum value subject to $A_1 = 0$ is $\frac{1}{2} \| A_d \|^2$. We should also calculate the minimum value subject to $\| A \| = \mu$. By applying the Lagrange multiplier method we found this value to be $\frac{1}{2}(\mu - \| A_d \|)^2$. Thus

$$c_1 = \min\{\frac{1}{2} \| A_{d1} \|^2 , \frac{1}{2} \| l_{d1} \|^2 , \frac{1}{2}(\mu - \| A_{d1} \|)^2\} \tag{5.94}$$

is the supremum of V_1 on the set $\Sigma_{e1} - \{(q_1, p_1)|A_1 = 0\}$. We proved that $S_1 \subset \Sigma_{e1} - \{(q_1, p_1)|A_1 = 0\}$.

Another observation is that $\pi(S_1)$ is a compact subset of D_1. Thus by corollary 5.2.2, S_1 is a compact subset of Σ_{e1}.

We can make the same arguments for the case when $i = 2$ to prove that S_2 is a compact subset of $\Sigma_{e2} - \{(q_2, p_2)|A_2 = 0\}$.

Hence by letting $c < \min\{c_1, c_2\}$, it is true that

$$S_M \subset S_1 \times S_2 \subset \Sigma_{e1} \times \Sigma_{e2} - \{z|A_1 = 0 \text{ or } A_2 = 0\} \; . \tag{5.95}$$

Thus, S_M is a compact subset of $\Sigma_{e1} \times \Sigma_{e2} - \{z | A_1 = 0 \text{ or } A_2 = 0\}$ ■

We can now apply LaSalle's invariance principle to show that the trajectory of the closed loop system, starting within S_M, converges to the maximal invariant subset of S_M where $u(t) = 0$ is satisfied for all t.

Proposition 5.5.2 *With V,c and u_i given as in (5.81) ,(5.88) and (5.86), the trajectory starting from point $(q_{10}, p_{10}, q_{20}, p_{20})$ which satisfies*

$$V(q_{10}, p_{10}, q_{20}, p_{20}) \leq c \tag{5.96}$$

will converge to the set where

$$\begin{aligned} l_i &= l_{di} \\ A_i &= A_{di} \\ (M_1 - M_2) &= \phi \end{aligned} \tag{5.97}$$

are satisfied for $i = 1, 2$.

Proof In order to calculate the invariant set,let $u_1 = 0$. When $\sin(E_1) \neq 0$, we get

$$\begin{aligned} &(l_1 - l_{d1} + \zeta_1 \sin(\frac{\Upsilon_1 - \Upsilon_2 \mp \phi}{2}) l_1) \times q_1 \\ &+ l_1 \times (A_1 - A_{d1} + \rho_1 \sin(\frac{\Upsilon_1 - \Upsilon_2 \mp \phi}{2}) \widetilde{A}_1) \\ &+ ((A_1 - A_{d1} + \rho_1 \sin(\frac{\Upsilon_1 - \Upsilon_2 \mp \phi}{2}) \widetilde{A}_1) \times p_1) \times q_1 \\ &= 0 \, . \end{aligned} \tag{5.98}$$

Take inner products on both sides with $q_1(t)$ to get

$$(l_1 \times (A_1 - A_{d1} + \rho_1 \sin(\frac{\Upsilon_1 - \Upsilon_2 \mp \phi}{2}) \widetilde{A}_1)) \cdot q_1 = 0 \, . \tag{5.99}$$

This is equivalent to

$$(l_1 \times q_1(t)) \cdot (A_1 - A_{d1} + \rho_1 \sin(\frac{\Upsilon_1 - \Upsilon_2 \mp \phi}{2})\widetilde{A}_1) = 0 \ . \tag{5.100}$$

Let

$$B = A_1 - A_{d1} + \rho_1 \sin(\frac{\Upsilon_1 - \Upsilon_2 \mp \phi}{2})\widetilde{A}_1 \ . \tag{5.101}$$

Equation (5.100) means B is perpendicular to the vector $l_1 \times q_1(t)$. We can see that vector B should stay in the plane spanned by l_1 and $q_1(t)$ as shown in Figure 5.2.

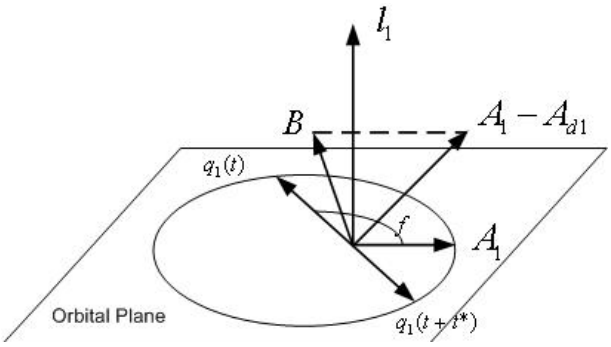

Figure 5.2: *The relationship between l_1,q_1, $A_1 - A_d$ and B*

However, from the assumption that $u_1(t) = 0$, we know that A_1 and l_1 are constant vectors. The time varying vector B will sweep a line segment passing the fixed point $(A_1 - A_{d1})$. The direction of this line segment is aligned with $\widetilde{A}_1$. So vector B will be the intersection of the (l_1, q_1) plane and this line segment. Because $q_1(t)$ is sweeping the orbital plane, the (l_1, q_1) plane is identical at t and $t + kT_1$ where k is an integer and T_1 is the period of the first satellite. Since the line segment is not changed, the intersection

points in these cases must be identical. Thus we must have

$$B(t) = B(t + kT_1) \ . \tag{5.102}$$

Without lost of generality, suppose at time t, $E_1(t), E_2(t) \in (-\epsilon, \pi+\epsilon)$. Then equation (5.102) requires that

$$\begin{aligned} & \rho_1(E_1(t)) \sin(\tfrac{\Upsilon_1(t)-\Upsilon_2(t)-\phi}{2}) \\ = \quad & \rho_1(E_1(t+kT_1)) \sin(\tfrac{\Upsilon_1(t+kT_1)-\Upsilon_2(t+kT_1)-\phi}{2}) \ . \end{aligned} \tag{5.103}$$

Let $k = 1$ in equation (5.103), because $\rho_1(E_1(t)) = \rho_1(E_1(t+T_1))$, the first observation we make is that the two satellites must have the same period. In fact, suppose at time t_0 equation (5.103) is satisfied. Then at time $t_0 + T_1$, since $E_1(t_0) = E_1(t_0+T_1)$,$\Upsilon_1(t_0) = \Upsilon_1(t_0+T_1)$ and all the angles(anomalies) are in the range of $[0, 2\pi)$, we must have $\Upsilon_2(t_0) = \Upsilon_2(t_0 + T_1)$. But

$$\Upsilon_2(t_0) - \Upsilon_2(t_0 + T_1) = -\sqrt{\frac{a_2^3}{a_d^3}}(M_2(t_0 + T_1) - M_2(t_0)) \ . \tag{5.104}$$

Then $\Upsilon_2(t_0) = \Upsilon_2(t_0 + T_1)$ will be satisfied only if $M_2(t_0 + T_1) = M_2(t_0)$. Thus we shall have $T_1 = k_1 T_2$ where k_1 is a positive integer. Remember we can apply the same argument to the second satellite to get $T_2 = k_1 T_1$. Thus we must have $T_1 = T_2$. Hence on the invariant set, we proved that $a_1 = a_2$.

On the other hand, for a specific time t, we know that there exists $t^* \in [0, T_1)$ such that

$$\pi + f_1(t) = f_1(t + t^*) \tag{5.105}$$

where f_1 is the true anomaly of the first satellite. The value of t^* depends on t. The plane spanned by (l_1, q_1) at time t will also be identical to the plane

spanned by (l_1, q_1) at time $t + t^*$. Thus we must have

$$B(t) = B(t + t^*) \tag{5.106}$$

which requires that

$$\begin{aligned} & \rho_1(E_1(t)) \sin(\tfrac{\Upsilon_1(t) - \Upsilon_2(t) - \phi}{2}) \\ = \quad & \rho_1(E_1(t + t^*)) \sin(\tfrac{\Upsilon_1(t+t^*) - \Upsilon_2(t+t^*) + \phi}{2}) \ . \end{aligned} \tag{5.107}$$

Further, $a_1 = a_2$ implies that $M_1(t) - M_2(t) = M_1(t + t^*) - M_2(t + t^*)$, one can verify that

$$\sin(\frac{\Upsilon_1(t) - \Upsilon_2(t) - \phi}{2}) = -\sin(\frac{\Upsilon_1(t + t^*) - \Upsilon_2(t + t^*) + \phi}{2}) \ . \tag{5.108}$$

For (5.107) to be satisfied, one possibility is that

$$\sin(\frac{\Upsilon_1(t) - \Upsilon_2(t) - \phi}{2}) = 0 \ . \tag{5.109}$$

Another possibility is that

$$\rho_1(E_1(t)) = -\rho_1(E_1(t + t^*)) \ . \tag{5.110}$$

By the definition of ρ_1, one can verify that (5.110) can only be satisfied when t takes value from a set of measure 0. Thus, for (5.107) to be satisfied, (5.109) must be true.

Because of (5.109), the time varying parts in equation (5.98) vanish. We can make the same argument as in the proof of the single satellite case [5] to show that

$$l_1 \quad = \quad l_{d1}$$

$$A_1 \;=\; A_{d1}\ . \tag{5.111}$$

We can apply similar arguments for the second satellite.

Thus we have

$$\begin{aligned} l_i &= l_{di} \\ A_i &= A_{di} \\ (\Upsilon_1 - \Upsilon_2) &= \pm\phi \end{aligned} \tag{5.112}$$

for $i = 1, 2$. By the definition of Υ_1 and Υ_2 in equation(5.75), we have

$$\sqrt{\frac{a_1^3}{a_d^3}}M_1 - \sqrt{\frac{a_2^3}{a_d^3}}M_2 = \phi\ . \tag{5.113}$$

But we already know $a_1 = a_2 = a_d$, so we conclude that

$$(M_1 - M_2) = \phi\ . \tag{5.114}$$

■

This proposition can be easily extended to m satellites where $m > 2$. Let the mth satellite be the leader of the formation. Let

$$V = \sum_i^m (V_i + 4\sin(\frac{\Upsilon_i - \Upsilon_m \mp \phi_i}{4})^2) \tag{5.115}$$

where $i = 1, 2, 3, ..., m$, $\phi_m = 0$ and

$$V_i = \frac{1}{2}\| l_i - l_{di} \|^2 + \| A_i - A_{di} \|^2\ . \tag{5.116}$$

It is easy to see that the control for the ith satellite with $i \leq m-1$ is the same as the control for the (i, m) pair of satellites. The initial value of V

should be less than the minimum value of c_i for $i = 1, 2, ..., (m-1)$. Then the solution will converge to the set where

$$\begin{aligned} l_i &= l_{di} \\ A_i &= A_{di} \\ M_i - M_n &= \phi_i \end{aligned} \tag{5.117}$$

are satisfied for $i = 1, 2, ..., m$.

5.6 Transfer of satellite formations to circular orbits

Formations on circular orbits are of great importance as addressed in [19]. If the destination of at least one of the satellites in a formation is circular, we will have difficulty to determine the mean anomaly. Since the Laplace vector A vanishes, the perigee point can not be determined. In such a case, the position of a satellite on the circular orbit is usually described by using the argument of latitude defined as the angle θ between the line of ascending node and the position vector q. It is easy to see that on an elliptic orbit, this angle

$$\theta = \omega + f \tag{5.118}$$

where ω is the argument of perigee and f is the true anomaly. On a circular orbit,we have

$$\theta = n(t - \tau) \tag{5.119}$$

where τ is the time when the satellite passing the ascending node for the first time. As we can see, θ serves as the mean anomaly for circular orbit.

Although θ and $\dot{\theta}$ can be easily determined as discussed in the appendix, they are not suitable for our Lyapunov function based control laws because θ is not affine in time on elliptic orbit. Thus, we will use the angle M_θ which is the mean anomaly measured from the line of node. M_θ can be determined from θ. But if the orbit is close to circular, we can use θ as an approximation for M_θ. Further analysis in the appendix shows that the derivative of M_θ is

$$\begin{aligned}\dot{M}_\theta &= n - \frac{r_w^2}{a^2\sqrt{1-e^2}}\frac{\cos(I)}{h\,\sin(I)}(\frac{\partial l}{\partial p})^T\widetilde{n}\cdot u \\ &\quad -(\sin(E)-\sin(E_\omega)+\frac{r\,\sin(E)-r_\omega\,\sin(E_\omega)}{a(1-e^2)})\frac{1}{\mu}(\frac{\partial A}{\partial p})^T\widetilde{A}\cdot u \\ &\quad +\frac{r^2-r_w^2}{\mu\,a^2\,e\,\sqrt{1-e^2}}((\frac{\partial A}{\partial p})^T\widetilde{A}_\perp\cdot u)\ . \end{aligned} \tag{5.120}$$

Here, ω is the argument of perigee, E and E_ω are the eccentric anomalies corresponding to $\theta-\omega$ and ω, r_ω denote the distance between the ascending node and the gravitational center. We let $\widetilde{n}=\frac{1}{\sqrt{l_x^2+l_y^2}}[-l_y,l_x,0]^T$, this $\widetilde{n}$ is the unit vector pointing to the ascending node. We let $\widetilde{A}_\perp$ be the unit vector perpendicular to $\widetilde{A}$ and l forming an acute angle with $\widetilde{n}$.

We will now study the case when we want to setup a formation of which all the members are on circular orbits with the same radius. According to the discussions made in section 5.4, this formation is a periodic formation. Let τ_i be the time when the ith satellite passes the line of ascending node for the first time. Similar to the perigee passage time in our elliptic orbit case, τ_i is a constant of the free motion for satellite i. Hence by specifying

the differences $\tau_i - \tau_j$ or $\theta_i - \theta_j$ between satellites, a periodic formation on circular orbits can be uniquely determined.

Similar to the elliptic orbit case, we introduce a variable Ψ_i which is defined as

$$\begin{aligned} \Psi_i &= \sqrt{\frac{a_i^3}{a_d^3}} M_{\theta_i}, \text{ if } \theta_i \in (-\epsilon, \pi + \epsilon) \\ \Psi_i &= \sqrt{\frac{a_i^3}{a_d^3}} (2\pi - M_{\theta_i}), \text{if } \theta_i \in (\pi - \epsilon, 2\pi + \epsilon) \end{aligned} \tag{5.121}$$

for $i = 1, 2$, where a_d is the common length of the semi-major axes (or radius) for the destination orbits. Here, the reasons for using two charts are the same as in the case of elliptic orbits.

Calculations in the appendix show that the derivative of Ψ is

$$\dot{\Psi} = \sqrt{\frac{\mu}{a_d^3}} + (\frac{\partial l}{\partial p})^T (\lambda \widetilde{n} + \kappa l) \cdot u + (\frac{\partial A}{\partial p})^T (\sigma \widetilde{A} + \varrho \widetilde{A}_\perp) \cdot u \tag{5.122}$$

where for $\theta \in (-\epsilon, \pi + \epsilon)$,

$$\begin{aligned} \lambda &= -\sqrt{\frac{a^3}{a_d^3}} \frac{r_w^2}{a^2 \sqrt{1-e^2}} \frac{\cos(I)}{h \sin(I)} \\ &\approx -\sqrt{\frac{a^3}{a_d^3}} \frac{r_w^2}{a^2} \frac{\cos(I)}{h \sin(I)} \\ \kappa &= \frac{3}{\mu a (1-e^2)} \Psi \\ \sigma &= \frac{3\, e}{\mu(1-e^2)} \Psi - \frac{1}{\mu} \sqrt{\frac{a^3}{a_d^3}} (\sin(E) - \sin(E_\omega) + \frac{r \sin(E) - r_\omega \sin(E_\omega)}{a(1-e^2)}) \\ &\approx -\frac{1}{\mu} \sqrt{\frac{a^3}{a_d^3}} (\sin(E) - \sin(E_\omega) + \frac{r \sin(E) - r_\omega \sin(E_\omega)}{a(1-e^2)}) \end{aligned}$$

$$
\begin{aligned}
\varrho &= \sqrt{\frac{a^3}{a_d^3}}\frac{r^2 - r_w^2}{\mu\, a^2\, e\, \sqrt{1-e^2}} \\
&\approx -\sqrt{\frac{a^3}{a_d^3}}\frac{2(\cos(E) - \cos(E_\omega))}{\mu}\ ,
\end{aligned} \tag{5.123}
$$

and for $\theta \in (\pi - \epsilon, 2\pi + \epsilon)$,

$$
\begin{aligned}
\lambda &= \sqrt{\frac{a^3}{a_d^3}}\frac{r_w^2}{a^2\sqrt{1-e^2}}\frac{\cos(I)}{h\,\sin(I)} \\
&\approx \sqrt{\frac{a^3}{a_d^3}}\frac{r_w^2}{a^2}\frac{\cos(I)}{h\,\sin(I)} \\
\kappa &= \frac{3}{\mu a(1-e^2)}\,\Psi \\
\sigma &= \frac{3\,e}{\mu(1-e^2)}\,\Psi + \frac{1}{\mu}\sqrt{\frac{a^3}{a_d^3}}(\sin(E) - \sin(E_\omega) + \frac{r\,\sin(E) - r_\omega\,\sin(E_\omega)}{a(1-e^2)}) \\
&\approx \frac{1}{\mu}\sqrt{\frac{a^3}{a_d^3}}(\sin(E) - \sin(E_\omega) + \frac{r\,\sin(E) - r_\omega\,\sin(E_\omega)}{a(1-e^2)}) \\
\varrho &= -\sqrt{\frac{a^3}{a_d^3}}\frac{r^2 - r_w^2}{\mu\, a^2\, e\, \sqrt{1-e^2}} \\
&\approx \sqrt{\frac{a^3}{a_d^3}}\frac{2(\cos(E) - \cos(E_\omega))}{\mu}\ .
\end{aligned} \tag{5.124}
$$

Here we use the "$\approx$" when the eccentricity of the orbits are very small. When the orbit is circular, E and E_w is not well defined, but we have $M_\theta = \theta$ and

$$
\dot{\theta} = n - \frac{\cos(I)}{h\,\sin(I)}(\frac{\partial l}{\partial p})^T\widetilde{n}\cdot u\ . \tag{5.125}
$$

Thus when $e = 0$

$$
\begin{aligned}
\lambda &= \mp\sqrt{\frac{a^3}{a_d^3}}\frac{\cos(I)}{h\,\sin(I)} \\
\kappa &= \frac{3}{\mu a(1-e^2)}\,\Psi
\end{aligned}
$$

$$\begin{aligned} \sigma &= 0 \\ \varrho &= 0 \,. \end{aligned} \tag{5.126}$$

This result agree with the limits of (5.123) and (5.124) as $e \to 0$.

Mimic what has been done in the elliptic orbit case, we design a Lyapunov function on the phase space of two satellites as

$$\begin{aligned} V &= V_1 + V_2 + 4\,\sin(\frac{\Psi_1 - \Psi_2 - \phi}{4})^2 \\ &\quad \text{if } \theta_i \in (-\epsilon, \pi + \epsilon) \\ V &= V_1 + V_2 + 4\,\sin(\frac{\Psi_1 - \Psi_2 + \phi}{4})^2 \\ &\quad \text{if } \theta_i \in (\pi - \epsilon, 2\pi + \epsilon) \end{aligned} \tag{5.127}$$

where

$$\begin{aligned} V_1 &= \frac{1}{2}(\| l_1 - l_{d1} \|^2 + \| A_1 \|^2) \\ V_2 &= \frac{1}{2}(\| l_2 - l_{d2} \|^2 + \| A_2 \|^2) \,. \end{aligned} \tag{5.128}$$

The derivative of this function has similar form as equation (5.85). And the control law u s.t. $\dot{V} \leq 0$ can be chosen as

$$\begin{aligned} u_1 &= -[(l_1 - l_{d1} + \sin(\tfrac{\Psi_1 - \Psi_2 \mp \phi}{2})(\lambda_1 \widetilde{n}_1 + \kappa_1 l_1)) \times q_1 + \\ &\quad l_1 \times (A_1 + \sin(\tfrac{\Psi_1 - \Psi_2 \mp \phi}{2})(\sigma_1 \widetilde{A}_1 + \varrho_1 \widetilde{A}_{1\perp})) + \\ &\quad ((A_1 + \sin(\tfrac{\Psi_1 - \Psi_2 \mp \phi}{2})(\sigma_1 \widetilde{A}_1 + \varrho_1 \widetilde{A}_{1\perp}) \times p_1) \times q_1] \\ u_2 &= -[(l_2 - l_{d2} - \sin(\tfrac{\Psi_1 - \Psi_2 \mp \phi}{2})(\lambda_2 \widetilde{n}_2 + \kappa_2 l_2)) \times q_2 + \\ &\quad l_2 \times (A_2 - \sin(\tfrac{\Psi_1 - \Psi_2 \mp \phi}{2})(\sigma_2 \widetilde{A}_2 + \varrho_2 \widetilde{A}_{2\perp})) + \\ &\quad ((A_2 - \sin(\tfrac{\Psi_1 - \Psi_2 \mp \phi}{2})(\sigma_2 \widetilde{A}_2 + \varrho_2 \widetilde{A}_{2\perp})) \times p_2) \times q_2] \,. \end{aligned} \tag{5.129}$$

Based on Lemma 5.5.1, the following lemma is obvious.

Lemma 5.6.1 *Let*

$$c < \min\{c_1, c_2\} \tag{5.130}$$

where

$$c_i = \min\{\frac{1}{2} \parallel l_{di} \parallel^2, \frac{1}{2}\mu^2\} \tag{5.131}$$

for $i = 1, 2$. *Then the set*

$$S_M = \{z | V(z) \leq c\} \tag{5.132}$$

is a compact subset of $\Sigma_{e1} \times \Sigma_{e2}$.

Hence we will prove that starting within the set S_M, the controlled dynamics will converge to the maximal invariant set where formation relationships are obtained.

Proposition 5.6.2 *With* V,c *and* u_i *given as in (5.127) ,(5.130) and (5.129), the trajectory starting from point* $(q_{10}, p_{10}, q_{20}, p_{20})$ *which satisfies*

$$V(q_{10}, p_{10}, q_{20}, p_{20}) \leq c \tag{5.133}$$

will converge to the set where

$$\begin{aligned} l_i &= l_{di} \\ A_i &= 0 \\ (\theta_1 - \theta_2) &= \phi \end{aligned} \tag{5.134}$$

are satisfied for $i = 1, 2$.

Proof Let $u_1 = 0$, and take the inner product with q_1 on both sides of the equation, we get

$$(l_1 \times B_1) \cdot q_1 = 0 \tag{5.135}$$

where

$$B_1 = A_1 + \sin(\frac{\Psi_1 - \Psi_2 \mp \phi}{2})(\sigma_1 \widetilde{A}_1 + \varrho_1 \widetilde{A}_{1\perp}) \; . \tag{5.136}$$

At the time t_0 when $E_1(t_0) = E_{\omega 1}$, since $M_{\theta 1} = 0$ and $r_1 = r_{\omega 1}$, we have

$$\varrho_1(t_0) = 0 \;\; \text{and} \;\; \sigma_1(t_0) = 0 \; , \tag{5.137}$$

hence

$$B_1(t_0) = A_1 \; . \tag{5.138}$$

On the other hand,

$$(q_1 \times l_1) \cdot B_1 = 0 \tag{5.139}$$

tells us that B_1 lies in the plane spanned by l_1 and q_1. Thus, when $q_1(t_0)$ is not aligned with A_1, $B_1(t_0)$ must vanish. This implies that

$$A_1 = 0 \; . \tag{5.140}$$

But it is also possible that $q_1(t_0)$ is aligned with A_1. In this case we have

$$E_{\omega 1} = 0 \;\; \text{and} \;\; \omega_1 = 0 \; . \tag{5.141}$$

Therefore, for all time t,

$$\varrho_1(t) \;\; = \;\; \pm \sqrt{\frac{a_1^3}{a_d^3}} \frac{r_1^2 - r_{w1}^2}{\mu \, a_1^2 \, e_1 \, \sqrt{1 - e_1^2}}$$

$$\sigma_1(t) \;=\; \frac{3\,e_1}{\mu(1-e_1^2)}\,\Psi_1 - \frac{1}{\mu}\sqrt{\frac{a_1^3}{a_d^3}}\sin(E_1)(1+\frac{r_1}{a_1(1-e_1^2)})\;. \quad (5.142)$$

Thus,

$$B_1(t) = A_1 + \sin(\frac{\Psi_1 - \Psi_2 \mp \phi}{2})(\sigma_1\widetilde{A}_1 + \varrho_1\widetilde{A}_{1\perp})\;, \quad (5.143)$$

and $B_1(t)$ has to be aligned with $q_1(t)$ for all time t. If we let T_1 to be the orbital period of the first satellite and T_2 be the orbital period of the second satellite, then after one period T_1 the first satellite will return to the same position, which implies that

$$\begin{aligned} &A_1 + \sin(\frac{\Psi_1(t+T_1) - \Psi_2(t+T_1) \mp \phi}{2})(\sigma_1(t+T_1)\widetilde{A}_1 + \varrho_1(t+T_1)\widetilde{A}_{1\perp}) \\ &= A_1 + \sin(\frac{\Psi_1(t) - \Psi_2(t) \mp \phi}{2})(\sigma_1(t)\widetilde{A}_1 + \varrho_1(t)\widetilde{A}_{1\perp})\;. \end{aligned} \quad (5.144)$$

Because $M_{\theta_1}(t) = M_{\theta_1}(t+T_1)$ and $E_1(t) = E_1(t+T_1)$, we know $\sigma_1(t+T_1) = \sigma_1(t)$ and $\varrho_1(t+T_1) = \varrho_1(t)$. Then the above equation results in

$$\begin{aligned} &\sin(\frac{\sqrt{\frac{a_1^3}{a_d^3}}M_{\theta_1}(t) - \sqrt{\frac{a_2^3}{a_d^3}}M_{\theta_2}(t) - \phi}{2}) = \\ &\sin(\frac{\sqrt{\frac{a_1^3}{a_d^3}}M_{\theta_1}(t) - \sqrt{\frac{a_2^3}{a_d^3}}M_{\theta_2}(t+T_1) - \phi}{2})\;. \end{aligned} \quad (5.145)$$

Therefore we must have

$$M_{\theta_2}(t) = M_{\theta_2}(t+T_1)\;. \quad (5.146)$$

So T_1/T_2 is a positive integer. On the other hand, the above arguments can be applied to the second satellite. If $A_2 \neq 0$, T_2/T_1 must be a positive integer. Hence $T_2 = T_1$ which implies that $a_1 = a_2$.

Still assuming $q_1(t_0)$ is aligned with A_1, we know that by the property of elliptic orbit, after half period, $q_1(t_0 + T_1/2)$ is aligned with A_1 again, which means that

$$\sin(\frac{\Psi_1(t_0 + T_1/2) - \Psi_2(t_0 + T_1/2) \mp \phi}{2})\varrho_1(t_0 + T_1/2) = 0. \tag{5.147}$$

According to the definition of Ψ, one can verify that

$$\sin(\frac{\Psi_1(t + T_1/2) - \Psi_2(t + T_1/2) \mp \phi}{2}) = -\sin(\frac{\Psi_1(t) - \Psi_2(t) \mp \phi}{2}) \ . \tag{5.148}$$

Therefore, the first possibility is that

$$\varrho_1(t_0 + T_1/2) = -\varrho_1(t_0) = 0 \ . \tag{5.149}$$

This further implies that $r_1(t_0 + T_1/2) = r_1(t_0)$. Because at time t_0 the satellite is at perigee and at time $t_0 + T_1/2$ the satellite is at apogee, we conclude that the orbit is circular i.e. $A_1 = 0$.

The second possibility for equation (5.147) to hold is that

$$\sin(\frac{\Psi_1(t_0) - \Psi_2(t_0) \mp \phi}{2}) = 0 \ . \tag{5.150}$$

But because $T_1 = T_2$, we must have

$$\Psi_1(t) - \Psi_2(t) = \Psi_1(t_0) - \Psi_2(t_0) \tag{5.151}$$

which implies that

$$\sin(\frac{\Psi_1(t) - \Psi_2(t) \mp \phi}{2}) = 0 \ . \tag{5.152}$$

One can then make the same argument as in the proof of the single satellite case [5] to show that

$$\begin{aligned} l_1 &= l_{d1} \\ A_1 &= 0 \end{aligned} \tag{5.153}$$

Up to this point, we have proved that our algorithm will cause either A_1 or A_2 to vanish. Without loss of generality, we proceed by assuming $A_1 = 0$. Then from $u_1 = 0$, we get

$$(l_1 - l_{d1} + \sin(\frac{\Psi_1 - \Psi_2 \mp \phi}{2})(\lambda_1 \widetilde{n}_1 + \kappa_1 l_1)) \times q_1 = 0 \; . \tag{5.154}$$

Let

$$D_1 = l_1 - l_{d1} + \sin(\frac{\Psi_1 - \Psi_2 \mp \phi}{2})(\lambda_1 \widetilde{n}_1 + \kappa_1 l_1) \; . \tag{5.155}$$

Such D_1 must be aligned with q_1 and also lies in the plane passing $(l_1 - l_{d1})$ spanned by l_1 and $\widetilde{n}_1$. Because the plane is fixed and q_1 is periodic in time, at time t and time $(t + T_1)$, the intersection of q_1 and the plane must be the same. This tells us that T_1/T_2 is a positive integer. Now if $A_2 = 0$, the above arguments can be repeated so that we conclude T_2/T_1 is also a positive integer. If $A_2 \neq 0$, we can repeat the arguments after equation (5.141) to conclude that T_2/T_1 is also a positive integer. Therefore, we conclude that $T_1 = T_2$ and $a_1 = a_2$

According to the property for circular orbit, at time t and $(t + T_1/2)$, the intersection of q_1 and the plane spanned by l_1 and q_1 passing $l_1 - l_d$ should be the same, i.e.

$$D_1(t) = D_1(t + T_1/2) \; . \tag{5.156}$$

Thus

$$\sin(\frac{\Psi_1(t) - \Psi_2(t) \mp \phi}{2})(\lambda_1(t)\widetilde{n}_1 + \kappa_1(t)l_1) =$$
$$\sin(\frac{\Psi_1(t + T_1/2) - \Psi_2(t + T_1/2) \mp \phi}{2})(\lambda_1(t + T_1/2)\widetilde{n}_1$$
$$+\kappa_1(t + T_1/2)l_1) \ . \tag{5.157}$$

Because of equation (5.148), equation (5.157) are satisfied only if

$$\sin(\frac{\Psi_1(t) - \Psi_2(t) \mp \phi}{2}) = 0 \tag{5.158}$$

or

$$\lambda_1(t)\widetilde{n}_1 + \kappa_1(t)l_1 = -\lambda_1(t + T_1/2)\widetilde{n}_1 - \kappa_1(t + T_1/2)l_1 \ . \tag{5.159}$$

Equation (5.159) implies that for all time t,

$$\kappa(t) = -\kappa(t + T_1/2) \tag{5.160}$$

which further implies that

$$M_{\theta_1}(t) = \frac{\pi}{2} \ . \tag{5.161}$$

This is impossible. Thus, the only possibility is to have

$$\sin(\frac{\Psi_1(t) - \Psi_2(t) \mp \phi}{2}) = 0 \ . \tag{5.162}$$

Because of (5.162), the time varying parts in equation $u_1 = 0$ vanish. We can make the same argument as in the proof of the single satellite case [5] to show that

$$l_1 \ = \ l_{d1}$$

$$A_1 \;=\; 0\,. \tag{5.163}$$

Now let $u_2(t) = 0$ and substitute equation (5.162) into it. We conclude that the second satellite will achieve

$$\begin{aligned} l_2 &= l_{d2} \\ A_2 &= 0\,. \end{aligned} \tag{5.164}$$

Thus we have

$$\begin{aligned} l_i &= l_{di} \\ A_i &= 0 \\ (\Psi_1 - \Psi_2) &= \pm\phi \end{aligned} \tag{5.165}$$

for $i = 1, 2$. By the definition of Ψ_1 and Ψ_2 in equation(5.121), we have

$$\sqrt{\frac{a_1^3}{a_d^3}} M_{\theta_1} - \sqrt{\frac{a_2^3}{a_d^3}} M_{\theta_2} = \phi\,. \tag{5.166}$$

But we already know $a_1 = a_2 = a_d$ and the orbits are circular, we conclude that

$$(\theta_1 - \theta_2) = \phi\,. \tag{5.167}$$

■

We would like to mention that this algorithm is not limited to set up formations on circular orbits. With slight modification to the proof one can show the convergence result hold for elliptic orbits.

5.7 Simulation results

To verify our algorithms, a series of simulations have been carried out in Matlab. First we show a controlled transfer of two satellites from orbit $[a, e, i, \omega, \Omega] = [20, 0.1, \pi/4, \pi/2, 0]$ with initial separation of mean anomaly being $\pi/90$ to the orbit $[a, e, i, \omega, \Omega] = [25, 0.05, \pi/3, \pi/2, 0]$ with final separation of mean anomaly being $\pi/18 \approx 0.175$. Only relative motion between the satellites is plotted in an inertial frame centered at one of the satellites. Figure 5.3 displays the desired relative motion between the satellites. Figure 5.4 displays the relative motion between the satellites using the control algorithm proposed. The final orbits for the two satellites are:

$$\begin{aligned} [a_1, e_1, I_1, \omega_1, \Omega_1] &= [25.10,\ 0.0495,\ 1.0472,\ 1.6231,\ 0] \\ [a_2, e_2, I_2, \omega_2, \Omega_2] &= [25.12,\ 0.0507,\ 1.0472,\ 1.6231,\ 0] \end{aligned}$$

and the final separation of mean anomaly is 0.168. As we can see, the desired orbit and separation are achieved with small error. We noticed that by adjusting the weight of the terms in our Lyapunov functions, we can control the distribution of errors among the orbital elements of final orbits.

Similar experiments are performed to set up a two satellite formation in circular orbits. Initially, the two satellites are on an elliptic orbit with $[a, e, i, \omega, \Omega] = [20, 0.1, \pi/4, \pi/2, 0]$ and the separation of argument of latitude is $\pi/90$. Their destination orbit is circular with $[a, e, i, \Omega] = [25, 0, \pi/3, \pi/4]$ and the separation $\pi/18$. Using our algorithm, the final orbits are

$$[a_1, e_1, I_1, \Omega_1] = [25.082,\ 0.0023,\ 1.0472,\ 0.7854]$$

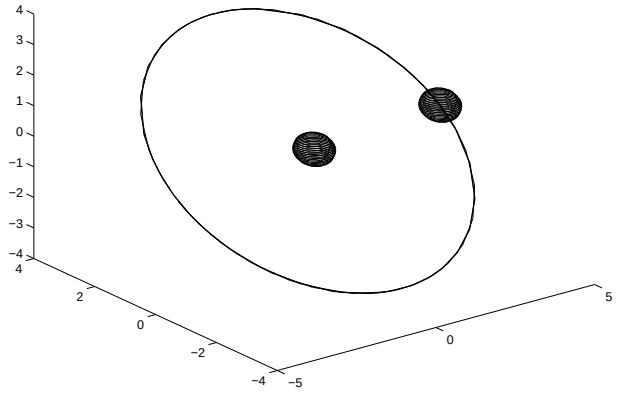

Figure 5.3: *The desired final relative motion of two satellites (length unit= one tenth of earth radius).*

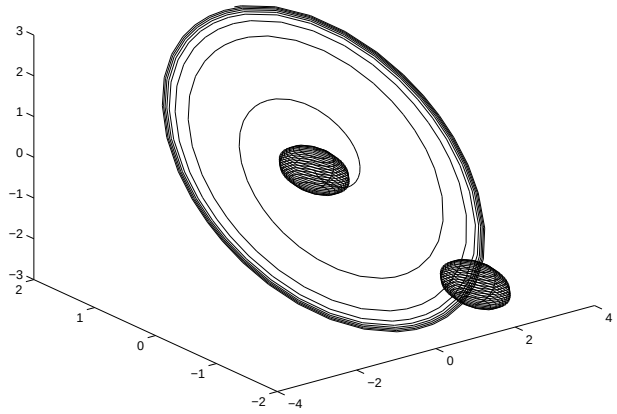

Figure 5.4: *The relative motion achieved by our algorithm.*

$$[a_2, e_2, I_2, \Omega_2] \quad = \quad [25.078,\ 0.0022,\ 1.0472,\ 0.7854]$$

and the final separation is 0.174. Again, the formation is achieved with small error.

Chapter 6

Summary and Future Directions

We have answered several questions related to how to control the formation of a team of robots. We model the robots as particles and use various shape theory to describe small formations in different contexts. Jacobi shape theory is the first such theory, which inspired the creation of shape theory on Lie groups in chapter 4 and shape theory on momentum maps in chapter 5. Of course, in order to understand complex teaming behaviors, especially when large number of objects are involved, such theories need to be significantly extended if still applicable.

Shape theory tells us what the system equations are for a formation. The equations often describe the dynamics of the shape only, which gives us an advantage of designing control laws using quantities that are independent of

choice of coordinate frame. In chapter 3, we tried to justify that this is an advantage that should not be neglected. By using gauge covariant controllers, one can improve the robustness of the formation and, at the same time, reduce the burden on communication links. These results might shed some light on how to cooperate more effectively. We admit that communication theory shall also play an important role here.

Chapter 2 fully illustrated the strength of shape theory. The fact that navigation problem can be considered as a formation control problem brings a new perspective. This is supported by experimental data in [50]. We have obtained a series of results that improve the known navigation algorithms. Although only the 2D case has been fully developed in this dissertation, we have obtained 3D results in very similar ways [46]. Besides, some preliminary results toward navigation for formations have also been developed[49]. The potential of this approach for navigation is yet to be fully explored. Meanwhile, this approach also inspired us to investigate related problems such as curvature estimation, boundary segmentation, and sensor fusion.

In chapter 5 we have proposed control algorithms that can be used to set up periodic formations of satellites on elliptic and circular orbits. The shape space formed by the angular momentum vectors and Laplace vectors is appropriate to describe satellite formations. The control laws we propose are based on a Lyapunov function on this shape space and proved to be convergent. We have not considered the effect of perturbations such as J_2 effect. This is currently being investigated.

BIBLIOGRAPHY

[1] S. S. Antman. *Nonlinear problems of elasticity*. Springer-Verlag, New York, 1995.

[2] V. Aquilanti and S. Cavalli. Coordinates for molecular dynamics: Orthogonal local system. *Journal of Chemical Physics*, 85(3):1355–1361, 1986.

[3] A. Bernhart. Polygons of pursuit. *Scripta Mathematica*, 24:23–50, 1959.

[4] H. Brocard. Solution of Lucas's problem. *Nouv. Corresp. Math.*, 3:280, 1877.

[5] D.E. Chang, D. Chichka, and J.E. Marsden. Lyapunov-based transfer between elliptic Keplerian orbits. *Discrete and Continuous Dynamical Systems*, B,2:57–67, 2002.

[6] D.F. Chichka. Satellite clusters with constant apparent distribution. *Journal of Guidance,Control,and Dynamics*, 24(1):117–122, 2001.

[7] R.H. Cushman and L.M. Bates. *Global aspects of classical integrable systems*. Birkhauser Verlag, Switzerland, 1997.

[8] J.M.A. Danby. *Fundamentals of Celestial Mechanics*. Macmillan, New York, 1962.

[9] B. R. Fajen and W. H. Warren. The behavioral dynamics of steering, obstacle avoidance, and route selection. *Journal of Experimental Psychology: Human Perception and Performance*, 29(2):343–362, 2003.

[10] B. R. Fajen, W. H. Warren, S. Temizer, and L. P. Kaelbling. A dynamical model of visually-guided steering, obstacle avoidance, and route selection. *International Journal of Computer Vision*, 54:13–34, 2003.

[11] Edward Fiorelli, Naomi Leonard, Pradeep Bhatta, Derek Paley, Ralf Bachmayer, and David Fratantoni. Multi-auv control and adaptive sampling in Monterey Bay. In *Proc. IEEE Autonomous Underwater Vehicles 2004: Workshop on Multiple AUV Operations(AUV04)*, pages 1–14. IEEE, 2004.

[12] F. Heppner. Three-dimensional structure and dynamics of bird flock. In J.K. Parrish and W.M. Hamner, editors, *Animal groups in three dimensions*. Cambridge University Press, 1997.

[13] A.G.Y. Johnston and C.R. McInnes. Autonomous control of a ring of satellites. *Advances in the Astronautical Sciences*, 95 part I:93–105, 1997.

[14] Eric Justh and P.S. Krishnaprasad. Equilibria and steering laws for planar formations. *System and Control Letters*, 52:25–38, 2004.

[15] D. G. Kendall. Shape manifolds, procrustean metrics, and complex projective spaces. *Bulletin of London Math. Society*, 16:81–121, 1984.

[16] D. G. Kendall, D. Barden, T. Karne, and H. Le. *Shape and shape theory*. Chichester, New York, 1999.

[17] L.E. Keshet. Trail following as an adaptable mechanism for popular behavior. In J.K. Parrish and W.M. Hamner, editors, *Animal groups in three dimensions*. Cambridge University Press, 1997.

[18] O. Khatib. Real-time obstacle avoidance for manipulators and mobile robots. *International Journal of Robotics Research*, 5:90–98, 1986.

[19] P. S. Krishnaprasad. Relative equilibria and stability of rings of satellites. In *Proc. 39th IEEE Conference on Decision and Control (CDROM)*, pages 1285–1288, New York, 2000. IEEE.

[20] D. R. Lewis. Lagrangian block diagonalization. *Journal of Dynamical Systems and Differential Equations*, 4:1–42, 1992.

[21] Z. Lin, M. Broucke, and B. Francis. Local control strategies for groups of mobile autonomous agents. *submitted to IEEE Transaction on Automatic Control*, 2003.

[22] R. Littlejohn and M. Reinsch. Internal or shape coordinates in the n-body problem. *Physical Review A*, 52(3):2035–2051, 1995.

[23] R. Littlejohn and M. Reinsch. Gauge fields in the separation of rotation and internal motions in the n-body problem. *Reviews of Modern Physics*, 69(1):213–275, 1997.

[24] V. J. Lumelsky and A. Stepanov. Path planning strategies for a point mobile automaton moving amidst unknown obstacles of arbitrary shape. *Algorithmica*, 2:403–430, 1987.

[25] J. E. Marsden, J. C. Simo, D. R. Lewis, and T.A. Posbergh. A block diagonalization theorem in the energy-momentum method. *Contemporary Mathematics*, 97:297–313, 1989.

[26] R. S. Millman and G. D. Parker. *Elements of Differential Geometry*. Prentice-Hall, 1977.

[27] J.K. Parrish. Individual decisions, traffic rules and emergent patterns in schooling fish. In J.K. Parrish and W.M. Hamner, editors, *Animal groups in three dimensions*. Cambridge University Press, 1997.

[28] E. Rimon and D. E. Koditschek. Exact robot navigation using artificial potential functions. *IEEE Transactions on Robotics and Automation*, 8(5):501–518, 1992.

[29] R.J.Sedwick, D.W.Miller, and E.M.C.Kong. Mitigation of differential perturbations in formation flying satellite clusters. *Journal of the Astronautical Sciences*, 47(3 and 4):309–331, 1999.

[30] H. Schaub, S.R. Vadali, J.L. Junkins, and K.T. Alfriend. Spacecraft formation flying control using mean orbit elements. *to appear in Journal of the Astronautical Sciences*, 2000.

[31] Hanspeter Schaub and Kyle T. Alfriend. J_2 invariant relative orbits for spacecraft formations. In *Proc. of the Flight Mechanics Symposium*. NASA/GSFC, 1999.

[32] G. Schöner and M. Dose. A dynamical systems approach to task-level system integration used to plan and control autonomous vehicle motion. *Robotics and Autonomous Systems*, 10:253–267, 1992.

[33] R. Shahidi. Mobile robot navigation using potential functions. Master's thesis, Department of Electrical and Computer Engineering, University of Maryland, 1989.

[34] Z. Shiller. Online suboptimal obstacle avoidance. *The International Journal of Robotics Research*, 19(5):480–497, 2000.

[35] J. C. Simo, D. R. Lewis, and J. E. Marsden. Stability of relative equilibria I: The reduced energy momentum method. *Archive for Rational Mechanics and Analysis*, 115:15–59, 1991.

[36] J. C. Simo, D. R. Lewis, and J. E. Marsden. Stability of relative equilibria II: Three dimensional elasticity. *Archive for Rational Mechanics and Analysis*, 115:61–100, 1991.

[37] L. Singh, H. Stephanou, and J. Wen. Real-time robot motion control with circulatory fields. In *Proc. 1996 IEEE International Conference on Robotics and Automation*, pages 2737–2742, Minneapolis, Minnesota, 1996. IEEE.

[38] L. Singh, J. Wen, and H. Stephanou. Motion planning and dynamic control of a linked manipulator using modified magnetic fields. In *Proc. 1997 IEEE International Conference on Control Applications*, pages 9–15, Hartford, CT, 1997. IEEE.

[39] D.P. Tsakiris. *Motion Control and Planning for Nonholonomic Kinematic Chains*. PhD thesis, University of Maryland, 1995.

[40] D.P. Tsakiris and P.S. Krishnaprasad. Oscillations, SE(2)-snakes and motion control: A study of the roller racer. *Dynamics and Stability of Systems*, 16(4):347–397, 2001.

[41] L.-S. Wang. *Geometry,Dynamics and Control of Coupled Systems*. PhD thesis, ISR Technical Report PhD90-5, University of Maryland, 1990.

[42] L.-S. Wang and P. S. Krishnaprasad. Gyroscopic control and stabilization. *Journal of Nonlinear Science*, 2:367–415, 1992.

[43] R. Yang. *Nonholonomic geometry, mechanics and control*. PhD thesis, University of Maryland, 1992.

[44] Fumin Zhang. Geometric control of formations. *Ph.D. proposal*, 2002.

[45] Fumin Zhang, Michael Goldgeier, and P.S. Krishnaprasad. Control of small formations using shape coordinates. In *Proc. of 2003 International Conference of Robotics and Automation*, pages 2510–2515, Taipei, Taiwan, 2003. IEEE.

[46] Fumin Zhang, Eric Justh, and P.S. Krishnaprasad. Boundary following using gyroscopic control. In *Proc. of 43rd IEEE Conference on Decision and Control*, Atlantis, Paradise Island, Bahamas, 2004. IEEE.

[47] Fumin Zhang and P.S. Krishnaprasad. Formation dynamics under a class of control laws. In *Proc. of 2002 American Control Conference*, volume 2, pages 1678–1685, Anchorage, Alaska, 2002.

[48] Fumin Zhang and P.S. Krishnaprasad. Co-ordinated orbit transfer of satellite clusters. *Astrodynamics, Space Missions, and Chaos, Annals of the New York Academy of Sciences*, 1017:112–137, 2004.

[49] Fumin Zhang, P.S. Krishnaprasad, and Salman Haq. Boundary tracking by a formation (preprint). 2004.

[50] Fumin Zhang, Alan O'Connor, Derek Luebke, and P.S. Krishnaprasad. Experimental study of curvature-based control laws for obstacle avoid-

ance. In *Proceedings of 2004 IEEE International Conference on Robotics and Automation*, pages 3849–3854, New Orleans, Tennessee, 2004. IEEE.